THE
PHYSICAL REVIEW
A Journal of Experimental and Theoretical Physics
VOL. 45, NO. 1 JANUARY 1, 1934 SECOND SERIES

Harmonic and Combination Bands in CO_2

E. F. BARKER AND TA-YOU WU, *University of Michigan*
(Received November 18, 1933)

The absorption bands of CO_2 at higher frequencies are important for the determination of anharmonic constants which characterize the potential function and for the location of upper levels in the vibration diagram of ν_1 and ν_2 in which resonance interaction appears. Only the odd harmonics are active. The band $3\nu_2$ at 5.0μ has been measured under high resolution and five zero branches identified, two originating in the normal state and three in the first excited state. The rotational structure of the strongest of these bands at 2078 cm^{-1} is resolved. The band $3\nu_3$ at 1.43μ is a typical doublet. Combination bands near 2μ and 1.6μ are sufficiently resolved to show their contours and to permit for the first time a satisfactory determination of their positions.

PROBABLY no other polyatomic molecule is as completely known in mechanical structure and behavior as is CO_2. The recent very successful formulation of this problem by Adel and Dennison[1] was based in large part upon infrared absorption measurements from this laboratory, including the following which were in progress at that time. The two fundamental bands had already[2] been located precisely and resolved. For observations upon the less intense harmonic and combination bands we have used an absorption cell seven meters long, with mica windows, filled by displacement with CO_2 to a maximum concentration of about 80 percent. The 4800 line grating used gives good resolution in the region near 5μ and, at shorter wave-lengths, adequate separation to show the contours of the bands but not to resolve their rotational structure.

With these measurements a sufficient number of vibrational levels are available to determine completely the arrangement and positions of all the terms, as indicated in Fig. 1. The levels involving V_1 and V_2 occur in groups designated by bracketed quantum numbers at the left of the figure, and, in any one group, the terms with equal l are mixed because of resonance interaction. These interacting levels are connected by brackets. The observed term values are indicated for all levels which have been identified in the spectrum and a few predicted levels are represented by broken lines, the term values in these cases being computed. Absorption bands arise only from transitions for which $\Delta V_2+\Delta V_3$ is odd. They are of the parallel (doublet) type when $\Delta l=0$ and perpendicular when $\Delta l=\pm 1$. The Venus bands observed by Adams and Dunham[3] determine the three highest levels by transitions from the normal state. For Raman lines $\Delta l=0$ and ΔV_2 is even, corresponding to transitions between groups in any one column. The groups of degenerate levels may be designated for convenience by the maximum value of V_2 involved. Thus group 2 consists of a pair of interacting levels with $l=0$ and a single level with $l=2$. None of the levels of group 5 has as yet been observed. A

[1] Adel and Dennison, Phys. Rev. **44**, 99 (1933).
[2] Martin and Barker, Phys. Rev. **41**, 291 (1932).
[3] Adams and Dunham, Pub. A. S. P. **44**, 243 (1932).

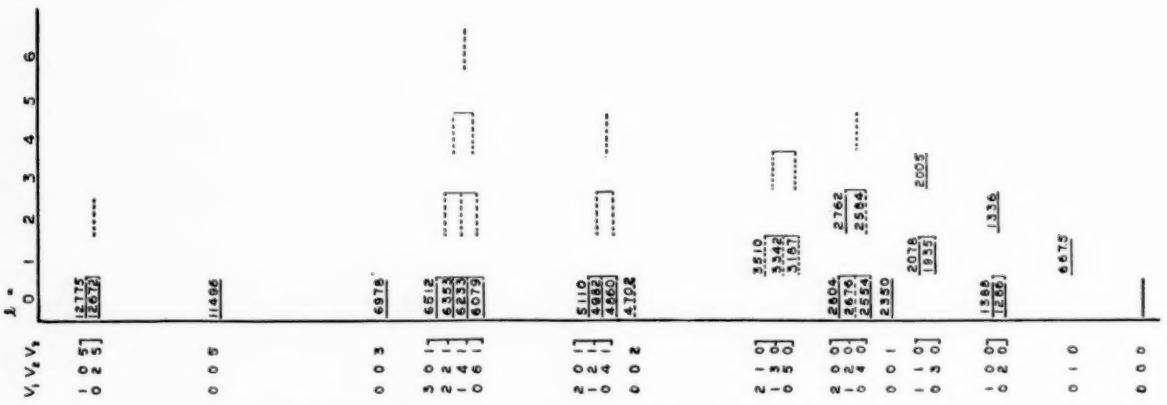

FIG. 1. Diagram of vibrational levels and term values for CO_2.

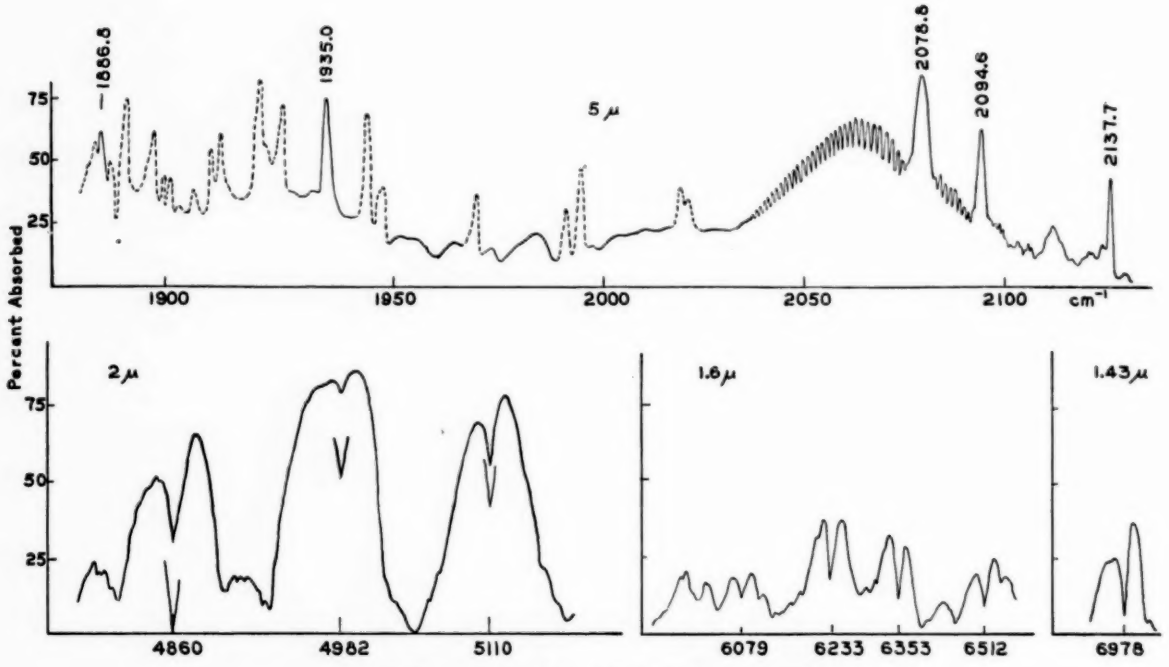

FIG. 2. Harmonic and combination bands of CO_2.

careful search was made for the three zero branches corresponding to ($5\nu_2$, $3\nu_2+\nu_1$, $\nu_2+2\nu_1$) but without success. Their computed positions are 3187, 3342 and 3510 cm^{-1}. They fall in a region of strong water vapor absorption but could have been observed if the maxima had been as great as 5 percent. Apparently a much longer cell would be required to find them.

THE BANDS AT 5μ

Absorption of ($3\nu_2$, $\nu_1+\nu_2$) by the normal molecule produces a pair of perpendicular bands shown in Fig. 2, with zero branches at 1935 cm^{-1} and 2078 cm^{-1}. A part of the rotation structure of the stronger band at 2078 cm^{-1} has been resolved, mostly in the negative branch which appears to be much more intense than the positive branch. For molecules already excited to the first vibration state the same transition defines three higher levels, namely 2554 and 2804 with $l=0$ and 2762 with $l=2$. These are indicated by the observed lines at 1886, 2137 and 2094 cm^{-1}. There are three other levels in group 4, one with $l=0$, one with $l=2$ and one with

$l=4$. The first two might have been expected here, the positions of the corresponding lines being 2008 and 1917 but apparently these transitions are too weak to be observed. In Fig. 2 the solid lines represent the only absorption attributable to CO_2. The other lines, which have not previously been measured, are probably due to water vapor.

The Bands at 2μ and 1.6μ

Transitions from the normal state to the three levels in group 4 having $l=0$ may be simultaneous with the change $0\rightarrow1$ in V_3, thus yielding three bands near 2μ, namely $\nu_3+(4\nu_2,\ 2\nu_2+\nu_1,\ 2\nu_1)$. They are analogous to the well-known pair $\nu_3+(2\nu_2,\ \nu_1)$ at 2.7μ. As indicated in the figure, the centers are observed at 4860, 4982 and 5110 cm^{-1}. Three weaker bands would also be expected corresponding to transitions from the first excited state but they cannot be located with confidence in the absorption pattern.

A similar set of transitions $\nu_3+(6\nu_2,\ 4\nu_2+\nu_1,\ 2\nu_2+2\nu_1,\ 3\nu_1)$ with $\Delta l=0$ gives rise to four bands near 1.6μ. These are shown at 6079, 6233, 6353 and 6512 cm^{-1}. The pattern is considerably complicated by irregular background and perhaps by weak bands arising from the first excited state.

The Band at 1.4μ

The position of the band $3\nu_3$ is of interest for the determination of x_{33}, which confirmed the identification of one of the Venus bands as $5\nu_3$. It is a doublet, the center being at 6978 cm^{-1}. This gives the large value -12.7 for x_{33}, indicating the strongly anharmonic character of the vibration ν_3.

The Structure of the Ultraviolet Absorption Spectrum of Formaldehyde. I

G. H. DIEKE[1] AND G. B. KISTIAKOWSKY,[2] *Communication No. 32 from the Alfred L. Loomis Laboratory in Tuxedo*

(Received October 18, 1933)

The ultraviolet absorption spectrum of formaldehyde was photographed under high dispersion so that the rotational structure could be analyzed. The present paper gives details of six bands at 3530, 3430, 3390, 3370, 3295 and 3260A. The bands are due to transitions in which the electric moment is in the plane of the molecule and perpendicular to the CO-axis. As the asymmetry of the molecule is very slight, the structure of the bands is very nearly the structure of vertical bands due to a symmetrical top. The position and intensity of the lines is in very good agreement with this except if the component K of the angular momentum along the CO-axis is smaller than four. In this case, the effect of the asymmetry makes itself felt in a shift and doubling of the lines in agreement with the theoretical expectations. A rigorous check of all the regularities is furnished by combination relations. The distortion of the molecule by the rotation can be studied in the deviations of the observed energy values from those of a rigid top. A value for the force between the two C−H bonds results from this. In the bands 3430 and 3295 there are strong perturbations which affect the dependence of the rotational energy on the quantum number K only, not that on the total angular momentum J. The molecular constants for the normal state of the molecule and six vibrational states of the excited electronic level can be obtained with good accuracy (see Table V and §10).

SOME time ago we reported on the analysis of the rotational structure of some ultraviolet absorption bands of formaldehyde.[3] Since then we photographed a number of additional bands under high dispersion and analyzed their structure. In the present paper the detailed results for six bands are given. Three of these, the bands at 3530, 3430 and 3390A were already described in the preliminary report, but the data on which the results were based were withheld then. They are given in full now, besides three more bands of the same structure at 3370, 3295 and 3260A. We hope to report on some more bands, some of them of different structure, in a subsequent paper and shall reserve also the discussion of the vibrational structure until then, as those bands are essential for its understanding.

§1. EXPERIMENTAL

All the bands discussed in this paper were photographed in the third order of the 40 ft. Tuxedo spectrograph[4] with a six-inch plane grating with 15,000 lines per inch. The Steinheil Uviol glass lens allowed one to photograph down to about 3200A. The light source for the continuous spectrum was a water-cooled quartz hydrogen tube described by one of us previously.[5] It took a current of about 1.5 amperes which was supplied by a 6500 volt transformer. The exposure times varied between two and ten hours. At the shorter wave-lengths the absorption of the uviol lens required a prolonged exposure. The whole spectrograph was thermostated, and the temperature fluctuations were of the order of 0.01°C.

In the earlier work a 30-cm long quartz absorption tube was used. At the high pressures which were necessary to obtain the fainter bands the formaldehyde polymerized rapidly, and it was difficult to keep the windows clean. Also, at the high pressures, the lines tend to broaden which has a detrimental influence on the resolution of the crowded parts of the bands. For that reason a two-meter long absorption tube was substituted. This tube was all quartz with two flat windows fused to the ends and could be heated electrically in order to study the absorption at higher temperatures. In order to avoid a deposit on the windows it was necessary in all

[1] The Johns Hopkins University.

[2] Harvard University.

[3] G. H. Dieke and G. B. Kistiakowsky, Proc. Nat. Acad. **18**, 367 (1932).

[4] A. L. Loomis and G. B. Kistiakowsky, J. Sci. Inst. **4**, 201 (1932).

[5] G. B. Kistiakowsky, Rev. Sci. Inst. **2**, 549 (1931).

cases to heat the windows separately to a slightly higher temperature than the rest of the tube.

Formaldehyde was obtained by heating commercial C.P.-grade paraformaldehyde. Early in the course of the work it was found that to obtain satisfactory photographs it was necessary to keep the formaldehyde pressure in the absorption tube very constant. This was accomplished by means of an automatic pressure regulating device. The solid paraformaldehyde was kept in a small glass vessel connected to the absorption tube and to a differential mercury manometer provided with electric contacts. On the other side of the differential manometer was a ballast flask and a closed-end manometer. The vessel with the paraformaldehyde was wound with Nicrome wire in series with a resistance and a relay operated through the contacts on the differential manometer. This latter had to be heated slightly (to 40–50°C) to prevent fouling of the contacts by the condensing paraformaldehyde. Air was admitted on one side of it to the desired pressure whereupon the formaldehyde pressure built up in the course of some 10–20 minutes and then stayed constant for prolonged time intervals, seldom varying by more than ± 1 mm.

At pressures above some 100 mm the condensation of paraformaldehyde was so rapid that the connecting tubes were rapidly clogged.

Here the regulation was accomplished by electric contacts on an open-end manometer and all the connecting lines as well as the manometer were electrically heated. We used pressures from a few mm to about 600 mm. Pressures above about 100 mm were, however, not of very much use, as the lines became too diffuse, and the resolution of the bands insufficient.

§2. Measurements

The plates which were obtained in this way have a dispersion of about 0.4A per mm. The absorption lines were measured under the comparator in the usual way against iron standards. As the number of lines was very large, in most cases the wave numbers of the lines were evaluated directly without the wave-lengths. Two plates, often more than two, were measured for every band. That was necessary, because on the low pressure plates the strong lines showed with very good definition and resolution, whereas on the high pressure plates, on which many fainter lines came out, the stronger lines, especially in the center of the bends, flowed together and could not be measured with any accuracy.[6] The centers of the bands are only partly resolved on all plates and the measurements there are at best very difficult. The agreement between the measurements of good lines on different plates was as a rule within a few hundreds of a wave number; for the congested regions the agreement was naturally less. Lines which are separated by less than 0.2 cm^{-1} could not be resolved. We believe that this is due to the character of the formaldehyde lines rather than to limitations of the spectrograph, as the full theoretical resolving power was obtained with other spectra.

§3. The Theoretical Structure of the Rotational Levels

The formaldehyde molecule must have a Y-shaped form (Fig. 1) and has therefore three different moments of inertia, i.e., it can be regarded in first approximation as an asymmetric top. The quantum-mechanical theory of the asymmetrical top has been given by Kramers

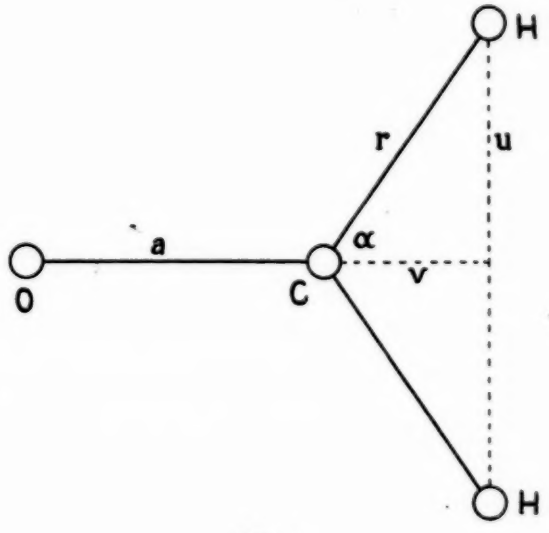

Fig. 1.

[6] In order to obtain the best results for a given region of a band it was essential that the pressure had a value deviating by not more than 50 percent from its optimum value. This means that a much larger number of plates had to be taken than were afterwards measured.

and Ittmann[7] and Wang.[8] All the rotational energy levels can be found from the general formulae given by these authors, but the process is somewhat laborious. Fortunately the asymmetry of the formaldehyde molecule is only very slight, and therefore most of the peculiarities of the absorption spectrum of formaldehyde can be understood from a consideration of the properties of the *symmetrical* top.

We shall therefore use the symmetrical top as starting point and investigate further on what changes are introduced when we take the asymmetry of the formaldehyde molecule into consideration. We call A, B, C the three principal moments of inertia of the molecule in the order of their size. A is then the moment about the axis perpendicular to the plane of the molecule, B about the axis in the plane perpendicular to the CO-axis, and C the moment of inertia about the CO-axis. We have

$$A=B+C \tag{1}$$

and, as C is very small on account of the small mass of the hydrogen atoms, A is very nearly equal to B. We consider now a symmetrical top with the moment of inertia C about the symmetry axis and the moment of inertia D about any axis perpendicular to it. D is connected with the moments of inertia A and B of our molecule by

$$1/D=\tfrac{1}{2}(1/A+1/B). \tag{2}$$

The rotational energy of this symmetrical top is[9]

$$W_0=\frac{h^2}{8\pi^2 D}J(J+1)+\frac{h^2}{8\pi^2}\left(\frac{1}{C}-\frac{1}{D}\right)K^2. \tag{3}$$

J is the total angular momentum, K its component along the axis of symmetry, both expressed in units $h/2\pi$.

If the deviations from the symmetrical top are small, this expression can be regarded as a good approximation, and the deviations from it can be calculated by the method of perturbations. This is what Wang did. The corrections can be expressed with the help of a parameter b which gives the degree of asymmetry.

$$b=[1/B-1/A]/[2(1/C-1/D)], \tag{4}$$

$b=0$ for the symmetrical top. If W is the energy of the asymmetrical top we can write

$$W=W_0+(h^2/8\pi^2)(1/C-1/D)x \tag{5}$$

and if $y=K^2+x$, y can be found immediately as the solution of the secular determinant characteristic of the perturbation problem. For every value of J there results an algebraic equation of degree $2J+1$ which splits up into four equations, three of degree $J/2$ and one of degree $J/2+1$ if J is even and three equations of degree $J/2+1$ and one of degree $J/2-1$, if J is odd. The coefficients of these equations contain the parameter b. The equations are given explicitly for $J\leq 8$ by Dennison[9] and for $J\leq 10$ by Nielsen.[10]

They are still rather inconvenient for numerical calculations and therefore we used the corresponding equations in x which have small quantities as solutions. They can be found for $J\leq 10$ from Nielsen's equations or directly from the secular determinants given by Wang. We found the latter course safer, as there are a few misprints in Nielsen's numbers. We used this method up to $J=15$ although for such high values of J the resulting equations became rather involved and an approximation method is better used.

There seems to be no need to reproduce here all the results of these calculations[11] especially in view of the fact that our hope to be able to use them to find an unambiguous assignment of quantum numbers also for the centers of the bands was not fulfilled.

A few general characteristics of the energy levels which can be obtained directly from the papers of Wang or Kramers and Ittmann are, however, useful for a discussion of the structure of the bands. For $b=0$, i.e., for the symmetrical

[7] H. A. Kramers and G. P. Ittmann, Zeits. f. Physik **53**, 553 (1929); **58**, 217 (1929); **60**, 663 (1930).

[8] S. C. Wang, Phys. Rev. **34**, 243 (1929).

[9] See D. M. Dennison, Rev. Mod. Phys. **3**, 280 (1931), where the literature is also given.

[10] H. Nielsen, Phys. Rev. **38**, 1432 (1931).

[11] In some of these calculations we were aided by Dr. J. W. Mauchly with the help of a special grant from The Johns Hopkins University for which we wish to express our appreciation.

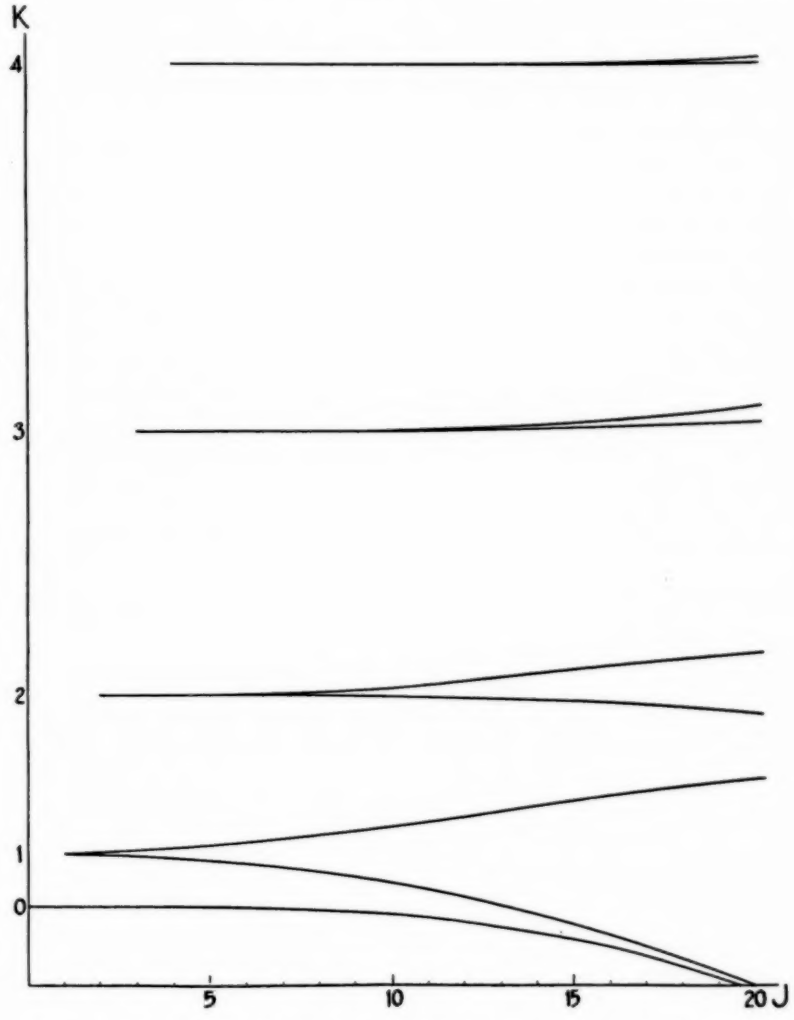

FIG. 2. The rotational energy of a slightly asymmetric top. (b about 0.01.) The term $h^2J(J+1)/8\pi^2D$ is subtracted. The deviations from the horizontal lines represent the deviations from the symmetrical top.

top there are $J+1$ different energy levels for each value of J, which are distinguished by different values of K, $(0 \leq K \leq J)$. As b gradually increases, all these energy levels split up into doublets except the ones with $K=0$. This splitting up is closely analogous to the Λ-doubling in the rotational energy levels of diatomic molecules. The doublet separation is negligible for large values of K and moderate values of J. Energy levels of this type are not appreciably affected by the small asymmetry of the molecule. That this must be the case can be seen easily from a classical model. If the rotation about the CO-axis is much faster than the precession about the invariable axis, only an average of the two large principal moments of inertia is of importance for the motion of the top. Therefore if

$$J/D \ll (1/C - 1/D)K$$

the asymmetrical top has acquired the properties of a symmetrical one.

For small values of K (for $K \leq 3$ for the degree of asymmetry found in the formaldehyde molecule) the deviations from the values for the symmetric top become appreciable. There is not only the doubling, but also the center of gravity of the doublet is shifted. The behavior of these levels is illustrated for $K \leq 4$ in Fig. 2.

§4. Selection Rules and Intensities

In order to find the appearance of a band it is not only necessary to know the rotational energy levels of the upper and lower electronic states, but we need also the selection rules and the expressions for the intensities of the lines. For our purpose it is first entirely sufficient to make use of the selection and intensity rules of the symmetrical top, as the deviations which are treated in §6 are only small for a very small degree of asymmetry.

There are two different cases to be considered for which the selection rules are different.

(A) The electric moment is perpendicular to the axis of symmetry. In this case we can have *pP*-, *pQ*-, *pR*-, *rP*-, *rQ*-, and *rR*-branches.[12]

(B) If the electric moment is parallel to the axis of symmetry *qP*-, *qQ*-, and *qR*-branches occur.

There are bands of both types in the ultraviolet absorption spectrum of formaldehyde, but as the bands given in this paper are all of type A, we need only consider this case here.

As the moment of inertia about the CO-axis is so much smaller than the other two principal moments of inertia, the factor of K^2 in (3) is much larger than the factor of $J(J+1)$, and a consequence of this is that a change of K by one results in a much larger energy change than a corresponding change in J. This means that all the lines belonging to a given $K' \rightarrow K''$ transition but different values of J lie much closer together than lines which have different values of K. Therefore the whole band can be divided up into a number of sub-bands each of which corresponds to a fixed K-transition and has a *P*-, *Q*- and *R*-branch. Each of these sub-bands is therefore closely analogous to a band of a diatomic molecule. The $K=1\rightarrow K=0$ sub-band, e.g., is in every respect analogous to a $^1\Pi \rightarrow {}^1\Sigma$ band of a diatomic molecule. The number of missing lines near the origin of each sub-band is determined by the condition $K \leq J$. For example, the $K=1\rightarrow K=0$ sub-band has one missing line in the *P*-branch and one in the *Q*-branch, the band $2\rightarrow 1$ two in the *P*-branch, two in the *Q*-branch and one in the *R*-branch, etc. If, therefore, the *K*-values are increased by one, that means that there is one more missing line in every branch for the corresponding sub-band.

The relative intensities of the individual lines in an absorption band are given by

$$J = P_{K'',\ J''}^{K',\ J'}\, e^{-W''/kT}, \tag{6}$$

in which W'' is the energy in the lower electronic states, and $P_{K'',\ J''}^{K',\ J'}$ factors in which the transition probabilities and weights *a priori* are contained. These intensity factors are for the different branches occurring in a vertical band.

$$\left.\begin{matrix} rR(K-1,\ J-1) \\ pP(K,\ J) \end{matrix}\right\} \frac{A(J+K-1)(J+K)}{8J},$$

$$\left.\begin{matrix} pQ(K,\ J) \\ rQ(K-1,\ J) \end{matrix}\right\} \frac{A(2J+1)(J-K+1)(J+K)}{8J(J+1)}, \tag{7}$$

$$\left.\begin{matrix} pR(K,\ J-1) \\ rP(K-1,\ J) \end{matrix}\right\} \frac{A(J-K+1)(J-K)}{(J+K)(J+K-1)},$$

If the constants of the molecule are known, so that the energy levels can be calculated, these expressions allow one to find the relative intensities of all lines in a given band. The formulae for the intensity factors show that the different branches have very unequal strengths. For not too small values of K only those branches are strong for which K and J change in the same direction, i.e., the *pP*- and *rR*-branches. The *Q*-branches though very strong for small values of K are much weaker for higher K's and the *pR*- and *rP*-branches are so weak that they are

[12] For the designation of the branches the following nomenclature which is an extension of that for the diatomic molecules is simple and useful. The change in J is designated, as for diatomic molecules, so that if $\Delta J=-1$, 0, or $+1$ we have *P*-, *Q*-, and *R*-branches. The corresponding *K*-transitions are given by the equivalent small letters. A *pQ*-branch, e.g., is a branch for which $\Delta K=-1$ and $\Delta J=0$. If it is desired to label a definite line, the quantum numbers of the lower state are given between brackets. *pQ*(*K*, *J*) means a line for which $K-1\rightarrow K$ and $J\rightarrow J$. In this paper all the transitions are written as if they occurred in *emission*. This nomenclature is very convenient for symmetrical or slightly asymmetrical molecules. In the latter case the two doublet components can be distinguished by subscripts. If the asymmetry is considerable, this nomenclature is still possible, and may in certain cases be preferable, as *K* always can be used to label the levels, even if it has lost its significance as component of the angular momentum along the symmetry axis.

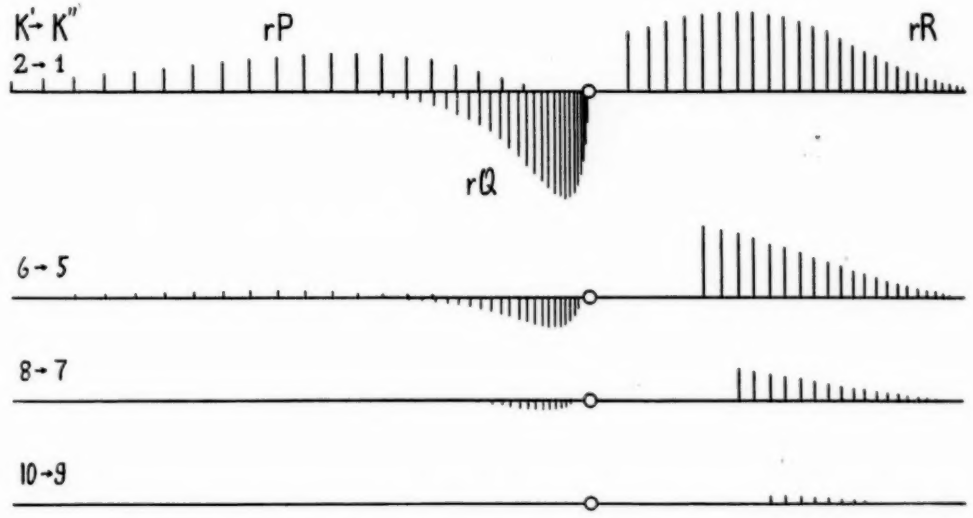

FIG. 3. The intensity distribution in a few typical sub-bands at room temperature. The spacing and convergence of the lines is chosen arbitrarily.

completely absent except for the lowest K-values. Fig. 3 gives an idea of the expected intensities for some characteristic values of K.

§5. Alternating Intensities

The formaldehyde molecule is symmetric with respect to a rotation of 180° about the CO-axis. It behaves in this respect exactly as an H_2-molecule. On account of the nuclear spin 1/2 in the hydrogen molecule successive rotational levels have alternately weights one and three, which results in the well-known alternating intensities in the molecular spectrum of hydrogen. In the formaldehyde molecule the same state of affairs must exist with respect to rotations about the CO-axis. As these rotations are characterized by the quantum number K, successive K-transitions will be alternately strong and weak and the intensities must correspond to a ratio three to one in the weights of the respective energy levels. Further on it will be shown that this is exactly what is observed in the absorption bands.

§6. Deviations from the Symmetric Top

The statements of the preceding paragraphs are strictly true only if the molecule is symmetric. There will be only slight changes in this picture if the asymmetry is only small. In the first place there will be a doubling of the lines. We have seen in §3 that a slight asymmetry results in a doubling of the energy levels and that this doubling is analogous to the Λ-doubling of diatomic molecules. The same kind of selection rules must hold here (see below) which means that only two of the possible four combinations are allowed, i.e., that all the lines (except those which involve levels with $K=0$) must be double. This doubling decreases rapidly with increasing K but increases roughly with the $2K$th power of J. For small values of K we have to expect besides a shift of the whole doublet from its position for the symmetric top.

The selection rules for the asymmetrical top can be derived from the symmetry properties of the rotational wave functions. The results can be expressed in a very simple way with the help of the quantum numbers K and J.

We have to consider two transformations. The first is an inversion at the C-axis, the axis of the smallest moment of inertia, the second a reflection at a plane perpendicular to this axis. The rotational wave functions can be either symmetric or antisymmetric to these transformations. If, as is customary, we designate by a $+$ that the wave function is symmetric and by a $-$ that it is antisymmetric, the symmetry properties of every state can be described by a pair of

TABLE I. *The bands at 3530, 3390, 3260, 3370, 3430 and 3295A.*

An * with a wave number means that the line has been used more than once. It is liable to be less accurate for this reason. The absence of an * does not mean that the line is necessarily single, as it may be confused with an unclassified line.
A wave number between [ ] means that a weak line should fall very close to a strong line of different origin, so that it cannot be separated from it. In this case the wave-lengtn is entirely unreliable.
The intensities (numbers between ( )) are rough estimates only. Their values for different bands cannot be compared. The meaning of the letters attached to the intensity figures is

b line broad.
c line very close to another line and not completely resolved from it.
d line diffuse.
h only found on the high temperature plates.
r degraded toward longer wave-lengths.
v degraded toward shorter wave-lengths.

Band at 3530A.

J''	$K''=3$		4	5	6	7	8	9	10	11	12	13
						pP-Branches						
3	282 61.44*(3)											
			28200+									
4	58.12 (1)		39.24 (1b)									
				28200+								
5	54.54 (2)		35.73 (1)	15.90 (3)								
					28100+							
6	50.70 (3)		31.87 (1)	12.03 (2)	91.33 (1)							
						28100+						
7	46.43 (2d)		27.57 (1)	07.87 (2)	87.15 (2c)	65.59 (3d)						
8	41.93 (2d)		23.16 (2)	03.35 (2)	[82.52] (2b)	61.07 (2)						
				28100+				28100+				
9	37.32 (0)	37.07 (0d)	18.33 (0)	98.60 (2)	—	56.35 (2c)		10.61 (0)				
10	32.35 (1)	31.87 (1)	13.29 (0)	93.53 (2d)	—	51.24 (1)		05.52 (0)				
										28000+		
11	27.08 (0)	26.51 (2b)	[07.87] (2)	88.16 (2)	67.46 (0)	45.88 (2)		00.13*(1)		51.35*(0bh)		
								28000+				
12	21.62 (2)	20.65 (1)	02.26 (0d)	82.55*(2b)	—	40.25 (1)		94.44 (0)		45.54 (0h)		
13	15.90*(3)	14.45 (1)		76.56 (2)	55.85 (0)	34.30 (1)		88.57 (0)		39.64 (0ch)		
14	09.87 (1)	07.87*(2c)		70.32 (2)	[49.72] (2)	28.03 (1)		82.31 (0)		33.42 (0h)		
15	03.63 (1)	01.20 (0)		63.74 (2)	—	21.56 (0)		75.80 (0ch)		26.81 (0h)		
		28100+										
16	97.16 (1d)	93.99 (1d)		56.90 (2)	36.32 (0)	14.63 (0)		68.94 (1h)		19.94 (0bh)		
							28000+					
17	90.38 (0)	86.33 (1c)		49.72 (2)		07.54*(0c)	85.00 (0h)	61.75*(2h)				
18				42.31 (1)		00.13*(1)	77.63 (0h)	54.34 (0bh)				
						28000+						
19				34.58 (1)		92.27 (0h)	69.84 (0bh)	46.59 (0h)				
20				26.51 (1)		84.29 (0h)	61.75*(2h)	38.61 (0h)				
21				18.20 (0)		75.98 (0ch)		30.21 (0h)				
22				09.52 (0)		67.35 (0ch)		21.56 (0ch)				
23				00.57 (0)		58.41 (1h)						
				28000+								
24				91.31 (0)		49.18 (0h)						
25				81.78 (0h)		39.64 (1ch)						
26				72.06 (0bc)		29.79 (0h)						
27				61.75*(2h)		19.52 (0h)						
28				51.35 (0bh)								

+ and − signs, the first referring to the first and the second to the second of the transformations mentioned above. For a given K and J we have two levels, and if we designate the upper one by D_1 and the lower one by D_2 the following scheme gives all the necessary information

$K+J$	even	even	odd	odd
K	even	odd	even	odd
D_1	++	+−	−+	−−
D_2	−+	−−	++	+−

For $K=0$ there is only D_1.

The selection rules are different according to whether the matrix component of the electric moment belonging to the transition in question has a component along the A-, B-, or C-axis. The selection rules are

Electric moment along	*first sign*	*second sign*
A	unchanged	changes
B	changes	changes
C	unchanged	unchanged

The connection between the possible branches and the values of K and $J+K$ is

Branch	$\Delta(K+J)$	ΔK
pP, rR	±2	±1
pR, rP	0	±1
pQ, rQ	±1	±1
qP, qR	±1	0
qQ	0	0

The combination of the last three schemes gives

TABLE I. (*Continued.*) *Band at 3530A.*

J''	$K''=3$	4	5	6	7	8	9	10	11	12	13
					pQ-Branches						
3	282 67.80 (1d)										
		28200+									
4	66.64 (3c)	47.84 (0d)									
			28200+								
5	65.23 (2)	[46.43] (3)	26.83 (0)								
6	63.48 (2)	—	24.85 (1)								
7	61.44*(3)	42.56 (0)	22.79 (1)								
8	59.21 (0) 58.95 (0)	40.04 (2c)	20.45 (1)								
					28100+						
9	56.73 (3) 56.27 (2)	37.59 (0)	17.82 (1)		75.45 (0c)						
10	53.81 (1) 53.28 (1)	34.64 (0)	14.87 (1)		—						
11	50.70*(3) 49.97 (1)	31.39 (2)	11.69 (2)		69.21*(1d)						
12	47.38 (1) 46.43*(3)		08.07 (2c)		—						
13	43.73 (2) 42.35 (1)		04.27 (2c)		—						
14	39.91 (2c) 38.07 (0)		00.22 (1)		57.91 (1)						
			28100+				28100+				
15	35.73 (1) 33.43 (1r)		95.75 (1)		53.39 (0)		07.54*(0c)				
16	31.39*(2) 28.47 (1)		91.03 (1d)		48.83 (1b)		02.95 (0)				
17			86.06 (1c)		43.73 (0)						
							28100+				
18			80.72 (1)		—		92.76 (0h)				
19			75.12 (1c)		32.76 (0)						
20			69.21 (1d)		26.87 (0)						
21			63.01 (0)								
					rQ-Branches						
4	283 58.73 (2)										
		28300+									
5	57.22*(3b)	[68.88] (3)									
			28300+								
6	55.48*(2d)	67.19 (0)	78.01*(2)								
7	53.40 (1)	65.17 (0)	75.82*(2d)	—							
8	51.07*(3d)	62.84 (0)	73.49 (1)	—	—						
9	48.42*(2)	60.16*(2)	70.84 (0)								
				28300+	28300+						
10	45.39 (2c)	[57.22] (3b)	[67.77] (4)	77.46 (0h)	86.10 (0)						
							28300+				
11	42.13 (3)	53.83 (1d)	64.61*(2c)	74.22*(1)	82.79 (0c)		96.85 (0h)				
12	38.51* (4)	50.28 (0)	61.02 (2)		79.20 (1c)		93.34 (0h)				
13	34.57 (2b)	[46.49] (2c)	57.22*(3b)		75.32 (1)		—				
14	30.56 (2b) 30.22 (1)		52.98*(1)		71.20 (0)		85.27 (0h)				
15	26.00 (1) 25.64 (1)		48.42*(2)		66.70 (0h)		[80.63] (1b)				
16	21.24 (2) 20.67 (0)		43.68 (2)		61.92 (0)		[75.82] (2d)				
17	16.10 (1) 15.34 (3c)		38.51*(4)								
18	10.71 (2c) 09.69 (0c)										
					rR-Branches						
3	283 68.46 (3)										
		28300+									
4	69.40 (3)	81.15 (1)									
			28300+								
5	70.09*(3c)	81.88*(2)	92.54*(3)								
				28400+							
6	70.49*(3c)	82.20*(2)	92.87*(3)	02.51*(2)							
					28400+						
7	70.49*(3c)	82.20*(2)	92.87*(3)	02.51*(2)	11.14 (2)						
						28400+					
8	70.25 (3c)	81.88*(2)	92.54*(3)	02.31 (1)	10.93 (2)	18.41 (0)					
							28400+				
9	69.72 (3)	81.49 (1)	92.13*(3)	01.75 (1)	10.35 (2)	17.89 (0)	24.43 (1)				
								28400+			
10	68.88 (3)	80.63 (1b)	91.31 (3)	00.92 (1c)	09.49 (2)	17.04*(1)	23.56 (1)	29.02*(1h)			
				28300+					28400+		
11	67.77 (4)	79.49 (1)	90.16 (3)	99.74 (1)	08.35 (2)	15.90 (0)	22.37 (1)	27.90 (0h)	32.37 (0h)		
										28400+	
12	66.24*(3)	78.01*(2)	88.71 (3)	98.33 (1)	06.88 (2)	14.38 (0)	20.88 (1)	26.36 (0bh)	30.80 (0h)	34.40 (0h)	
											28400+
13	64.61*(2c) 64.39 (2c)	76.30 (1)	86.99 (2)	96.62 (0)	05.12 (1)	12.68 (0)	19.11 (0)	[24.43] (1)	29.02*(1h)		34.98 (0h)
14	62.54 (1) 62.24 (1)	74.22 (1)	84.94 (2)	94.52 (0)	03.07 (1)	10.57 (0h)	17.04*(1)	[22.37] (1)	26.92 (0h)		32.84 (0h)
15	60.16 (1) 59.73 (1)	71.88 (1)	82.57 (1)	92.13*(3)	00.72 (1c)	08.35*(2)	14.71 (0)		[24.43] (1)		30.42 (0h)
					28300+						
16	57.54 (2) 56.89 (0)		79.94 (1)	89.50 (0)	98.09 (1)	05.65*(0h)	11.98 (0d)		21.80 (0h)		27.64 (0h)
17	54.46*(1d) 53.83 (1d)		76.96 (2)	—	95.09 (0)		09.05 (0h)		18.77 (0h)		
18			73.68 (1)	83.21 (0)	91.77 (0)		05.65 (1bh)		15.44 (0h)		
19			70.09*(3)		88.23 (0)		02.13 (0h)				
20			66.24*(3)		84.36 (0)						
21			61.90 (10)		80.12 (0h)						
22			57.54*(2c)		75.82*(2d)						
23					70.84*(0)						

TABLE I. (*Continued.*) *Band at 3390A.*

J''	$K''=3$	4	5	6	7	8	9	10	11
				pP-Branches					
3	294 43.82 (2c)								
4	40.45 (2)	29400+ 21.36 (0)							
5	36.74 (2)	17.67 (1)	29300+ 97.57 (2)						
6	32.71 (2)	13.66*(3)	93.58 (2)	29300+ 72.48 (0)					
7	28.37 (2)	—	89.24 (2)	68.18 (0)	29300+ 46.19*(2)				
8	23.79 (1c) 23.64 (1c)	04.66 (0)	84.62 (2)	63.58 (0)	41.53 (1)	29300+ 18.59 (0)			
9	18.92 (1e) 18.71*(1e)	29300+ 99.84*(3r)	79.71*(2e)	58.68*(1c)	36.57*(2)	13.60*(2)	29200+ 89.89 (1)		
10	13.66*(3) 13.19 (0)	94.46 (0)	74.34 (2e)	53.28 (0)	31.29 (1)	08.37 (1)	84.66 (1)	29200+ 59.97 (0)	
11	08.25*(2) [a]	—	68.77 (1)	47.70 (1)	25.74 (1)	02.77 (0d)	79.04 (1)	54.54*(0d)	29200+ 29.14 (0d)
12	02.46*(1e) 01.53 (0e)	82.99 (1)	62.88 (1)	41.84 (0)	19.80 (1)	29200+ 96.91 (0d)	73.12 (2d)	48.58 (0)	23.21 (0e)
13	96.45 (1) 95.11 (0)	76.72 (0)	56.64 (1)	35.54 (1)	13.60*(2)	90.60 (0d)	66.91*(1)	42.32 (0)	16.99 (0e)
14	90.10 (0) 88.27*(1d)	70.15 (0)	50.11 (1)	29.05 (0)	07.05 (1)	84.08 (0)	60.41 (1)	35.70 (0)	10.48*(0e)
15	83.56 (0) 81.17 (0)	63.33 (1e) 63.13*(1e)	43.27 (1)	22.13 (2)	00.17 (1)	77.23 (0)	53.56 (0)		03.57 (0)
16	76.72*(1) 73.66 (0)	57.06 (0d) 55.57*(1)	36.06 (1)	—	29200+ 93.02 (1)	70.00 (0)	46.38*(1)		
17	69.81*(1r) 65.64 (1)	48.42 (1) 47.70 (0)	28.52 (1)	07.48 (0)	85.48 (2c)	62.50 (0)	38.87 (0)		
18	62.83 (0) 57.27 (0)		20.69 (1)	—	77.69 (1)	54.54 (0)	31.08 (0)		
19			12.54 (1)	29200+ 91.50 (0d)	69.52 (1)	46.38*(1)	22.85*(1)		
20			03.99 (1e)	83.08 (0)	61.09 (1)	38.15 (0d)	14.48 (0)		
21	[a] Emission line superimposed		29200+ 95.26 (1)	74.23 (0e)	52.30 (1)		05.73 (0e)		
22			86.13 (1)	65.14 (0)	43.14 (0e)				
23			76.66 (1)		33.70 (0)				
24			66.91*(1)		24.07 (1e)				
25			56.70 (0)		13.91 (0)				
				pQ-Branches					
3	29400+ 50.13 (2c)								
4	48.84 (2)	—							
5	37.34 (4v)	—	29400+ 08.25*(2)						
6	45.41 (1)	29400+ 26.14 (2)	06.24 (0)	29300+ 85.03 (0)					
7	43.25 (1d) 43.10 (0)	24.04 (1)	04.09*(1d)	82.99*(1)	—				
8	40.80 (1) 40.45*(2)	21.61 (0)	01.53 (1)	80.43 (0)	29300+ 58.50 (1c)	—			
9	38.02 (1) 37.66 (1e)	18.71*(1e)	29300+ 98.68 (1)	—	55.57 (1)	29300+ 32.60 (1)			
10	34.98 (1) 34.46 (1)	15.62 (0)	95.48*(1)	74.55 (1e)	52.39 (1)	29.38 (0)	—		
11	31.61 (1) 30.89 (1)	12.15 (0)	92.02 (1)	—	48.88 (1)	—	29300+ 02.17 (0d)		
12	27.96 (1) 26.95 (1)	08.25*(2)	88.27*(1d)	67.13 (1d)	45.13 (1)	22.13*(2)	29200+ 98.41 (0d)		
13	24.04 (1) 22.71 (0e)	04.09*(1d)	84.10 (1)	63.13 (1e)	40.97 (1)	—	—		
14	19.81 (1) 18.09 (1)		79.71*(2e)	58.68*(1dc)	36.57*(2)	13.60*(2)	89.89*(1)		
15	15.29 (0) 13.19*(0d)[a]		74.79 (1)	53.82 (0)	31.78 (1)		85.18 (1e)		
16	10.80 (0) 08.25*(0)		69.81 (1r)		26.75 (1)		80.07 (1v)		
17	06.24*(0) 03.22 (0)		64.42 (1)		21.33 (1)		74.60 (1dc)		
18			58.68*(1e)		15.64 (1d)		68.96 (0e)		
19	[a] close to Emission line.		52.64 (1)		09.61 (2)		62.95 (0)		
20			46.19*(2)		03.24 (1)		56.70 (1b)		
21			39.62*(1)		96.50 (0d)				
22					89.53 (0)				
23					82.23 (0)				
24					74.60 (1dc)				

the following selection rules:

Electric moment along	*A*	*B*	*C*
pP, rR, pR, rP	$D_1 \rightarrow D_1$, $D_2 \rightarrow D_2$	$D_1 \leftrightarrow D_2$	absent
pQ, rQ	$D_1 \leftrightarrow D_2$	$D_1 \rightarrow D_1$, $D_2 \rightarrow D_2$	absent
qP, qR	absent	absent	$D_1 \leftrightarrow D_2$
qQ	absent	absent	$D_1 \rightarrow D_1$, $D_2 \rightarrow D_2$

The selection rules for the symmetrical top given in §4 are a special case of the rules given here. The two first cases which interest us here differ in that there is crossing over in the Q-branches if the electric moment is along the greatest moment of inertia, and in the P- and R-branches if it is along the middle moment of inertia. (Figs. 4 and 5.)

TABLE I. (*Continued.*) *Band at 3390A.*

J''	$K''=0$	4	5	6	7	8	9	10	11
				rQ-Branches					
3									
4	29500+ 40.36 (2)								
5	38.94*(3d)	29500+ 50.13 (2c)							
6	36.89 (1)	48.25 (0)	29500+ 58.52 (2)						
7	34.68 (2)	46.06*(0)	56.32 (1d)	29500+ 65.47 (1c)					
8	32.10 (2)	—	53.78 (0)	62.86*(2)	29500+ [70.90] (3)				
9	29.22 (2)	40.63 (0)	50.99*(3c)	60.00 (1)	68 19 (1)	—			
10	26.00*(2)	37.45 (1c)	47.77*(4)	56.85 (0)	64.97 (2)	—	—		
11	22.47 (2c)	33.87 (0)	44.13 (3c)		61.46 (2c)	29500+ 68.56 (0)	—		
12	18.30 (3)	30.04 (0)	40.36*(2)		57.54*(2)	64.64 (0)	29500+ 70.69 (c)		
13	14.40 (2)	26.00*(2)	—			[60.50] (2c)	66.41 (0)		
14	10.02 (1) 09.67 (1)	21.37 (2)	31.70 (1)				[61.71] (2c)		
15	05.13 (1) 04.73*(2)		26.75 (2)				57.20 (0)		
16	00.01 (2c) 99.45*(1d)		21.77 (0)				—		
17	94.51 (0) 93.76 (2)		16.26 (1c)				46.46 (0)		
18	88.73 (0) 87.65 (0)		10.49 (0)				40.63 (0)		
19			04.32 (1)						
20			29400+ 97.82 (0)						
21			90.96 (1)						
22			83.95 (0)						
				rR-Branches					
3	29500+ 50.13 (2c)								
4	50.99*(3c)	29500+ 62.29 (2c)							
5	51.57*(4)	62.86 (2)	29500+ 73.19 (3c)						
6	51.57*(4)	63.06*(2)	73.33*(4c)	29500+ 82.40*(2)					
7	51.57*(4)	63.06*(2)	73.33*(4c)	82.40*(2)	29500+ 90.46 (2)				
8	51.11 (3c)	62.48 (2c)	72.73 (3c)	81.84 (2)	90.00*(2)	29500+ 97.06 (1)			
9	50.35 (3c)	61.71 (2c)	71.98 (2b)	81.10 (2)	89.24 (3)	96.30 (1)	29600+ 02.33 (2v)		
10	49.26 (2)	60.68 (2c)	70.90 (3c)	80.01 (2)	88.16 (3)	95.16 (1)	01.22 (2)	29600+ 06.22 (0c)	
11	47.77*(4)	59.29 (2c)	69.52 (3b)	78.54 (2)	86.77 (3)	93.75 (1c)	29500+ 99.78 (2)	04.78*(1c)	29600+ 08.78 (0)
12	46.06 (2)	57.54*(2)	67.74 (3)	76.85 (2c)	85.00 (3r)	92.06 (1r)	98.01 (2)	02.96 (1)	07.02 (0c)
13	44.13*(3) 43.91 (1)	55.39 (2c)	65.68 (3c)	74.82*(3)	82.95 (2)	90.00*(2)	95.90 (2r)	—	04.78*(1c)
14	— 41.37 (1)	52.96 (0)	63.30 (2)	72.38 (1)	80.60 (2)	87.49 (0c)	93.56 (1c)	98.45 (0)	[02.33] (2v)
15	38.94*(3d) 38.49 (1d)		60.50 (2c)	69.52*(3b)	77.89 (2)	[85.00] (3r)	90.80 (1)	[95.90] (2r)	[99.78] (2)
16	— —		57.54*(2)	66.60 (2)	74.82*(3)		87.71 (0c)		
17	32.62 (0) 31.70 (0)		54.19 (0d)		71.47 (1)		84.39 (0)		
18			—		67.74*(3)		[80.60] (2)		
19			46.46 (0)		63.80 (2c)		76.59 (2c)		
20			—		59.51 (2c)		[72.38] (1)		
21			37.29 (1c)						

These selection rules are, of course, the same as those given by Kramers and Ittmann or Dennison. They are, however, in a form much more convenient for our purpose. Even if the asymmetry is larger so that the symmetrical top is no more a good approximation, the quantum number K can be used for the classification of the levels, and this may often be found convenient. In that case it cannot be interpreted, however, as the angular momentum about the symmetry axis.

It needs hardly mentioning that all these considerations, even if the deviations due to the asymmetry are strictly taken into account, lead only to approximative results for an actual molecule. The results are true only to such an extent as the molecule can be regarded as a rigid top. Especially for higher values of the rotational quantum numbers deformations will take place, which are of an analogous though more complicated nature, as those observed for diatomic molecules. The effect of such deformations can be detected in the formaldehyde bands, but it is in general very small compared with the total rotational energy.

TABLE I. (*Continued.*) *Band at 3260A.*

J''	$K''=3$	4	5	6	7	$K''=3$	4	5	6	7
	pP-Branches					*rQ-Branches*				
3	306 07.07 (1c)									
		30500+								
4	03.64 (2)	84.40 (0)				307 03.10 (0)				
			30500+							
5	305 99.79 (2c)	80.57 (0)	60.21 (1)			01.28 (0)				
				30500+				30700+		
6	95.75 (2)	76.53 (1)	56.13 (1)	34.67 (0)		306 99.32 (1)		20.15*(0)		
					30500+					
7	91.27 (2)	72.01 (0)	51.62 (2)	[30.46] (1b)	07.86 (1)	96.91 (1)		17.79 (0)		
										30700+
8	86.53 (2b)	67.25 (1)	46.85 (2c)	—	03.04 (1)	94.16 (1c)		15.22 (0c)		31.52 (0c)
					30400+					
9	81.52 (0c) 81.21 (0c)	62.17 (1)	41.77 (2)	20.31 (0r)	97.94 (1)	91.12 (1c)		12.01*(2)		28.52 (0)
10	76.01 (1) 75.63 (1c)	56.60*(1)	36.30 (1)	14.94 (0d)	92.49 (1)	87.66 (1)		08.56 (0)		24.94*(1)
11	70.38 (1) 69.79 (1)	50.82 (1)	30.46 (1b)	—	86.69 (1)	83.92 (1)		04.96 (0c)		21.13*(0)
12	64.39 (0) 63.55*(1)	44.63*(1c)	24.35 (2b)	03.04*(1)	80.58 (0)	79.74 (1c)		00.82 (0)		
				30400+						
13	57.98 (0) 56.60*(1)	38.12 (1)	17.87 (1)	96.44*(1c)	74.02 (1)	75.43 (1c) 75.13 (1c)				
14	51.37 (0) 43.49 (0)		10.97 (1)		—	70.58 (0b) 70.25 (0)				
15	44.63 (1) 42.23 (1)		03.77 (0b)		60.07 (0)	65.44 (1) 64.98 (1)				
			30400+							
16	37.40 (1) 34.67 (0)		96.23 (1c)			59.81 (2c) 59.26 (1c)				
17			88.45 (1d)							
	pQ-Branches					*rR-Branches*				
3	306 13.35 (0)					307 12.98*(2)				
		30500+					30700+			
4	12.03 (1)	92.80*(1)				13.52*(3c)	24.62*(1d)			
			30500+					30700+		
5	10.36 (2c)	91.27*(2)	70.77 (1)			13.90*(3c)	24.94*(1r)	34.81*(2c)		
6	08.29 (0)	89.01 (1)	68.65 (1)			13.90*(3c)	24.94*(1r)	34.81*(2c)		
				30500+						30700+
7	06.07 (1c) 05.92 (1c)	[86.53] (2b)	66.31 (1)	44.99*(2)		13.52*(3c)	24.62*(1d)	34.50 (1e)		50.94 (0)
					30500+					
8	03.40 (0c) 03.16 (1c)	84.00*(1d)	63.55 (2)	42.23*(1)	19.75 (0)	12.98*(2)	24.10 (0)	33.90 (1)		50.27 (0)
9	00.46 (1c) 00.07 (1c)	80.81*(1b)	60.59 (1)	39.19 (0)	16.73 (0)	12.01 (2)	23.06 (1c)	32.96 (1)		49.18 (0)
10	97.03 (1) 96.60 (1)	77.61 (2)	57.17 (1)	35.93 (0)	13.32 (0)	10.69 (1)	21.77 (0)	31.63 (1e)		47.80 (0)
11	93.41 (2) 92.80 (1)		53.53 (0)		09.68 (0)	09.00 (1)	20.15*(0)	29.95 (1)		46.15 (0)
12	89.49 (1) 88.65 (0)		49.49 (0)		05.58 (0)	06.95 (1)	18.13 (0)	27.90 (1)		44.06 (0)
13	85.29 (2) 84.00*(1d)		44.99*(2)		01.19 (0)	01.80 (1d) 01.54 (1)		25.62 (1)		41.60 (0)
					30400+	30600+				
14	80.81 (1b) 79.16 (0)		40.28 (1)		96.44 (1c)	98.83 (1b) 98.36 (0)		22.83 (1e)		38.72 (0)
15	76.01*(1) 74.29 (1)		35.11 (1)		91.40 (0)	95.67 (0) 94.90 (0)		19.75*(0c)		
16			29.71 (1)					16.37 (0)		
17								[12.72] (2c)		

§7. OBSERVED STRUCTURE

All the absorption bands under consideration have the following features in common. In the center of the bands the absorption is strongest, but the lines are so close together that this region is only partly resolved and there are no obvious regularities. On the violet end there is a number of regular progressions of lines (called further on the violet branches) each of which comes to a head toward the shorter wave-length side. The heads themselves form also a regular sequence. It can be observed that in this sequence of violet branches subsequent members are alternately strong and weak. The intensity of the branches diminishes gradually toward the outside of the band. Furthermore it is at once apparent that the outermost branches have fewer lines than those nearer to the center, and a closer inspection reveals that as one goes from the center of the band toward its violet side every subsequent progression has one line less near its head than the preceding one.

On the red side of the bands some regular progressions are also apparent (called in this paper the red branches). The spacing of the lines in these red branches is much wider than in the violet branches and they do not form heads. Also there is no such *apparent* connection between the different red branches as was found between the violet ones.

These are the empirical facts which can be deduced from the plates even without a measurement of the lines. An inspection of the frequencies of the lines shows that the lines in the branches satisfy Deslandres' law very closely and that in most bands also the corresponding lines of the violet branches satisfy a quadratic

TABLE I. (*Continued.*) *Band at 3370A.*[a]

J″	K″=3	4	5	6	7	8	9	11
				rQ-Branches				
4	296 82.88 (0)							
5	81.43 (2)							
			29700+					
6	79.60 (2)		[04.92] (2)					
		29600+						
7	77.56 (2)	90.59 (0)	02.92 (1)					
					29700+			
8	75.17 (2c)	88.21 (1c)	00.53*(2)		22.85 (0)			
			29600+					
9	72.46 (2b)	—	97.79*(2b)		—			
10	69.46 (2c)	82.54 (0)	94.99 (1c)		17.15*(3)			
11	66.16 (2c)	79.26 (0)	91.55 (2c)		13.88*(3)			
12	62.57 (3)58	75.75 (0)	88.00 (2c)		10.29 (0)			
13	58.64 (1)	71.76 (1c)	84.11*(2)		06.44*(1)			
14	54.50 (1c) 54.30 (2c)	67.56 (0c)	79.89 (1)		02.21 (1d)			
15	50.03 (2b) 49.56 (2b)	63.13 (0)	75.44 (1c)		97.79*(2b)			
16	45.18 (2) 44.65 (1)		70.62 (1)		92.59*(2)			
17	40.12 (1) 39.29 (1)		65.48 (1r)		87.82 (1)			
18			60.06 (1)		82.34 (0)			
				rR-Branches				
3	296 92.59 (2)							
		29700+						
4	93.50 (2c)	06.77*(2c)						
			29700+					
5	94.18 (3c)	07.29*(2c)	19.55*(3c)					
				29700+				
6	94.53*(3c)	07.62*(2c)	19.91*(3c)	31.45*(3b)				
					29700+			
7	94.53*(3c)	07.62*(2c)	19.91*(3c)	31.45*(3b)	42.25 (3)			
						29700+		
8	94.36 (3c)	07.29*(2c)	19.55*(3c)	31.45*(3b)	41.98 (3)	52.05 (1)		
							29700+	
9	93.79 (2c)	06.77 (2c)	19.11 (3)	30.66 (1)	41.43 (2)	51.43 (1c)	60.73 (1)	
10	92.94 (2)	05.97 (1b)	18.26 (3)	29.79 (2)	40.56 (2)	50.62*(1b)	59.79 (1)	
								29700+
11	91.75 (2c)	04.92*(2b)	17.15*(3)	28.61 (2)	39.39 (2)	49.32 (0)	58.58 (1)	74.86 (1)
12	90.36 (2)	03.36 (1)	15.66 (3)	27.17 (2)	37.91 (2)	47.90*(1)	57.08 (1c)	73.37 (0)
13	88.45 (2c)	01.62 (1)	13.88*(3)	25.40 (1)	36.15 (2)	46.02 (0)	55.25 (1)	71.31 (0)
		29600+						
14	86.52 (1c) 86.27 (1c)	99.54 (1)	11.86 (2v)	23.27 (0)	34.05 (2)	43.94 (0)	53.15 (1)	69.36 (0)
15	84.11*(1) 83.74 (0)		09.45 (2)	20.87 (0)	[31.45] (3b)		50.62*(1b)	
16	81.43*(2) 80.89 (1c)		06.77*(2c)	[18.26] (3)	29.01 (1)		47.90*(1)	
17	78.44 (2c) 77.56*(2)		03.79 (1)	15.21 (0)	26.03 (1)		44.96 (0)	
18			00.53*(2)		22.65 (1c)			
			29600+					
19			96.85 (1)					
20			92.94*(2)					
21			88.64 (2c)					
22			84.11*(2)					

[a] The *p*-branches of the 3370 band fall in the region where the much stronger 3390 band is well developed. At pressures sufficiently high to bring out the lines of λ3370, the absorption of 3390 is so strong that there is no chance to observe any of the *p*-branches of the 3370 band.

formula. All the violet branches have very nearly the same constants, i.e., they can be shifted in such a way that they all coincide. One can do the same thing with the red branches and in this way identify corresponding lines. It becomes then at once apparent that corresponding lines of the different red branches also follow Deslandres' law and that also in these sequences the branches are alternately strong and weak. The spacing of the red branches is much wider than the spacing of the violet progressions. Also in the red branches, as in the violet ones, there is one more line missing in every branch, as one goes toward the outside of the band.

§8. INTERPRETATION

These are roughly the observed facts. With the results of §3–§5 in mind, it is not difficult to see how they must be interpreted. Let us consider first the sequence of violet branches. The fact that subsequent branches in this sequence show the intensity alternations indicates that they must be due to subsequent K-transitions. The individual lines of each branch are then due to a fixed K-transition and different J-transitions. The behavior of the missing lines shows clearly that they are rR-branches. In the same way it is shown that the red branches must be pP-branches. This explains also the fact that their

TABLE I. (*Continued.*) *Band at 3430A.*

J''	$K''=3$	4	5	6	7	8	9	$K''=3$	(4)	5
			pP-Branches						*rQ-Branches*	
3	290 84.03 (3)							291 79.70 (2r)		
		29000+								
4	80.72 (2)	61.02 (1)						78.14*(2)		
			29000+							
5	77.15 (3v)	57.43 (1)	36.84 (2c)					76.36 (3d)		
				29000+						29100+
6	73.19 (3)	53.58 (1)	32.94 (2)	11.72*(2)				74.31*(3d)		98.73 (1d)
					28900+					
7	68.97 (3d)	49.47 (1c)	28.80*(3v)	07.59 (0)	86.27*(3)			71.92*(2)		96.58 (2c)
8	64.61 (1c) 64.46 (1c)	44.89 (1)	24.27 (2c)	03.05 (0c)	81.78 (1)			69.27 (3c)		94.23 (2d)
							28900+			
9	59.87 (1c) 59.59 (1c)	40.16 (2d)	19.41 (3)	98.21 (2)	76.90 (2)		36.57 (0)	66.24 (2)		91.37*(3)
10	54.86 (2) 54.49 (1)	35.00 (1)	14.41 (3)	93.14 (1)	71.87 (2)		31.45 (0)	62.94 (2)		88.50*(2)
11	49.70 (1c) 49.04 (1)	29.63 (0)	08.99 (3)	87.75 (0)	66.43 (1)		26.01 (0)	59.38 (2)		85.15 (2v)
12	44.03 (1) 43.26 (2)	23.93 (1c)	03.30 (2c)	82.08 (0)	60.69 (1)		20.35 (0c)	55.49 (2)		81.48 (1)
			28900+							
13	38.18 (1) 37.12 (1c)	17.94 (0)	97.34 (2)	76.06 (0)	54.64 (1)		14.33 (0c)	50.97 (2db)		77.49 (2)
14	32.03 (1) 30.59 (0)	11.72*(2)	91.05 (2)	69.84 (1)	48.38 (1)		07.99 (0)	46.74 (0) 46.17 (0)		
15	25.82 (2) 23.75 (0)	05.25 (1c)	84.40 (1)	63.20 (0)	41.69 (1)		01.40 (0)	41.97 (2c) 41.34 (2)		
							28800+			
16	19.43*(3) 16.48 (2)		77.56 (1)		34.85 (1)		94.46 (0)	36.78 (1) 35.87 (1c)		
17			70.38 (1)		27.58 (0)		87.22 (0c)	31.21 (1c) 30.24 (1)		
18			62.86 (1c)		20.06 (0c)		79.70 (0)			
19			55.13 (1v)		12.24 (0r)					
20			46.99 (1)		04.15 (0)					
					28800+					
21			38.57 (0)		95.34 (0)					
22			29.88 (0)		86.78 (0)					
23			20.85 (0)							

J''	$K''=3$	4	5	6	7	$K''=3$	4	5	6	7
		pQ-Branches					*rR-Branches*			
3	290 90.49 (1)					291 89.40 (3)				
							29200+			
4	89.35 (2v)					90.35 (3c)	01.59 (2c)			
		29000+	29000+					29200+		
5	87.87 (3d)	68.14 (1)	47.54 (0)			91.02 (4d)	02.27*(3)	13.24*(4)		
				29000+					29200+	
6	96.09 (2)	66.34 (1)	45.76 (2)	24.49 (0c)		91.37*(2c)	02.63*(3)	13.56*(4)	25.86*(2d)	
					29000+					29200+
7	84.03*(3)	69.31 (1c)	43.67 (1)	22.49 (0)	01.27*(1)	91.37*(4c)	02.63*(3)	13.56*(4)	25.86*(2d)	37.20 (1d)
8	81.76 (1c) 81.59 (1c)	62.00 (2)	41.33 (2c)	00.09 (0)	98.79 (0)	91.20 (2c)	02.27*(3)	13.24*(4)	25.50 (1)	36.90 (1d)
9	79.15 (2c) 78.83 (2)	59.33 (1c)	38.62 (2)	17.40 (0)	96.08 (0)	90.59 (3c)	01.73 (2c)	12.69 (3)	25.00 (2c)	36.26 (0d)
10	76.24 (2) 75.86 (1)	—	35.70 (1)	14.41*(3)	93.14*(1)	89.71 (3)	00.88 (1d)	11.82 (3)	24.15 (2d)	35.32 (0d)
							29100+			
11	73.19*(3) 72.53 (2)	[53.20] (2d)	32.45 (1)	11.17 (0)	89.70*(1d)	88.50*(2)	99.72 (1c)	10.56 (3)	22.93 (2)	34.77 (0)
12	69.71 (3d) 68.97*(3d)	49.47*(1c)	28.80*(3v)	07.59 (0)	86.27*(3)	86.94 (2c)	98.20 (1)	09.11 (2)	21.53 (0)	32.60 (0)
13	66.02 (1) 64.93 (1)	45.76*(2)	25.05 (1)	03.78 (0c)	82.34 (0)	85.15 (2v)	96.45 (2c)	07.27 (2)	19.61 (0)	30.90 (0)
14	62.00*(2) 60.63 (1)		20.90 (1)	99.62 (1d)	78.15 (0)	83.19 (1c) 82.96 (1c)		05.15 (1d)	17.52 (0)	
15	57.96 (2c) 55.97 (1d)		16.47 (2)		73.68 (0)	80.80 (1) 80.42 (1)		02.63*(3)		
								29100+		
16			11.72*(2)		68.84 (0)	78.14*(1) 77.49 (1)		99.96 (1c)		
17			06.63 (1)		63.71 (0b)	75.11 (0) 74.31*(2d)				
18			01.27 (1)		58.33 (1)	71.92*(2) 70.67 (1)				
19			95.59 (1)		52.63 (0)	68.35 (2d) 66.64 (0)				
20			89.70*(1d)		46.53 (0)					
21			83.41 (1c)		40.24 (0)					

spacing is so much wider than that of the violet branches, for the band is degraded toward the red. We have seen that the *rR*- and the *pP*-branches are for not too small values of K the only ones with an appreciable intensity, but that for smaller values of K also *rQ*- and *pQ*- branches must exist and, with a smaller intensity, also *rP*- and *pR*-branches. If the *rR*-branches are given, the position of the *rP*-lines can be found by extrapolation, and with a suitable assumption about the numbering of the lines also the *rQ*-branches. (In each sub-band everything is exactly as in a band of a diatomic molecule.) These calculated branches are actually found and are more intensive if we go toward the center of the band where the sub-bands with small values of K lie. In this way the numbering of the lines can be fixed, as only with one definite numbering the *Q*-branches are found in their right places.

In Table I the wave numbers and intensities of the classified lines are given. Whereas on both sides of the bands almost all the observed lines are classified, there is a large number of unclassified lines in the center of the bands. These lines

TABLE I. (*Continued.*) *Band at 3925A.*

J''	$K''=3$	4	5	(6)	7	$K''=3$	(4)	5	(6)	7
		pP-Branches						*rQ-Branches*		
3	302 86.95 (1)									
		30200+								
4	83.58 (1c)	[62.39] (1c)				303 78.51 (2c)				
			30200+							
5	79.89 (1)	58.56 (0c)	35.55 (1c)			76.76 (2)				
								30300+		
6	75.90 (1)	54.58 (0d)	31.50 (1)			74.76 (1)		89.34*(2c)		
					30100+					
7	71.73 (2b)	50.22 (0c)	27.11 (0)		77.00 (0)	72.54 (1)		87.10*(2)		
8	67.00 (2c)	45.58 (1b)	22.48 (1)		72.36 (1)	69.94 (1)		84.73 (0)		
										30300+
9	[62.39] (1c) 61.94*(1c)	40.60*(1b)	17.47*(1b)		67.51 (0)	67.08 (1c)		81.81*(1d)		93.71 (0)
10	56.83 (0c) 56.52*(2c)	35.35 (1c)	12.23 (1)		62.29 (0)	63.94 (2d)		78.81 (0)		90.49 (0)
11	51.35 (1) 50.87 (1)	29.81*(1)	06.64 (1)		56.77 (0)	60.30 (2)		75.35 (1c)		87.10*(2)
12	45.58*(1b) 44.89*(0b)	23.79 (0d)	00.71 (0)		50.96 (0)	56.48 (1c)		71.67*(2dc)		83.21 (0)
			30100+							
13	39.37 (0) 38.51 (0)	17.65*(0c)	94.42 (0)		44.84 (0)	52.37 (2c) 52.12 (0c)		67.45 (1c)		78.81*(1d)
14		11.37 (0) 11.08 (0)	87.87 (0)					63.11*(0c)		74.21 (0)
15			81.00 (0)					58.27 (1)		69.44*(0)
16			73.80 (0)					53.31 (1)		
17			66.27 (0)					48.17 (1c)		
18			58.44 (0)							
		pQ-Branches						*rR-Branches*		
3	302 93.30 (1)					303 87.92 (2c)				
		30200+								
4	92.09 (1)	[70.99] (1b)				88.85*(2c)				
			30200+					30400+		
5	90.48 (1c)	69.07 (0)	46.15 (1b)			89.34*(2c)		03.84*(1c)		
6	88.29 (0)	67.35 (0c)	44.17 (0)			89.52*(2c)		04.17*(2c)		
					30100+					30400+
7	86.40 (1)	64.97 (0)	41.84 (0)		91.99 (0)	89.52*(2c)		04.17*(2c)		15.81 (0)
8	84.15 (1c) 83.89 (1)	62.39 (1c)	39.37 (0)		89.37 (0)	88.85*(2)		03.84*(1c)		15.32 (0)
9	81.21 (1c) 80.91 (1c)	59.55 (1)	36.55 (1)		86.46 (0)	88.21 (2c)		03.04 (1b)		14.63 (0)
10	78.11 (0) 77.66 (2)	56.53 (3c)	33.35 (1)		83.35 (0)	87.10*(2)		02.07 (1)		13.62 (0c)
11	74.75 (1) 74.19 (1)	52.91 (1)	29.81 (1)		—	85.33 (2c)		00.72 (1)		12.18 (0)
								30300+		
12	70.99*(1b) 70.29 (1)	49.06 (0c)	26.01 (1)		76.29 (0d)	83.84 (1)		99.03 (1d)		10.53 (0)
13	67.00*(2c) 66.09 (1)	44.94(0)	21.83 (0)		—	81.81*(1d)		97.09 (2r)		
14	62.82 (1c) 61.50 (1)		17.47*(1v)		67.51*(0)	79.27*(2b)		94.73 (1)		
15			12.65 (0)			76.76* 76.26 (0)		92.48 (0d)		
16			07.55 (0)					89.52*(2c)		
17			02.19 (0)							
18			96.38 (0)							
19			90.66 (0)							
20			84.40 (0)							

belong to the branches with low values of K which were omitted from the tables for reasons discussed in §11. The rP- and pR-branches are omitted as their intensity is so low that they can be observed only very incompletely and only in the crowded center portion of the bands where many strong lines interfere with them.

After the bands have been analyzed, the values for the rotational energies of the lower state can be found, and therefore the intensities of all the lines calculated according to (6) and (7). The observed intensities agree very well with the calculated values although a very accurate comparison is not possible, as only intensity estimates are available. However by comparing lines which are just at the limit of visibility it is possible to get nevertheless a fairly good confirmation of the intensity relations. In particular it is found that the intensity ratio between the strong and weak branches conforms with the expected ratio 3 : 1 (§5).

In order to obtain a further check of the classification and the intensity relations the band at 3530A was photographed with the formaldehyde vapor at varying temperatures up to 300°C. The changes which occurred in the bands are exactly those to be expected. Lines belonging to higher rotational quantum numbers come out relatively more strongly. In this way the rR-branches up to $K=14\rightarrow K=13$ could be identified. There is, however, a limit to the usefulness of increased temperatures for the development of higher lines. At room temperature practically all the molecules are in the lowest vibrational state. With rising temperatures an increasing number of molecules is brought into the next higher vibrational states, and there is accordingly the possibility of a great number of new bands arising from the absorption of molecules in these higher vibrational levels. These bands are partly confused with the low temperature bands, and

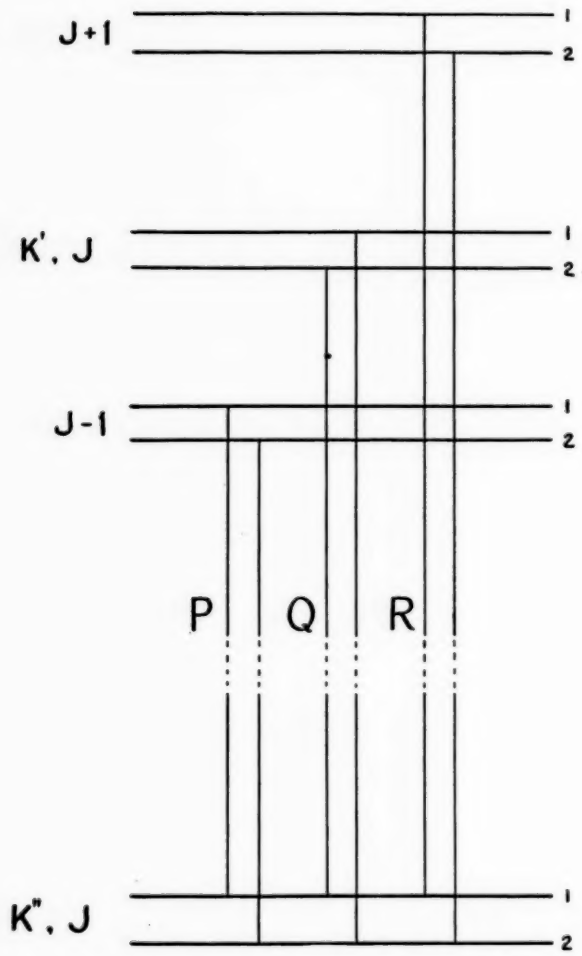

FIG. 4. Allowed transitions, if the electric moment is along the axis of the greatest moment of inertia.

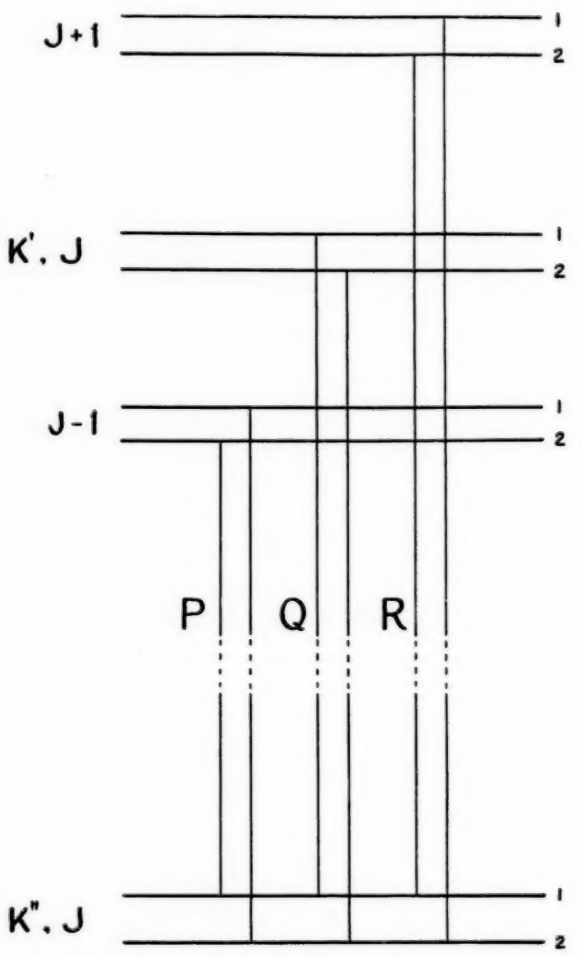

FIG. 5. Allowed transitions, if the electric moment is along the axis of the middle moment of inertia.

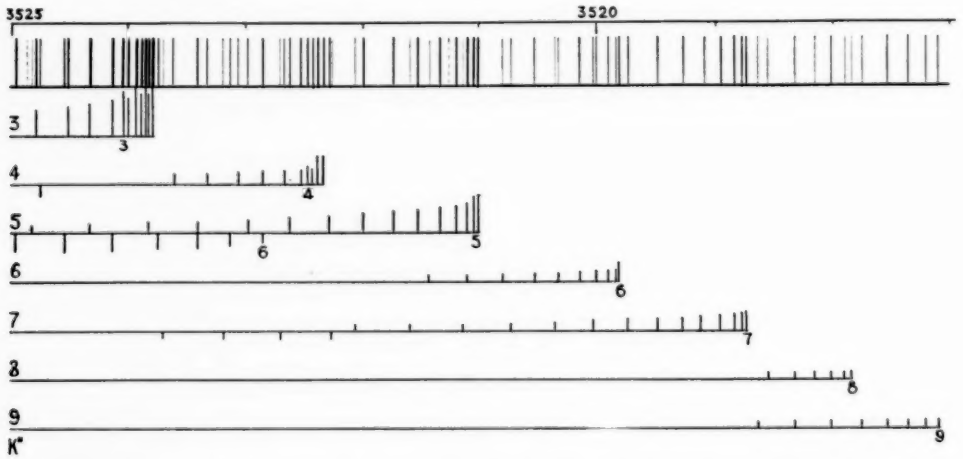

FIG. 6. Short wave-length end of the 3530 band at room temperature, with the classification into the different sub-bands. Lines drawn upward represent rR-lines, those drawn downward rQ-lines.

form an almost continuous background against which weak lines disappear.

In order to give an idea of the actual appearance of the bands in Fig. 6 the violet side of the 3530 band is drawn. The intensity of the lines is roughly indicated by their thickness. Below, the arrangement of the lines into different branches is shown. Each horizontal line represents one sub-band. Only two weak lines, shown in the figure as dotted lines could not be classified in this region. At higher pressures more lines appear some of which do not fit into the band. This is not surprising, as at high enough pressures new bands appear almost everywhere so that the absorption becomes almost continuous.

§9. Combination Relations

The correctness of the numbering of the lines can be tested in a much more direct way with the help of combination relations, which also furnish a general proof of the correctness of the interpretation, which is free from any particular assumption about the shape of the molecule or any formula for the rotational energy levels. If $F(K, J)$ is the rotational energy (divided by h) of the upper state as function of J and K, and $f(K, J)$ that of the lower state we can write the six kinds of branches.

$$\left.\begin{aligned} pP(K, J) &= F(K-1, J-1) - f(K, J), \\ pQ(K, J) &= F(K-1, J) - f(K, J), \\ pR(K, J) &= F(K-1, J+1) - f(K, J), \\ rP(K, J) &= F(K+1, J-1) - f(K, J), \\ rQ(K, J) &= F(K+1, J) - f(K, J), \\ rR(K, J) &= F(K+1, J+1) - f(K, J). \end{aligned}\right\} \quad (8)$$

From this it follows that

$$\left.\begin{aligned} rR(K-1, J-1) - pP(K+1, J+1) &= f(K+1, J+1) - f(K-1, J-1), \\ rR(K, J-1) - rP(K, J+1) &= f(K, J+1) - f(K, J-1), \\ pR(K, J-1) - pP(K, J+1) &= f(K, J+1) - f(K, J-1), \\ rR(K, J) - rQ(K, J+1) &= f(K, J+1) - f(K, J), \\ pQ(K, J) - pP(K, J+1) &= f(K, J+1) - f(K, J). \end{aligned}\right\} \quad (9)$$

The right sides of all these equations contain only term differences of the lower state. If we form these differences for different bands which have all the same lower but different upper states they must be identical for all the bands. All the bands considered here have the normal state of the formaldehyde molecule as lower state. The fact that the differences for the six bands turn out to be identical proves that the interpretation and the numbering of the lines must be correct.

In Tables II and III the combination relations are given, and it is seen that the agreement is very satisfactory. These combination relations were a very great help for the analysis of additional bands when the analysis of one or two were completed, as it was possible then to calculate the position of all other lines, if one set of branches only was known.

§10. Calculation of the Constants

If we restrict ourselves to those lines which follow Deslandres' formula well (those deviating from it will be discussed in the next paragraph), and show no doubling, we can be assured that (3) is a good approximation for the rotational energy levels, and by substituting this expression for $f(K, J)$ in (9) we can calculate the moments of inertia from the values of Tables II and III. If we introduce the abbreviations

$$\alpha = \frac{h}{8\pi^2 cA};\ \beta = \frac{h}{8\pi^2 cB};\ \gamma = \frac{h}{8\pi^2 cC};\ \delta = \frac{h}{8\pi^2 cD}, \quad (10)$$

we have

$$f(K, J+1) - f(K, J) = 2\delta(J+1), \quad (11)$$

$$f(K+1, J+1) - f(K-1, J-1) = 4(\gamma-\delta)K + 4\delta(J+\tfrac{1}{2}). \quad (12)$$

TABLE II. $pQ(K, J)-pP(K, J+1)$.

J	K=3 3530	3390	3200	3430	3295	K=4 3530	3350	3260	3430	3295
3	9.68	9.68	9.71	9.77	9.72					
4	12.10	12.10	12.24	12.20	12.25	12.11	—	12.23*	—	[12.43]
5	14.53	14.63	14.61	14.68	14.58	[14.56]	—	14.74*	14.56	14.49
6	17.05	17.04	17.02	17.12	16.92	—	—	17.00	16.87	17.15
7	19.51*	19.46 19.46	19.54 19.39	19.41* 19.57*	19.40	19.40	19.38	[19.28]	19.42	19.39
8	21.89 21.88	21.88 21.76*	21.88 21.95	21.89 22.00	— 21.95	21.71	21.77	21.83*	21.84	21.79*
9	24.38 24.40	24.36* 24.47	24.45 24.44	24.29 24.34	24.38 24.39	24.30	24.25*	24.21*	24.33	24.20
10	26.73 26.77	26.73* —	26.65 26.81	26.54 26.82	26.76 26.79	[26.77]	—	26.79	—	26.72*
11	29.08* 29.32	29.15* 29.36	29.02 29.25*	29.16* 29.27	29.17 29.30	29.13	29.16		[29.27]	29.12
12	31.48* 31.98*	31.51 31.84	31.51 32.05*	31.53 31.85*	31.62 31.78		31.53*		31.73*	31.41*
13	33.86 34.48*	33.94 34.44*	33.92 34.51*	33.89 34.34			33.94*		34.04	
14	36.28 36.87	36.25 36.92	36.18 36.93	36.18* 36.88			36.51			
15	38.57 39.44	38.57* 39.53	38.61* 39.62	38.53* 39.49						
16	41.01* 42.14	40.99* 42.61								
17		43.36* 45.95								

J	K=5 3530	3390	3260	3430	3235	K=6 3390	3260	3430	K=7 3530	3390	3260	3430	3295	K=9 3530	3390
3															
4															
5	14.80	14.67	14.64	14.58	14.65										
6	16.98	17.00	17.03	16.98*	17.06	16.85	—	16.90							
7	13.44	19.47*	19.46	19.39	19.36	19.41*	—	19.44	—	—	—	[19.48]	19.54		
8	21.85	21.82*	21.78	21.88	21.90*	21.75*	21.92	21.88	—	21.93*	21.79	21.88	21.86		
9	24.29	24.34	24.29	24.20	24.32	—	24.25	24.26	24.21	24.28	24.24	24.21	24.17	—	—
10	26.70	26.71*	26.71	26.69	26.69	26.85		26.66	—	26.65	26.63	26.73*	26.58	—	—
11	29.14*	29.14*	29.18	29.14	29.11	—		29.09	28.96*	29.08	29.10	29.02*	—	—	29.05
12	31.51	31.63*	31.62	31.45*	31.59	31.59		31.53	—	31.53	31.56	31.64*	31.45*	—	31.50*
13	33.95	33.98	34.02	33.99	33.96	34.08		33.94	—	33.92		33.95		—	—
14	36.48	36.44*	36.51	36.49	36.47*	36.55*		36.42	36.35	36.40*		36.46		—	36.63*
15	38.85	38.91	38.88	38.92	38.85				38.76	38.76		38.83		38.60*	38.80*
16	41.31	41.29	41.26	41.34*	41.28				41.29	41.27		41.26		41.20*	41.20
17	43.75	43.73		43.83	43.75				43.60*	43.64		43.65			43.58
18	46.14	46.14*		46.15					—	46.12		46.09		46.17	46.11*
19	48.61	48.65		48.63					48.47	48.52		48.48			48.47
20	51.01	50.93*		51.13*					50.89	50.94		—			50.97
21	53.49	53.49*		53.53						53.36		53.48			
22										55.83					
23										58.16					
24										60.69					

TABLE II. (*Continued.*) $rR(K, J)-rQ(K, J+1)$.

J	K=3 3530	3390	3260	3370	3430	3295	K=4 3530	3350	3370
3	9.73	9.77*	9.88*	9.71*	9.70	9.41			
4	12.18*	12.05*	12.14*	12.07	12.21*	12.09*	[12.27]	12.16	—
5	14.51*	14.68*	14.58*	14.58	14.64	14.58*	14.69*	14.61	—
6	17.09*	16.89*	16.99*	16.97*	17.06*	16.98*	17.03*	17.00*	17.03*
7	19.42*	19.47*	19.36*	19.36*	19.45*	19.58*	19.36*	—	19.41*
8	21.83*	21.89	21.86*	21.90	21.93	21.77*	21.72*	21.85	—
9	24.33	24.35*	24.35	24.33	24.35	24.27	[24.27]	24.26	24.23
10	26.75	26.79	26.77	26.78	26.77	26.80*	26.80	26.81	26.71
11	29.26*	29.17	29.26	29.18	29.12*	29.15	29.21	29.25	29.17*
12	31.67*	31.66	31.52 31.82	31.62	31.45	31.47 31.69	[31.52]	31.54*	31.60
13	33.83 34.39*	33.89 34.46	33.95 34.28	33.95 34.15	34.18	33.91*		34.02	34.06
14	36.24 36.80	36.24 —	36.30 36.82	36.24 36.96	36.22 37.02				36.41
15	38.47 39.49	38.48 39.49*	38.55 39.57	38.56 39.46*	38.45 39.46				
16	40.79 42.20	— —		40.77 42.14*	40.71 42.27*				
17	43.12 44.77	42.97 44.97			42.10 44.87				

J	K=5 3530	3390	3260	3370	3430	3295	K=6 3530	3390	K=7 3530	3390	3260	3370	K=8 3390	K=9 3530	3390
3															
4															
5	14.53*	14.67	14.66*	[14.63]	14.51*	14.50*									
6	17.05*	17.01*	17.02*	16.98*	16.98*	17.07*	—	16.93							
7	19.38*	19.55*	19.28	19.38*	19.33*	19.44*	—	19.54*	—	—	19.42	19.40			
8	21.70*	21.74*	21.89*	21.76*	21.87*	22.03*	—	21.84	—	[21.81]	21.75	—	—		
9	24.36	24.21*	24.40	24.23	24.19*	24.23	24.29	24.25	24.26	24.27	24.24*	24.28*	—	—	—
10	[26.92]	26.77	26.93	26.71	26.67	26.72	26.70*		26.70	26.70	26.67*	26.68*	26.60	26.72	—
11	29.14*	29.16*	29.13	29.15*	29.08	29.05*			29.17	29.23*		29.10	29.11	29.03	29.03
12	31.49	—		31.55	31.62	31.58			31.55			31.47*	[31.56]	—	31.60
13	34.01*	33.98		33.99*		33.98*			33.92			33.94		33.84	[34.19]
14	36.52*	36.55		36.42		36.46			36.38			36.26*		[36.41]	36.36
15	38.89*	38.73		38.83		39.17			38.80			[38.86]		[38.89]	—
16	41.43*	41.28*		41 29*		41.35*						41.19			41.25
17		43.70		43.73								43.69			43.76
18		—													
19		48.64													
20		—													
21		53.34													

TABLE III. $rR(K-1, J-1)-pP(K+1, J+1)$.

	$K=4$								$K=5$			
J	3530		3390		3260	3430		3295	3530	3390	3260	3430
4	152.56		152.56		152.77*	152.55		152.37				
5	157.37		157.41*		157.39*	157.41		157.35*	189.82	189.81	189.95*	189.81*
6	162.22*		162.33*		162.28*	162.25*		162.23*	194.73	194.68	—	194.68*
7	167.14*		166.95*		167.05*	166.93*		167.03*	[199.65]	199.48*	—	199.58*
8	171.89*		171.86*		171.75*	171.94		171.87*	—	204.38*	204.31*	204.42*
9	176.72		176.77		176.68*	176.79		176.60*	—	209.20	209.16	209.13*
10	181.56		181.58*		181.55	181.60		181.57	214.03	214.01	—	213.98
11	186.33*		186.38		186.34	186.41*		186.40*	—	218.84	218.73*	218.80
12	191.21		191.13*		191.13	191.16		191.21	223.64	223.75	223.71*	223.66
13	195.92*		195.95		195.98	195.89		195.97	[228.29]	228.49*		228.36
14	200.87*	200.65	200.86*	200.64	200.76	200.75		200.81*	—	233.26		233.25
15	206.04	205.34	—	205.31	205.57	205.31	205.63	205.40	205.47*	237.90		
16	210.44	210.01	210.42*	209.97	210.38	209.91	210.42	210.04	210.49*	209.99		
17	215.23	214.58	—	—			215.26*	214.63				
18			220.08	219.16			219.98	219.18*				
19							224.93*	223.68				
20							229.78	228.07				

	$K=6$					$K=7$		$K=8$			$K=9$	$K=10$	
J	3530	3390	3260	3430	3295	3530	3390	3530	3390	3430	3390	3530	3390
4													
5													
6	226.95*	227.00*	226.95*	226.96*	226.84*								
7	231.80*	231.80*	231.77*	231.78*	231.81*	—	263.81*						
8	236.52*	236.76*	236.56	236.66*	236.66*	—	268.80*	300.53	300.57	300.63			
9	241.30*	241.44	241.41	241.36*	241.55*	—	273.47	305.41	305.34*	305.45	337.09		
10	246.25*	246.24	246.27	246.28	246.27	—	278.33	310.23*	310.19	310.25	341.76*	373.07	373.19
11	251.06	251.10	251.05	251.13	251.11	—	283.10	315.05	315.03	314.97	346.58	378.02	378.01
12	255.86	255.92	255.93	255.95	255.83	—	287.94	319.80	319.85*	319.84	351.43	382.71	382.79
13	260.68	260.69	—	260.72		—	292.77	324.56	324.58	324.61	356.36	387.46	387.53
14	265.43	265.51	265.55	265.58		—	297.59*	329.32	329.39	329.50		392.30	
15	270.31	270.28		270.30		—	302.38	334.14	334.22*			397.11	
16	275.03*	275.01		275.05*		307.13*	307.02*	338.97*	339.02			402.47	
17	279.81*	279.83*		279.90		311.87	312.06	343.75	343.74*				
18	284.69	284.67				—		348.50	348.62*				
19	289.39	—				321.46*		353.16	353.26*				
20	294.11*	294.16						358.02	358.07				
21	298.89*	—						362.80					
22	303.49	303.59											
23	308.36*												

Table II gives the observed values of $f(K, J+1)-f(K, J)$. They can be represented within the limits of experimental errors by (11). The values for $K=5$, and $K=7$ may serve here as an example (Table IV).

TABLE IV.

	$K=5$		$K=7$	
J	obs.	calc.	obs.	calc.
5	14.61	14.57		
6	16.99	17.00		
7	19.44	19.43	19.41	19.40
8	21.83	21.86	21.83	21.83
9	24.28	24.29	24.24	24.25
10	26.71	26.72	26.67	26.68
11	29.15	29.15	29.08	29.10
12	31.57	31.58	31.55	31.53
13	34.00	34.01	33.93	33.95
14	36.49	36.44	36.39	36.38
15	38.89	38.87	38.79	38.80
16	41.31	41.29	41.25	41.23
17	43.74	43.72	43.65	43.65
18	46.14	46.15	46.10	46.08
19	48.63	48.58	48.49	48.50
20			50.92	50.93
21			53.42	53.35

The second column gives the averages for $K=5$ obtained from Table II and the fourth column those for $K=7$. In forming these averages all values originating from obviously bad lines were excluded. Assuming now the validity of (11) a value for δ can be calculated by dividing the sum of the values in one column by the sum of the $J+1$ values involved. We obtain thus $2\delta=2.4291$ for $K=5$ and $2\delta=2.4250$ for $K=7$. If we calculate $2\delta(J+1)$ with these values for δ we get the third and fifth columns. Table IV shows clearly that the agreement between the calculated and observed values is as perfect as the experimental errors permit, and that therefore (11) holds within the limits of experimental errors. The value of δ for $K=7$ is a little smaller than that for $K=5$, and this difference is real and outside the limits of experimental errors. It shows in the table in that the observed values for $K=7$ are systematically all a little smaller than those for $K=5$. More generally it was found

that in all the states investigated the value of δ depends on K and that it decreases with K.[13] It is easy to verify that for the lower electronic state from Table II.

The reason for the variation of δ with K must be sought in the deformation of the molecule by the rotation. We can disregard it for the purpose of this paper, except that it necessitates small corrections for the calculation of the other constants of the molecule.

With the help of (12) and the values of Table III, it is possible to calculate γ. As δ is not a constant, (12) must be modified to

$$f(K+1, J+1)-f(K-1, J-1)=(4\gamma-\delta)K + 4\delta_{K+1}(J+\tfrac{1}{2})-(\delta_{K-1}-\delta_{K+1})(J-\tfrac{1}{2})^2. \quad (13)$$

As δ_K is known this equation can be used to calculate γ. In order to do so we subtract $4\delta_{K+1}(J+\frac{1}{2})-(\delta_{K-1}-\delta_{K+1})(J-\frac{1}{2})^2$ from the observed average values of Table III. The result should be a constant independent of J. It appears that this is in general not the case, but that there is a slight though definite variation. That is due to the fact that the quadratic term is not known with sufficient accuracy. It is easy however to adjust in every case the value of $\delta_{K-1}-\delta_{K+1}$ in such a way that there is no more systematic variation. This is then at the same time a method to obtain more accurate information about the variation of δ with K.

This procedure is carried out in the same way for all the available values of K. The result is

K	4	5	6	7	8	9	10
obs.	130.83	163.26	195.45	227.67	259.51	291.33	322.59
calc.	130.71	163.18	195.52	227.68	259.54	291.41	322.92

and the values (obs.) thus found should be proportional to K. It is found that this is not the case, but that there are deviations which exceed by far the observational errors. Also here these deviations are due to the deformation of the molecule by the rotation. The main effect here is easily accounted for quantitatively. It is the centrifugal force acting on the hydrogen atoms due to the rapid rotation about the CO-axis. This force is of the same nature as the centrifugal expansion of a diatomic molecule and we expect therefore that it can be represented by a negative term of the form $-\mu K^4$. The value of μ turns out to be 5.8×10^{-4}. If this correction term is taken into account, the above values are fairly well proportional to K. The value of $\gamma-\delta$ turns out to be 8.189, the values of $4(\gamma-\delta)K-8\mu(K^3+K)$ calculated with these values for γ and μ are given in the row "calc." of the above table. The agreement between the observed and calculated values is fairly good, although there are still some slight systematic deviations, which, however, are too small to be of any interest to us here.

Combination relations analogous to (9) allow us to obtain the rotational differences of the upper electronic level. They are omitted here in order to save space. From these combination differences we obtain the constants of the six upper levels by the same process which was used for the calculations of the constants of the ground state. All the constants obtained in this way are collected in Table V.

A few comments concerning these constants are necessary. It was already mentioned that the expression (3) for the energy of a symmetrical top, though a very good approximation, does not represent exactly the rotational states of the formaldehyde molecule. The deviations which are due to the fact that the molecule is slightly asymmetric, and which occur for low K-values only, will be discussed in §11. Besides, we saw that the rotational distortion of the molecule has the effect that the moments of inertia are not constants but depend on K. Due to uncertainty about the exact nature of the deviations an extrapolation to the rotationless state of the molecule cannot be carried out exactly. For this reason the constant δ is given for $K=5$ for the ground level and for $K=4$ for the upper levels. The possible deviations of this value from that for the rotationless molecule are very small, probably of the same order as the uncertainty

[13] As the variation of δ with K is very small the exact law of the variation cannot be established from the present data. The values for $K=3$, 5 and 7 which are the most reliable ones seem to indicate a linear decrease with K. It seems highly probable though that this apparent linear decrease results from two terms of higher power with opposite sign. This would also agree better with the theoretical results. Preliminary calculations about the distortion of the formaldehyde molecule by rotation have shown that there is no possibility of a linear term, but that there is a term proportional to K^2 and one proportional to K^3 with opposite sign.

TABLE V. *Rotational constants of formaldehyde.*

	δ	$\gamma-\delta$	γ	$\mu\times10^4$	ν_0	α	β	$A\times10^{40}$	$B\times10^{40}$	$C\times10^{40}$	b
Normal state	1.215	8.189	9.404	5.8		1.137	1.293	24.33	21.39	2.941	0.0095
Upper level of											
3530	1.067	7.682	8.749		28,312.66	1.002	1.132	27.61	24.44	3.162	0.0084
3390	1.056	7.645	8.701	3.8	29,495.12	0.992	1.120	27.88	24.70	3.179	0.0084
3260	1.046	7.606	8.653		30,658.67	0.983	1.110	28.14	24.92	3.197	0.0083
3370	1.066	7.827	8.893		29,634.45	1.002	1.130	27.61	24.48	3.110	0.0081
3430	1.067	7.546	8.613		29,136.6						
3295	1.055	7.19	8.24		30,340.1						

due to experimental errors. Besides, for further information about the nature of the upper electronic state, the absolute values of the constants are not as important as their variation with the vibrational states. If, therefore, the way in which the constants are calculated might introduce a slight systematic error, this will be of no great importance provided it is the same for all the different levels. For this reason the constants of all the bands were as much as possible calculated in exactly the same manner, so that very probably the relative values of the constants are free from any, even slight, systematic errors.[14]

In all cases it was found that the dependence of the rotational energy on J was strictly of the form $\delta_K J(J+1)$. No deviations from this formula could be detected. It was already mentioned that there occur, however, appreciable deviations from the quadratic dependence of the rotational energy on K, and that these deviations can be expressed satisfactorily by a term in K^4. The same thing is true for the initial levels of the bands 3530, 3390, 3260, and 3370. This is illustrated by Table VI in which the K differences extrapolated to $J=0$ are tabulated for the upper levels of the different bands. They are compared with the values calculated from the formula $4(\gamma-\delta)K-8\mu(K^3+K)$. The value $\mu=3.8\times10^{-4}$ is obtained from the 3390 band for which the most complete and reliable data are available. The same value for μ was used for the upper levels of the other bands, as it must be expected that it does not depend much on the vibrational state. Table VI shows that the agreement between calculated and observed values is satisfactory for the bands 3530, 3390, and 3260. The same is true for the band 3370 for which, however, as the p-branches could not be observed, a slightly different mode of procedure had to be adopted.

If one tries, however, to represent the differences for the upper levels of the 3430 and 3295 bands by a formula of the same type, there is no possible way to get any agreement. Table VI shows that if the calculated values are made to agree for $K=3$ there is a wide discrepancy for the higher values of K. This discrepancy does not seem to obey a simple law. This is shown, e.g., by the following figures which are the K differences of Table VI (corrected for the fourth power term) for the 3430 band divided by K.

3	4	5	6	7	8	9
30.19	30.41	30.67	31.23	30.72	——	30.71

If no anomaly were present, all these values should be identical and equal to $4(\gamma-\delta)$.

In view of the fact that no adequate formula can be found to represent the rotational levels of these two bands, and that certainly the expression (3) cannot be valid even with the corrections for the nonrigidity of the molecule, the question may be raised, in how far we can be sure of the correctness of the analysis of the bands. As far as the four regular bands are concerned, we believe that there is hardly any possibility for doubt. Most of the regularities suggest themselves readily and the fact that they agree in all details with the theoretical expectations is a strong confirmation for their genuineness. In the band 3430 some of the branches are quite as regular and well developed as those of the other bands and the Tables II and III show that the

[14] To give an example the value for δ given in Table V, is 1.067 for the 3530 band and 1.066 for the 3370 band. Although there may be an error of a few units of the last decimal in the absolute values of these constants, their difference 0.001 is accurate to a fraction of this value.

TABLE VI.

K	3530 obs.	3530 calc.	3390 obs.	3390 calc.	3260 obs.	3260 calc.	3430 obs.	3430 calc.	3295 obs.*	3295 calc.
3	92.32	92.18	91.58	91.62	91.17	91.17	90.47	90.47	86.44	86.44
4	122.98	122.91	122.06	122.07			121.39	120.53		115.16
5	153.66	153.64	152.44	152.43	151.64	151.67	152.89	150.51	142.24	143.79
6	184.45	184.37	182.59	182.69			186.62	180.38		
7	215.06	215.10	212.86	212.82	211.78	211.75	213.83	210.12	208.24	200.72
8			242.83	242.80						
9	276.35	276.55	272.62	272.61			273.75	269.14		
10			302.25	305.23						
11			331.61	331.63						

* Obtained from the zero lines of the sub-bands.

combination relations are fulfilled with the same accuracy as for the other bands. It is hard to imagine how all these regularities could be anything but genuine. We must have then here a perturbation of the rotational energy levels, as far as we know the first one of this type observed in a polyatomic molecule. The perturbation affects only the dependence of the energy levels on K.

The band at 3295A is a little less well developed than the other bands, and the regularities are less obvious. But also in this case we believe that the analysis presented here is essentially correct and that we have here a similar perturbation.

In order to clear up completely the nature of the perturbations further investigations are necessary which are still under way. The perturbations must originate from the interaction of the level in question with another level which is very close to it. This second level might be another vibrational level of the same electronic state, or might belong to a different electronic state. Because of the predissociation in the higher vibrational states we know that there is a second electronic state close to the upper state of our bands which is at least partly continuous. Whether this level is also responsible for the perturbations observed here is doubtful though not impossible.

The fact that the rotational levels of the upper state of the bands 3430 and 3295 do not follow a quadratic formula makes an accurate calculation of the constant γ impossible. As the figures on the preceding page show, the apparent value of $\gamma-\delta$ in 3430 decreases for decreasing values of K and if this decrease continues it seems plausible that the value for 4 $(\gamma-\delta)$ should be smaller than 30.19. For the band 3295 the value for $\gamma-\delta$ is also calculated from the lowest K available, but this is, of course, no guarantee that it is very close to the real value.

The zero lines

The wave numbers for the lines in the rR-branches can be written

$$rR(K_1J)=\nu_0+\gamma''+2K(\gamma''-\delta'')$$
$$-(\gamma''-\gamma'+\delta'-\delta'')(K+1)^2-\mu'(K+1)^4+\mu''K^4$$
$$+(2J+1)\delta_K''-(\delta_K''-\delta_{K+1}')(J+1)^2 \quad (13)$$

and, as all the other constants are known, ν_0 can be calculated with the help of this expression. In doing so it is most convenient to calculate first the zero lines of the individual sub-bands. The difference $(\delta''-\delta')$ is multiplied with much larger numbers than δ'' and should therefore be known with about the 20-fold accuracy. Therefore often a slight adjustment of $\delta''-\delta'$ is necessary in order to assure that the zero line calculated from the different lines of a branch has the same value. With such an adjustment it is not difficult to get a perfect agreement within the limits of experimental errors. Naturally for the bands 3430 and 3295 no accurate value for the zero lines can be obtained and the value given in Table V may be in error by several wave numbers.

The relations (1), (2) and (10) allow us to calculate the three principal moments of inertia, if γ and δ are known. We get, e.g., α as the positive root of the quadratic equation

$$\alpha^2-2(\gamma+\delta)\alpha+2\gamma\delta=0.$$

Finally the asymmetry constant b can be found from (4) which can be written

$$b=(\beta-\alpha)/2(\gamma-\delta)\leqq\delta^2/2\gamma.$$

§11. The Deviations from the Symmetrical Top

The deviations from the symmetrical top must be noticeable for small values of K. It is unfortunate that the lines due to the low K-transitions fall into the very crowded center region of the bands. Some of the strongest sub-bands are crowded together here. Each of these sub-bands is much richer in lines than those due to higher K-values, as fewer lines near the origin are missing. Besides, the P-, Q- and R-branches have much more nearly the same intensity and each line is split into a doublet. All this causes the structure in this part of the band to be extremely complex, many lines fall so close together that they cannot be separated and no obvious structure is apparent. For these reasons it is rather futile to attempt an analysis of this section. It is perfectly possible to find all the lines to be expected, but such an analysis would have very little value, as there would be no way to test its correctness. Because of the incomplete resolution one would have to allow much larger errors in the combination relations and the intensities would have no meaning. Under these conditions almost any expected arrangement of lines could be verified.

Only in the $4\rightarrow3$ and $2\rightarrow3$ sub-bands conditions are more favorable so that an unambiguous identification of the lines seems possible. Both are strong sub-bands, and both have still the symmetric top characteristics for small values of J. But if one tries to find the higher lines with the help of the symmetrical top formula, it appears that they show deviations from about $J=13$ in the $4\rightarrow3$ sub-band and from about $J=8$ in the $2\rightarrow3$ sub-band. As must be expected the lines become doublets of increasing width. As all the constants of the molecule are known, the position of the lines can be calculated with the help of the formulae for the asymmetrical top. But in order to obtain entirely unbiased results an empirical analysis was first attempted, and only after this was completed it was compared with the theoretical expectations. The procedure was as follows: The approximate positions for all the lines under the assumption that the molecule is strictly a symmetrical top were calculated. For high enough values of J, of course no lines were found in these positions, but there would be several lines near. As for all the bands the asymmetry is about the same, the deviations of the correct lines from their calculated positions should be about the same. Therefore the lines which showed about the same deviation from the calculated positions in all the bands were taken to be the correct ones. This allowed in general an unambiguous identification of the lines except near the end of the branches where the lines became too weak in some bands.

It is now necessary to investigate, how the lines found in this way without any assumption about the theoretical structure of the bands, fit into the theoretical scheme. In the $4\rightarrow3$ sub-band the doublet separation will be due almost entirely to the separation of the lower level (see Fig. 2) whereas in the $2\rightarrow3$ sub-bands the situation will be just the opposite. The Figs. 4 and 5 show, that in order to obtain the differences for the final state it is necessary to subtract the longer wave-length doublet component from the shorter wave-length one and *vice versa*, if the doublet separation of the upper levels is less than that of the lower ones. We have therefore, if the index 1 refers to the upper and the index 2 to the lower component of a given doublet level

$$\left.\begin{aligned} R_s(K,J)-Q_l(K,J+1)&=f_1(K,J+1)-f_2(K,J),\\ R_l(K,J)-Q_s(K,J+1)&=f_2(K,J+1)-f_1(K,J)\end{aligned}\right\} \tag{14}$$

independent on whether the electric moment is in the plane of the molecule or perpendicular to it. If the doublet separation in the upper level is bigger than in the lower one we have to take the differences

$$\left.\begin{aligned} Q_l(K,J)-P_l(K,J+1)&=f_1(K,J+1)-f_2(K,J),\\ Q_s(K,J)-P_s(K,J+1)&=f_2(K,J+1)-f_1(K,J).\end{aligned}\right\} \tag{15}$$

The right sides are correct if the electric moment is in the plane of the molecule (Fig. 4). If it is perpendicular to it, (Fig. 5) the indices 1 and 2 must be interchanged. The differences of the two Eqs. (15) give

$$P_s(K, J+1)-P_l(K, J+1)-[Q_s(K, J)-Q_l(K, J)]=\Delta P(K, J+1)-\Delta Q(K, J)$$
$$=f_1(K, J+1)-f_2(K, J+1)+f_1(K, J)-f_2(K, J).$$

TABLE VII. $\Delta f(3, J)+\Delta f(3, J+1)$.

	1. From 2→3 sub-band					2. From 4→3 sub-band							
J	3530	3390	3260	3430	3295	3530	3390	3260	3370	3430	Ave.$_1$	Ave.$_2$	Calc.
8	−0.01	−0.14	+0.07	0.11	—						0.01		0.02
9	+ .02	+ .11	− .01	.05	0.01						.04		.05
10	.04	—	+ .17	.28	.03						.10		.10
11	.24	.21	.23	.11	.13						.18		.17
12	.50	.33	.54	.32	.16						.37		.26
13	.62	.50	.59	.35		0.34	59	0.33	0.20	—	.52	0.37	.41
14	.57	.67	.75	.70		.66	—	72	.72	0.80	.67	.72	.62
15	.87	.96	1.01	.66		1.00	1.01	1.02	.90	1.01	.95	.99	.91
16	1.13	1.62				1.41	—		1.37	1.56		1.44	1.32
17						1.65	2.00			1.77		1.81	1.88
18						2.15				2.75			

TABLE VIII. *Doublet separation in the $K'=2\rightarrow K''=3$ sub-band.*

	pP-Branch						*pQ-Branch*					
J	3530	3390	3260	3430	3295	calc.	3530	3390	3260	3430	3295	calc.
7	0	0	0	0	0	0.10	0	0.15	0.15	0	0	0.20
8	0	0.15	0	0.15	0.17	.20	0.26	.35	.24	0.17	0.26	.33
9	0.25	.21	0.31	.28	.32	.34	.46	.36	.39	.32	.30	.51
10	.48	.47	.38	.37	.38	.55	.53	.52	.42	.38	.45	.74
11	.57	—	.59	.66	.66	.84	.73	.72	.61	.66	.56	1.03
12	.97	.93	.84	.77	.74	1.20	.95	1.01	.84	.74	.70	1.42
13	1.45	1.34	1.38	1.06	1.09	1.68	1.38	1.33	1.29	1.09	.91	1.88
14	2.00	1.83	1.88	1.44	1.37	2.29	1.84	1.72	1.65	1.37	1.32	2.40
15	2.43	2.39	2.40	2.07	1.99	3.04	2.30	2.10	1.72	1.99		3.00
16	3.17	3.06	2.73	2.65		3.92	2.92	2.55				3.64
17	4.05	4.17				4.96						

The right side, a positive quantity, is the sum of the doublet separations of two successive rotational levels. It would change its sign, if the electric momentum were not in the plane of the molecule, but perpendicular to it.

In the formaldehyde bands the doublet separation of the $pQ(3, J)$ lines is consistently smaller than that of the $pP(3, J+1)$ lines, which proves that for the electronic transition in question the resultant electric moment is in the plane of the molecule and perpendicular to the CO-axis.

In Table VII the sum of the doublet separations of two successive rotational levels is given for $K=3$ of the lower electronic level. The method of calculation is indicated by the heads of the table. In each of the values so obtained four lines are involved of which one or more, as a rule, are incompletely resolved. In view of this circumstance the rather large differences between the values of the individual bands is not surprising. The averages are compared with the theoretical values calculated with the value $b=0.0095$ given in Table V. The agreement is very satisfactory.

In Table VIII the observed doublet separations in the 2→3 sub-bands are compared with the theoretical ones. We have

$$\Delta pP(K, J)=\Delta F(K, J-1)+\Delta f(K, J),$$
$$\Delta pQ(K, J)=\Delta F(K, J)-\Delta f(K, J).$$

The calculated values are those for the band 3390. The values for the other bands should not be more than about 3 percent different. The

observed values are all systematically lower than the calculated ones. One would get agreement within the limits of experimental errors if the asymmetry constant were about $b=0.0073$ instead of 0.0083. We see, therefore, that although the general trend of the doublet separation agrees well within the theoretical one, there is a definite discrepancy in the exact numerical agreement. It is probable that the cause for this discrepancy is the same which produces the perturbations in the 4330 and 3295 bands. In the normal state where there is no such possibility for the interaction of different levels the agreement between the observed and theoretical values is entirely within the limits of experimental errors.

§12. The Shape of the Formaldehyde Molecule

From the values for the moments of inertia (see Table V) the shape of the formaldehyde molecule can be determined to a certain extent. A complete determination of the shape is not possible, as we have only two independent data, say the moments of inertia B and C (the third moment of inertia is not independent of the two others as it is given by the relation $A=B+C$) for the determination of the three quantities which determine the structure of the molecule. These three quantities are (see Fig. 1) the CO-distance a, the CH-distance r and the angle 2α between the two CH-bonds. If we call $u=r\sin\alpha$ and $v=r\cos\alpha$, we have

$$C=2m_{\mathrm{H}}u^2.$$

From the observed values of C we obtain for the distance $2u$ between the hydrogen atoms 1.88A for the normal state of the molecule and 1.95A cm for the excited state of 3530. In the normal hydrogen molecule the distance between the two H-atoms is 0.75A.

We have further

$$B=[m_{\mathrm{O}}(m_{\mathrm{C}}+2m_{\mathrm{H}})a^2+4m_{\mathrm{O}}m_{\mathrm{H}}av+2m_{\mathrm{H}}(m_{\mathrm{O}}+m_{\mathrm{C}})v^2]/M, \tag{16}$$

in which m_{O}, m_{C}, and m_{H} are the masses of the oxygen, carbon and hydrogen atoms and $M=m_{\mathrm{O}}+m_{\mathrm{C}}+2m_{\mathrm{H}}$ the total mass of the molecule. By substituting the values for the masses we obtain

$$B=7.471(a^2+0.2876\,av+0.2516\,v^2)m_1$$

in which $m_1=1.649\times10^{-24}$ g is the mass of an atom with atomic weight one.

It is necessary to know one of the two quantities a or v in order to determine the other one from this relation. If we assume that the angle 2α between the two CH-bonds is the tetrahedron angle (110°), $v=u\,\mathrm{ctg}\,\alpha=0.659$A. We obtain then for the CO-distance $a=1.185$A, and the CH-distance becomes $r=1.15$A. In the normal state of the CO-molecule the internuclear distance is 1.15A. It is perhaps better to compare the CO-distance in formaldehyde with that in CO_2, where it is 1.16A.[16] In almost all compounds the CH-distance is found to be about 1.1A (for the lowest state of the CH-molecule the internuclear distance is 1.13A). We see therefore that the dimensions obtained for the formaldehyde molecule are about what we should expect.

It is rather problematic whether we are justified in assuming that also in the excited state of formaldehyde the angle between the CH-bonds is about 110°. If we make this assumption nevertheless for want of something better, we get for the CO-distance $a=1.27$A and for the CH-distance 1.19A.

In §10 we saw that the centrifugal force due to the rotation about the CO-axis enlarges the distance between the two H-atoms. The amount of this centrifugal expansion depends on the strength of the CH-bond and the force between the two CH-bonds. A quantitative relation between the different constants involved can easily be obtained by the following simple calculation.

If we call x_1 a displacement of an H-atom from the equilibrium position in the direction of the CH-bond, and x_2 a displacement perpendicular to it, the restoring forces can be written f_1x_1 and $2f_2x_2$. (Both hydrogen atoms are affected in the same way.) If k is the angular momentum

[16] From the value $70.6\cdot10^{-40}$ g cm² for the moment of inertia given by Barker and Adel, Phys. Rev. **44**, 185 (1933).

about the CO-axis, ($k=Kh/2\pi$) the centrifugal force acting on a hydrogen atom is $k^2/2Cu$ and the equilibrium is determined by

$$\left.\begin{aligned} k^2/2Cu &= f_1x_1\sin\alpha+2f_2x_2\cos\alpha,\\ 0 &= f_1x_1\cos\alpha-2f_2x_2\sin\alpha,\\ x &= x_1\sin\alpha+x_2\cos\alpha, \end{aligned}\right\} \quad (17)$$

in which x is the increase in the distance u from the CO-axis. The potential energy is $f_1x_1^2+2f_2x_2^2$ and the kinetic energy in first approximation

$$k^2/2C=(k^2/2C_0)(1-2x/u_0);$$

therefore the total change in energy in first approximation

$$E=-\frac{k^2x}{C_0u_0}+f_1x_1^2+2f_2x_2^2$$
$$=-\frac{k^4m_H}{2C_0^3}\left(\frac{\sin^2\alpha}{f_1}+\frac{\cos^2\alpha}{2f_2}\right). \quad (18)$$

If we call $2\pi\omega_1=(f_1/m_H)^{\frac{1}{2}}$ and $2\pi\omega_2=(2f_2/m_H)^{\frac{1}{2}}$ we obtain

$$\Delta E/h=-\mu K^4 \quad (19)$$

with

$$\mu=4\gamma^3[(\sin^2\alpha)/\omega_1^2+(\cos^2\alpha)/\omega_2^2]. \quad (20)$$

ω_1 is the frequency with a force constant f_1 and a reduced mass m_H, ω_2 the frequency with f_2 as force constant and a reduced mass $\frac{1}{2}m_H$. For $\alpha=90°$ the expression for μ becomes the well-known expression for the diatomic molecule.

(20) can be used to obtain a rough value for the frequency ω_2, as the value for ω_1 is well known from Raman and infrared data of other molecules which contain a CH-bond. With the observed value 5.8×10^{-4} for μ and $\omega_1=3000$ cm^{-1}, we obtain $\omega_2=2000$ cm^{-1}. The accuracy of this value is not very great, probably not better than about 20 percent, but it seems to be definitely larger than the value generally assumed. With the above value for ω_2 it follows that the CH-force is about four times larger than the apparent force between the two hydrogen atoms.

In conclusion it is a great pleasure to express our sincere thanks to Mr. A. L. Loomis for his continued hospitality and the opportunity to use the facilities of his laboratory. We are also grateful to Mrs. Hildegard Kistiakowsky for her help with the wave-length calculations.

The Measurement of Natural Alpha-Particles Ejected from Solids

ROBLEY D. EVANS,* *Physics Department, University of California, Berkeley, California*

(Received August 24, 1933)

Exact expressions for the ionization due to the emission of alpha-particles from radioactive solids are set up and the results of their graphical integration are given. The total ionization per cm² of surface, both with and without absorbers; the variation of ionization with height above the radioactive surface; the ionization from thin films; the ionization from substances containing all members of the U, Th and Ac series, both with and without absorbers; and the counting rate for alpha-particle counting chambers, are given in equations accompanied by appropriate graphs and tables. The older approximate theories break down for actual alpha-particles, particularly those of short range. If q is ion pairs per cm² per sec. formed above the surface of a radioactive solid; N, the number of alpha-particles per sec. per cm³ emitted in the solid; k, ion pairs per alpha-particle of range R in air; and R', the alpha-particle range in the solid: then $q=\epsilon NkR'$, and the numerical coefficient ϵ has values between 0.114 and 0.150 for the alpha-particles from all known radioactive substances.

I. INTRODUCTION

TWENTY years ago McCoy,[1] v. Schweidler,[2] and Flamm[3] gave an approximate theory of the ionization above a solid radioactive body, due to its emission of alpha-particles. Their work was based on the assumption that the ionization produced by an alpha-particle of range R is $k_0R^{\frac{3}{2}}$, where k_0 is a constant. Although this expression is quite accurate for all the alpha-particles of the U, Th and Ac series, where $R>2.5$ cm of air, it breaks down seriously for shorter range alpha-particles, such as are being investigated by v. Hevesy, Pahl and Hosemann,[4] Latimer and Libby,[5] Langer and Raitt,[6] and Evans and Henderson[7] and it also fails for the short residual ends of originally long range alpha-particles emerging from solids such as ordinary rocks.[8] By combining the reliable empirical ionization curves for alpha-particles obtained by G. H. Henderson[9] and others,[10] with a new mode of analytical attack, an exact solution of the problems can now be given.

II. COMPARISON OF APPROXIMATE AND ACTUAL ALPHA-PARTICLE IONIZATION CURVES

If R is the range of an alpha-particle in air at 0°C and 760 mm Hg, and r is the distance, also expressed in cm of standard air, from the origin of the track to a point under consideration, then provided $R-r\geq 2.5$ cm, we have the approximate empirical law that the number of ion pairs, I,

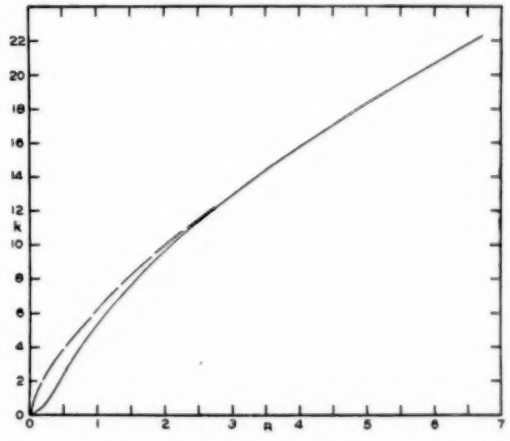

FIG. 1. The solid curve shows the empirical total ionization, k, per alpha-particle in ion pairs $\times 10^{-4}$, obtained by graphical integration over curve I of Fig. 4. The dotted curve shows the approximate value of the total ionization as given by the two-thirds power rule of Eq. (1). R is the range of the alpha-particle in cm of air at 0°C and 760 mm Hg.

* National Research Fellow.

[1] McCoy, Phys. Rev. **1**, 393 (1913).

[2] v. Schweidler, Phys. Zeits. **14**, 505, 728 (1913).

[3] Flamm, Phys. Zeits. **14**, 812, 1122 (1913).

[4] v. Hevesy, Pahl and Hosemann, Zeits. f. Physik **83**, 43 (1933).

[5] Latimer and Libby, J. Am. Chem. Soc. **55**, 433 (1933).

[6] Langer and Raitt, Phys. Rev. **43**, 585 (1933).

[7] Evans and Henderson, Phys. Rev. **44**, 59 (1933).

[8] Evans, Phys. Rev. **45**, 38 (1934).

[9] G. H. Henderson, Phil. Mag. **42**, 538 (1921).

[10] H. Geiger, Zeits. f. Physik **8**, 45 (1921); I. Curie and Behounek, J. de Physique **7**, 125 (1926); G. H. Briggs, Proc. Roy. Soc. **A114**, 341 (1927).

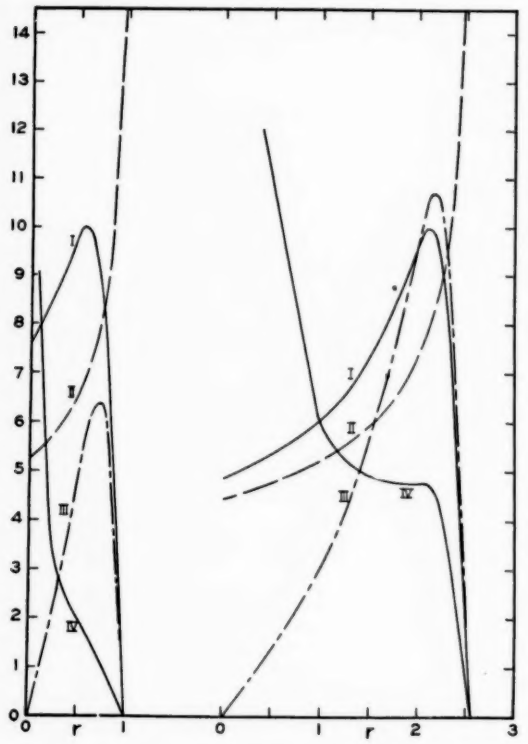

FIG. 2 FIG. 3

FIG. 2. The characteristic curves for a 1.0 cm alpha-particle in air at 0°C and 760 mm Hg. Curve I shows $\varphi(r)$, the Henderson empirical ionization per cm. Curve II shows $\Phi(r)$, the ionization per cm derived from the two-thirds power rule of Eq. (3). Curve III shows the function $r\,\varphi(r)$ and curve IV the function $1/r\,\varphi(r)$ of Eq. (6). The ordinates, on the same scale for all curves, are arbitrary. Abscissas are in cm at 0°C and 760 mm Hg.

FIG. 3. The characteristic curves for the 2.56 cm alpha-particles from U I. As in Fig. 2, curve I is $\varphi(r)$, curve II is $\Phi(r)$, curve III is $r\,\varphi(r)$, curve IV is $(1/r)\varphi(r)$. The numerical value of the ordinates for curve III are twice those shown on the scale. The areas under curves I and II are equal. Abscissas are in cm at 0°C and 760 mm Hg.

produced between r and the end of the track is

$$I=k_0(R-r)^{\frac{3}{2}} \tag{1}$$

where k_0 is a constant. The ionization per unit length of path, $\Phi(r)$, at any r is therefore

$$\Phi(r)=-\partial I/\partial r=(2/3)k_0(R-r)^{-\frac{1}{2}} \tag{2}$$

and if K is the number of ion pairs produced along the entire track from $r=0$ to $r=R$, then $K=k_0R^{\frac{3}{2}}$, and

$$\Phi(r)=(2/3)KR^{-\frac{3}{2}}(R-r)^{-\frac{1}{2}}. \tag{3}$$

This approximate expression has been used by Siegl[11] and others; it will be compared with the experimental ionization-density, $\varphi(r)$, *vs.* r curves. In the computations described below, Henderson's ionization-density *vs.* r curve for Ra C′ has been taken as accurately representing the number of ion pairs per cm, $\varphi(r)$, produced at any distance $R-r$ from the end of any alpha-particle track. The total ionization due to short range alpha-particles is obtained by graphical integration of the end portion of this $\varphi(r)$ *vs.* r curve.

Fig. 1 compares this empirical total ionization, k, with the approximate values, K, computed from the equation $K=k_0R^{\frac{3}{2}}$, k_0 being chosen to make the curves coincide at $R=6.59$ cm, Henderson's value for Ra C′ alpha-particles at 0°C and 760 mm Hg. The approximate and empirical curves agree for $R>2.56$ cm, the shortest (uranium-I) alpha-particle in the U, Th or Ac series, but K is 16 percent high for $R=1$ cm (samarium[4]), and 100 percent high for $R=0.4$ cm.

Figs. 2, 3, 4 illustrate the contrast between the empirical ionization-density curve, $\varphi(r)$, and the approximate analytic expression $\Phi(r)$, for alpha-particles of 1 cm (Sm, Be?), 2.56 cm (U I), and

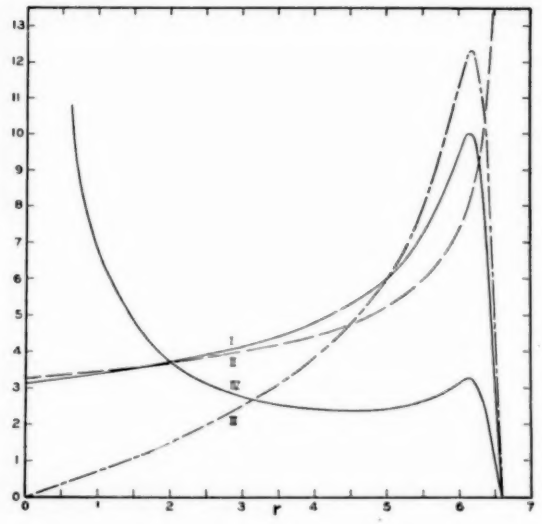

FIG. 4. The characteristic curves for the 6.60 cm alpha-particles from Ra C′. Curve I is Henderson's[9] empirical ionization curve. As in Fig. 2, curve I is $\varphi(r)$, curve II is $\Phi(r)$, curve III is $r\varphi(r)$, curve IV is $(1/r)\varphi(r)$. The ordinates are arbitrary for curve I; for curve II read ordinates as shown; for curve III multiply ordinates by 5; for curve IV multiply ordinates by 0.5. The area under curves I and II are equal. Abscissas are in cm at 0°C and 760 mm Hg.

[11] Siegl, Akad. Wiss. Wien, Ber. IIa **134**, 11 (1925).

6.59 cm (Ra C′) range. The ordinates are adjusted so that the areas under the $\varphi(r)$ and $\Phi(r)$ curves are identical, i.e., $K=k$. It is evident that agreement between $\varphi(r)$ and $\Phi(r)$ is not even remote, except in the Ra C′ curve for $r \leq 0.6\ R$.

III. Total Ionization above a Thick Solid Emitting Alpha-Particles

As here used, a thick plate is one whose thickness is greater than the range, R', of the alpha-particle in the solid, while a thin plate has a thickness less than R'. In Fig. 5, let AA' be the

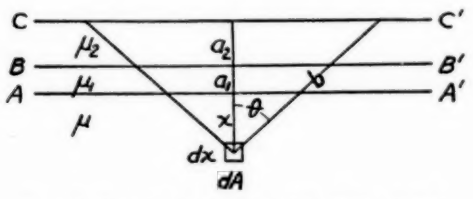

FIG. 5. Geometry for Eqs. (6), (9) and (10).

interface between a thick solid body of infinite extent emitting N alpha-particles per cm³ per sec., and an absorber of thickness a_1, above it. Similarly, let BB' be the interface between this first absorber and a second absorber of thickness a_2, and let CC' be the boundary between the second absorber and an ionization chamber. Let the stopping power of the air relative to the solid, i.e., the ratio of the alpha-particle range in the solid to its range in air, be μ for the radioactive source, μ_1 for the first absorber, μ_2 for the second absorber.

From geometry, the number of alpha-particles from a volume element $dx\,dA$ which spend the portion of their range between r and $r+dr$ above the interface CC', is the number of alpha-particles formed in the volume element $dx\,dA$, times the solid angle for emergence, or

$$[N\,dx\,dA]\left[\frac{1}{2}\left(1-\frac{x+a_1+a_2}{b}\right)\right],$$

where b is the geometrical length corresponding to a path equivalent to r cm of air. Thus $b\cos\vartheta = x+a_1+a_2$, while $r\cos\vartheta = x/\mu+a_1/\mu_1+a_2/\mu_2$, and hence $b=r(x+a_1+a_2)/(x/\mu+a_1/\mu_1+a_2/\mu_2)$. The total number, n_a, of alpha-particles per cm² of surface with the range-element between r and $r+dr$ above the interface CC', is:

$$n_a=\frac{N}{2}\int_0^{\mu(r-a_1/\mu_1-a_2/\mu_2)} 1-\frac{(x/\mu+a_1/\mu_1+a_2/\mu_2)}{r}dx \quad (4)$$

$$=\frac{N}{4}\mu(r-a)^2/r, \text{ where } a\equiv a_1/\mu_1+a_2/\mu_2+\cdots, \quad (5)$$

a being the total absorber thickness, measured in equivalent cm of air. Since the stopping power varies slightly[12] with the velocity of the alpha-particle the values of μ, μ_1, μ_2, $\cdots$ chosen for numerical work may be taken as the mean values for the range under consideration. Eq. (5) is easily generalized for any number of absorbers.

The ionization, q_a, in ion pairs per cm² per sec. due to these emergent alpha-particles is

$$q_a=\int_a^R n_a\varphi(r)dr$$

$$=\frac{N}{4}\mu\left\{\int_a^R r\varphi(r)dr-2a\int_a^R\varphi(r)dr+a^2\int_a^R\frac{1}{r}\varphi(r)dr\right\} \quad (6)$$

$$\equiv\epsilon_a kRN\mu, \quad (7)$$

where the dimensionless numerical coefficient ϵ_a is defined by Eqs. (6) and (7).

Graphical integration of Eq. (6) shows that ϵ_a depends upon R in the manner shown in Figs. 6 and 7. With no absorption (i.e., $a=0$; $\epsilon_a\equiv\epsilon$) Fig. 6 shows that ϵ is always less than 0.150, and falls to low values for short range alpha-particles. The ratio ϵ_a/ϵ, or q_a/q, is the fraction of the total ionization appearing above an absorber having a stopping power equal to a cm of air. This ratio is also a function of R and is shown in Fig. 7.

[12] Harper and Salaman, Proc. Roy. Soc. **A127**, 175 (1930).

In the limiting case of a very long range alpha-particle Eqs. (1) and (3), describing the two-thirds power rule, give nearly the same result as the exact theory. Substituting $\Phi(r)$ from Eq. (3) for $\varphi(r)$ in Eq. (6), and integrating, we obtain

$$q_a=\frac{3}{20}NKR\left\{\left(1-\frac{a}{R}\right)^{\frac{5}{3}}-\frac{5}{3}\frac{a}{R}\left(1-\frac{a}{R}\right)^{\frac{2}{3}}+\frac{5}{9}\frac{a^2}{R^2}\log\frac{1+(1-a/R)^{\frac{1}{3}}+(1-a/R)^{\frac{2}{3}}}{a^2/R^2}\right.$$
$$\left.-\frac{10}{9}3^{\frac{1}{2}}\frac{a^2}{R^2}\left[\tan^{-1}\frac{2(1-a/R)^{\frac{1}{3}}+1}{3^{\frac{1}{2}}}-\tan^{-1}\frac{1}{3^{\frac{1}{2}}}\right]\right\}. \quad (8)$$

Eq. (8) corresponds to the solutions of McCoy,[1] v. Schweidler[2] and Flamm[3] and is plotted on Figs. 6 and 7 for comparison with the exact result of Eq. (6). When $a=0$, Eq. (8) gives $\epsilon=0.150$, whereas the true value of ϵ is always lower; see Fig. 6.

Fig. 8 shows the ionization factor $\epsilon_a kR$ for all known alpha-particles. Three absorbers $a=0$, $a=0.5$ cm, $a=1.63$ cm of air at 0°C and 760 m Hg are considered. The factor $\epsilon_a kR$ is a direct measure of the ionization as a function of R above sources having the same N and μ. Such a case is presented when a single source contains several radioactive substances in equilibrium, e.g., an igneous rock source which contains all members of the U, Ac and Th series.

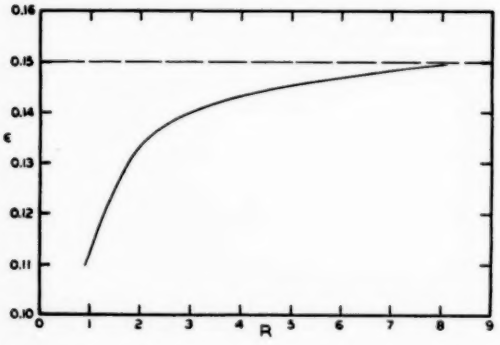

FIG. 6. The solid curve is the empirical value of ϵ, the coefficient of Eq. (7), as a function of the range, R, of the alpha-particle in air at 0°C and 760 mm Hg. The dotted line is the value of ϵ given by the approximate theory of Eq. (8), employing the two-thirds power rule of Eqs. (1) and (3).

IV. Stratification of Ionization above a Thick Plate

The total ionization to any height above a thick source may be derived from the results of Section III. The ionization chamber, of thickness a' is regarded as an additional absorber. The ionization measured in it is the ionization lost in an additional absorber of thickness a', or $q_a-q_{a+a'}$. The fraction of the total available ionization which is observed in the chamber is then $q_a/q-q_{a+a'}/q$. Numerical values, for alpha-particles of any range, R, may be read from Fig. 7. For the special case in which $a=0$, the fractional ionization absorbed in the chamber is $1-q_{a'}/q$. Ordinates corresponding to this case are shown at the right side of Fig. 7.

The exact nature of the variation of ionization with distance is important in measurements on very feeble sources, such as rocks, where the ionization chamber must be made as shallow as possible, so that its background ionization from cosmic and local radiation will be sufficiently low.

V. Ionization above Thin Sources

The ionization above a thick source may be thought of as composed of two parts: first, the ionization from a thin surface layer; second, the ionization from below this layer. The ionization from below equals that due to a thick source surmounted by the thin surface layer acting as an absorber. The equations are therefore the same as those of the preceding section. The total ionization from a thin layer of thickness a is $q-q_a$, hence the fractional ionization relative to that from a thick source is $1-q_a/q$; these values are shown as ordinates on the right side of Fig. 7.

VI. Counting Individual Alpha-Particles

In examining weak sources it is sometimes more convenient to count individual alpha-particles than to measure the ionization current produced by them. Several devices, aside from cloud chambers, are available for such measure-

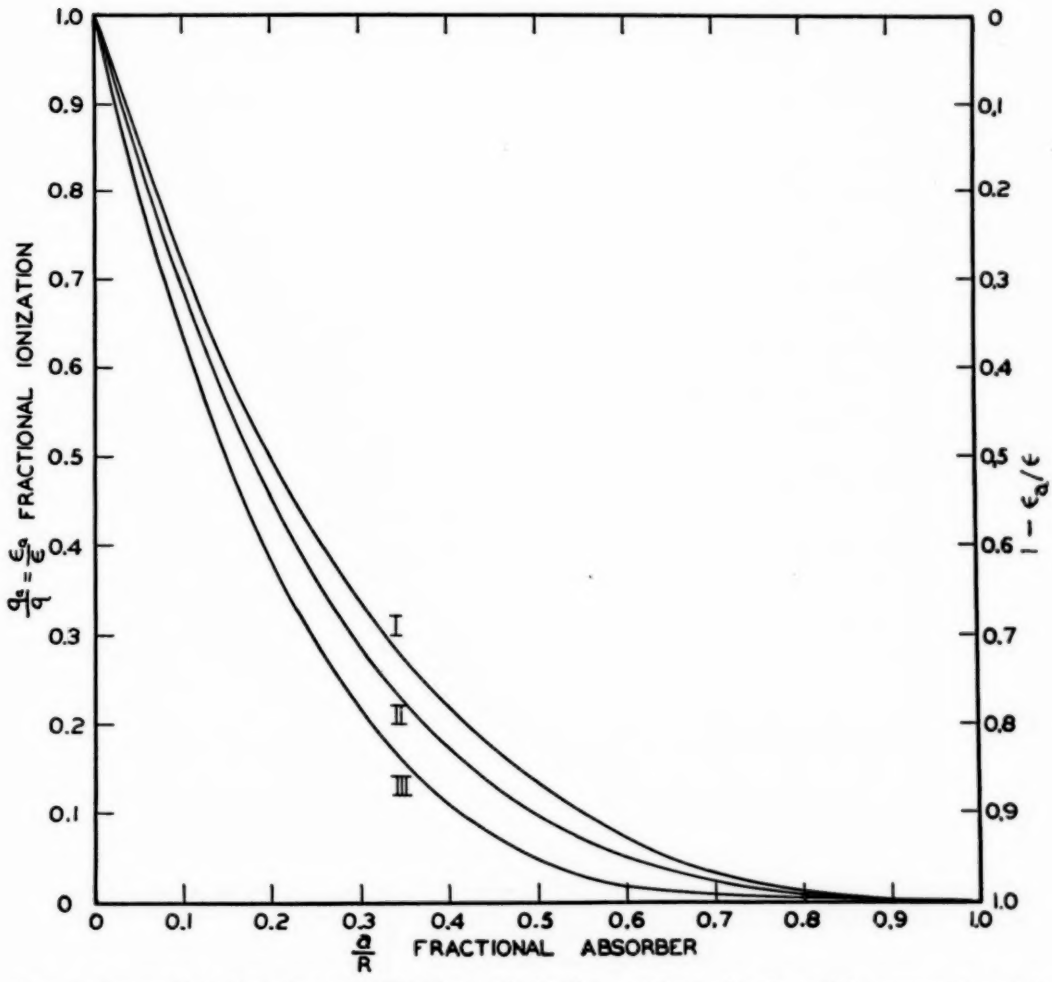

FIG. 7. Curves for absorption, stratification of ionization, and ionization from thin sources, for alpha-particles. Ordinates at the left, q_a/q or ϵ_a/ϵ, show the fraction of the maximum ionization which remains above the absorber; see Section III of the text. The ordinates at the right are $1-\epsilon_a/\epsilon$; see Sections IV and V of the text. Curve I is for long range alpha-particles; the computed values from the exact theory for 6.6 cm alpha-particles coincide with the values from the approximate theory of Eq. (8). Curve II is for the 2.56 cm alpha-particles from U I. Curve III is for 1.0 cm alpha-particles.

ments.[13] Where the alpha-particle pulse counter is an air-filled ionization chamber connected to a linear amplifier, it is possible to recognize a particle whose path in the ionization chamber is 0.2 cm or greater. If we designate this minimum track length for detection as ρ cm of air, then the following analysis applies.

In Fig. 5 let the source have a thickness μd and hence be equivalent in stopping power to d cm of air. The number of particles per cm² of surface which spend their range beyond r in the counting apparatus and hence emerge from the interface CC' with residual ranges $\rho \geq R-r$ is given by integrating Eq. (4) between the limits $x=0$ and $x=\mu d$, and making the substitution $r \equiv R-\rho$. This is:

$$n_a = (N\mu d/4)\cdot[2(R-\rho-a)-d]/(R-\rho), \quad (9)$$

which is the counting rate for thin films surmounted by absorbers.

For thick films, d has its maximum value which is $d=r-a=R-\rho-a$; substituting in Eq.

[13] Greinacher, Zeits. f. Physik **36**, 364 (1926); **44**, 319 (1927). Wynn-Williams and Ward, Proc. Roy. Soc. **A131**, 391 (1931). Curtiss, Bur. Standards J. Research **9**, 115 (1932). Bearden, Rev. Sci. Inst. **4**, 271 (1933). Hafstad, Phys. Rev. **44**, 201 (1933).

(9) we have the counting rate for thick films:

$$n_a=(N\mu/4)\cdot(R-\rho-a)^2/(R-\rho). \qquad (10)$$

As an example consider counting the 1.13 cm alpha-particles from samarium.[4, 5] If the emitter is a block of samarium sulfate, $Sm_2(SO_4)_3\cdot 8H_2O$, then the Bragg-Kleeman rule gives $\mu=3.49\times10^{-4}$. Having a density of 2.93 g per cm³, the material should emit[4] 90 alpha-particles per cm³ per sec. If the counting chamber is separated from the source by 1 mm of air, then $a=0.1$ cm, and if residual ranges of 2 mm or greater will operate the counter, then $\rho=0.2$ cm. Substituting in Eq. (10), we find 0.35 counts per cm² per min. In determining the effective area, the counting chamber's geometry must be considered.

VII. Corrections for Straggling

The use of the extrapolated ionization curve of Fig. 4 automatically corrects the ionization Eq. (6) for straggling.

The probability, P_l, that the range-element r, (measured from the origin of the track, in equivalent cm of air) will be lengthened or shortened by l cm is

$$P_l=(1/\rho_3 r\pi^{\frac{1}{2}})e^{-l^2/\rho_3^2 r^2}.$$

Eqs. (9) and (10), for counting individual particles, are corrected for straggling by integrating the above error function describing straggling over the appropriate solid angles. Since the error function is symmetrical, the gain due to straggling is only slightly less than the loss. Detailed treatment shows that the fractional loss, $\Delta n/n$, of countable particles is:

$$\Delta n/n=\tfrac{1}{2}(\rho_3)^2, \qquad (11)$$

where the fourth power of ρ_3 is neglected, and $\rho_3 r$ is the usual straggling or distribution coefficient. Briggs[14] has determined ρ_3 experimentally at various points along the range of Ra C′ alpha-particles, finding values between 0.0778 at $r=0.5$ cm and 0.0177 at 6.5 cm. The maximum loss in counting rate due to straggling is therefore only 0.3 percent. Strictly, the range employed in Eqs. (9) and (10) for counting alpha-particles is the most probable range, which, according to Kurie's[15] analysis of Briggs[14] data, is shorter than the usual extrapolated ionization range by $0.042\ (R-1.51)^{\frac{1}{2}}$ cm.

[14] Briggs, Proc. Roy. Soc **A114**, 313 (1927).
[15] Kurie, Phys. Rev. **41**, 701 (1932).

VIII. Total Ionization above Plates with Mixed Ranges

In considering the radiation from polished surfaces of ordinary rocks, we deal with the integrated effect of all the different alpha-particles of the U, Th and Ac series. If no absorber is used, $a=0$, $q_a\equiv q$, $\epsilon_a\equiv\epsilon$, and for the uranium series Eq. (7) becomes:

$$q^U=N^U\sum\epsilon kR\mu, \qquad (12)$$

where the summation extends over all the alpha-ray emitting elements in the uranium series, and is evaluated with the aid of Figs. 1 and 6. Similar expressions may be written for the thorium and actinium series.

For every element which has been proved to emit alpha-rays, Table I gives the extrapolated ionization range, $R_{15°}$, in air at 15°C, 760 mm; the

Table I. *Extrapolated ionization range, ionization, ϵ, and ionization factor for all known alpha-particles.*

Element	$R_{15°}$	R	$k\times10^5$	ϵ	$\epsilon kR\times10^5$	$\Sigma\epsilon kR$
U I	2.70	2.56	1.17	0.138	0.41	
U II	3.28	3.11	1.33	0.140	0.58	
Io	3.19	3.03	1.31	0.140	0.55	
Ra	3.39	3.21	1.36	0.141	0.62	corrected for C, C′, C″ branching
Rn	4.12	3.91	1.55	0.143	0.87	
Ra A	4.72	4.48	1.70	0.144	1.10	
Ra C	4.14	3.92	1.56	0.143	0.87	
Ra C′	6.97	6.60	2.20	0.148	2.15	
Ra F	3.92	3.72	1.50	0.142	0.79	
U series						7.07×10^5
Th	2.90	2.75	1.22	0.139	0.47	
Rd Th	4.02	3.81	1.53	0.143	0.83	
Th X	4.35	4.12	1.61	0.144	0.96	
Tn	5.06	4.80	1.78	0.145	1.24	
Th A	5.68	5.39	1.92	0.146	1.51	
Th C	4.79	4.54	1.71	0.144	1.12	
Th C′	8.62	8.17	2.54	0.150	3.11	
Th series						7.42×10^5
Ac U	3.2(?)	3.0	1.31	0.140	0.54	
Pa	3.67	3.48	1.43	0.142	0.71	
Rd Ac	4.68	4.43	1.69	0.144	1.08	
Ac X	4.37	4.14	1.62	0.143	0.96	
An	5.79	5.49	1.95	0.146	1.57	
Ac A	6.58	6.24	2.12	0.147	1.95	
Ac C	5.51	5.22	1.89	0.146	1.44	
Ac C′	6.5	6.2	2.10	0.147	1.92	
Ac series						8.25×10^5
Sm	1.13	1.06	0.56	0.114	0.068	

range, R, at 0°C, 760 mm; the total ionization, k, per alpha-particle; the coefficient ϵ of Eq. (7); and the ionization factor ϵkR. The last column gives $\sum \epsilon kR$ for the U, Th and Ac series, where the branching ratios of the C, C′ and C″ bodies have been taken into account in making the summation. The range of the actinouranium (Ac U) alpha-particle was estimated from the half-value period given by v. Grosse,[16] combined with the Geiger-Nuttall relation by using Geiger's values for the Ac series.[10]

The stopping power of rocks relative to air at 0°C and 760 mm depends on the composition of the rock, in accord with the Bragg-Kleeman rule. We can form an independent estimate of μ for rocks from measurements of the radius of the Ra C′ pleochroic halo ring, which has values between 28 and 34×10^{-4} cm in various minerals.[17] Taking 31×10^{-4} cm as an average value, we find $\mu=4.7\times10^{-4}$, and this is in fair agreement with the value computed from the chemical composition, using the Bragg-Kleeman rule.

If U is the concentration of uranium I in g per g of rock, and d the density of the rock, then since the decay constant[18] $\lambda_{U\,I}$ is 4.77×10^{-18} sec.$^{-1}$, and the atomic weight 238.14, we can express N^U, the number of uranium-I alpha-particles per cm^3 of rock per sec., as

$$N^U = \mathrm{U}\cdot d\cdot\frac{6.06\times10^{23}\times4.77\times10^{-18}}{238.14} = 1.22\times10^4\ \mathrm{U}\cdot d. \quad (13)$$

Similarly we find for N^{Th}, the number of thorium alpha-particles per cm^3 of rock per sec.,

$$N^{Th} = \mathrm{Th}\cdot d\cdot\frac{6.06\times10^{23}\times1.2\times10^{-18}}{232.12} = 0.31\times10^4\ \mathrm{Th}\cdot d, \quad (14)$$

where Th is the concentration of thorium in g per g of rock. For the actinium series, whose parent is Ac U, an isotope of U I, we take the activity ratio of v. Grosse;[16] thus 0.04 alpha-particles from Ac U accompany each alpha-particle from U I, hence:

$$N^{Ac} = 0.04\ N^U = 0.05\times10^4\ \mathrm{U}\cdot d. \quad (15)$$

Combining Eqs. (12) to (15) with the data of Table I, then taking $\mu=4.7\times10^{-4}$ we find

$$q^U = 8.62\times10^9\mu\mathrm{U}\cdot d = 4.06\times10^6\ \mathrm{U}\cdot d, \quad (16)$$
$$q^{Ac} = 0.43\times10^9\mu\mathrm{U}\cdot d = 0.20\times10^6\ \mathrm{U}\cdot d,$$
$$q^{Th} = 2.30\times10^9\mu\mathrm{Th}\cdot d = 1.08\times10^6\ \mathrm{Th}\cdot d.$$

Since ordinary granites have a uranium content of *ca.* 3×10^{-6} g U per g, a thorium content of *ca.* 6×10^{-6} g Th per g, and a density of *ca.* 2.7 g per cm^3, the total ionization is $\sum q = q^U+q^{Ac}+q^{Th} = 32.8+1.6+17.5 = 51.9$ ion pairs per cm^2 of rock surface per second. Where a shallow ionization chamber is employed, this alpha-ray ionization will more than double the background ionization from cosmic and local gamma-radiation, and is therefore within the range of modern apparatus. The saturation current is the order of 10^{-15} amp. per 100 cm^2 of rock.

The ranges given in Table I are those of Rutherford, Chadwick and Ellis.[19] Recent determinations by various workers, as summarized by Kurie and Knopf,[20] suggest no striking changes. The decay constant, 1.2×10^{-18} sec.$^{-1}$, for Th is that of the International Radium-Standards Commission.[21] If the higher value of 1.7×10^{-18} sec.$^{-1}$ found by Geiger and Rutherford[22] is taken, then the numerical constant of Eq. (14) *et seq.* would be correspondingly modified. The actinium series branching ratio is taken[16] as 0.04 in Eqs. (15) and (16). If the lower value of 0.03 as obtained by Hahn and Meitner,[23] who used tantalum for the separation of protactinium, is employed, then the numerical coefficient of Eq. (15) and of the actinium member of Eq. (16) would be reduced correspondingly.

[16] A. v. Grosse, Phys. Rev. **42**, 565 (1932).

[17] Holmes, Nat. Res. Council, Bull. **80**, 162 (1931).

[18] Kovarik and Adams, Phys. Rev. **40**, 718 (1932) give $\lambda_{U\,I}=4.865\times10^{-18}$ sec.$^{-1}$. When corrected for AcU, this value becomes 4.77×10^{-18} sec.$^{-1}$.

[19] Rutherford, Chadwick and Ellis, *Radiations from Radioactive Substances* pp. 24–27 (1930).

[20] Kurie and Knopf, Phys. Rev. **43**, 311 (1933).

[21] Rev. Mod. Phys. **3**, 427 (1931).

[22] Geiger and Rutherford, Phil. Mag. **20**, 691 (1910).

[23] Hahn and Meitner, Phys. Zeits. **20**, 529 (1919); Zeits. f. Physik **8**, 202 (1922).

IX. Total Ionization above Plates with Mixed Ranges and Surmounted by Absorbers

In measuring the ionization above say 100 cm² of polished rock surface, the specimen cannot be placed inside the ionization chamber, both because of its size and because of the distortion it would produce in the electrostatic ion-collecting field with a resultant influence on the relative saturation of the ion current. If the rock surface is brought close to a thin aluminum foil window in the ionization chamber, and if the total stopping power of the window and air between the rock surface and the inside of the ionization chamber is equivalent to a cm of air at 0°C and 760 mm, then a/R can be computed for each alpha-particle range involved. Fig. 7 then gives ϵ_a/ϵ, and combined with the values of ϵkR from Table I we can easily evaluate the total ionization, q_a, per cm² per sec. for each radiaoctive element, using Eq. (7). Fig. 8 shows the value of the ionization factor $\epsilon_a kR$ for all values of R and for $a=0$ (no absorber); $a=0.5$ cm air-equivalent at 0°C, 760 mm; and $a=1.63$ cm air-equivalent at 0°C, 760 mm. For the present case, with absorption, Eq. (12) becomes

$$q_a{}^{U} = N^{U}\Sigma\epsilon_a kR\mu \qquad (17)$$

with similar equations for the thorium and actinium series. Tabulating $\epsilon_a kR$ from Fig. 8, and summing over each of the radioactive series, we obtain the values shown in Table II for the

Table II. *Series ionization factors and relative ionization for U, Th, Ac series and Sm, with and without absorbers.*

	$a=0$		$a=0.5$ cm air 0°C, 760 mm		$a=1.63$ cm air 0°C, 760 mm	
	$10^{-5}\Sigma\epsilon kR$	q/q	$10^{-5}\Sigma\epsilon_a kR$	q_a/q	$10^{-5}\Sigma\epsilon_a kR$	q_a/q
U series	7.07	1.00	4.58	0.65	1.60	0.23
Th series	7.42	1.00	5.23	0.70	2.27	0.31
Ac series	8.25	1.00	5.72	0.69	2.30	0.28
Sm	0.068	1.00	0.0041	0.06	0	0

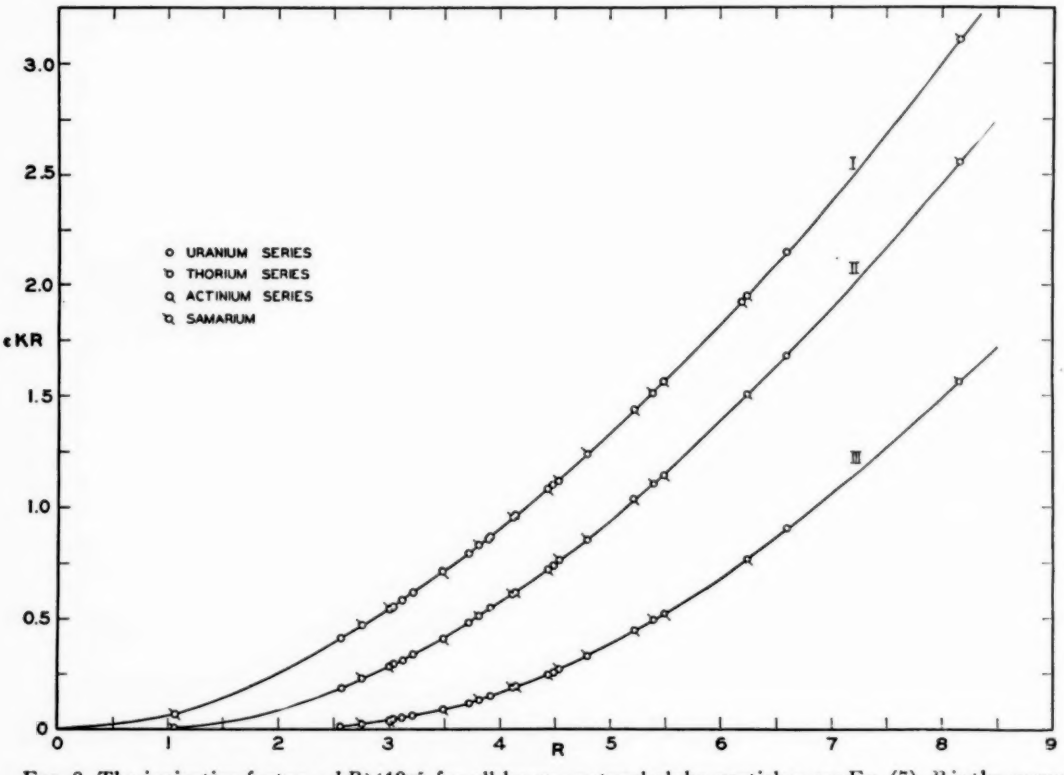

Fig. 8. The ionization factor, $\epsilon_a kR\times10^{-5}$, for all known natural alpha-particles; see Eq. (7). R is the range of the alpha-particle in cm of air at 0°C and 760 mm Hg. Curve I shows ϵkR (no absorber). Curve II shows $\epsilon_a kR$ with an absorber of 0.5 cm air-equivalent at 0°C and 760 mm Hg. Curve III shows $\epsilon_a kR$ when $a=1.63$ cm air-equivalent. Intermediate values for other absorbers may be obtained by interpolation or by computation from Figs. 1, 6 and 7.

series ionization factor $\sum \epsilon_a k R$, and for the fraction, q_a/q, of the total ionization from the radioactive surface which is able to penetrate the absorber and appear in the ionization chamber. It will be noted that, when radioactive equilibrium exists, the uranium series is more strongly absorbed by a given absorber than is the actinium series, and that the thorium series is absorbed the least of the three. This is due, of course, to the longer ranges of many of the thorium series alpha-particles. The difference in absorbability between the U, Th and Ac series is, however, not great enough to afford a means of separating these effects and determining, from absorption measurements, both the uranium and thorium content of feebly radioactive materials.

The Radioactive Radiations from the Surfaces of Solids and the Measurement of the Thorium Content of Rocks

ROBLEY D. EVANS,* *Department of Physics, University of California, Berkeley, California*

(Received August 24, 1933)

Ordinary granite, containing *ca.* 3×10^{-6} g U per g and *ca.* 6×10^{-6} g Th per g of rock, will support an ionization current of *ca.* 10^{-15} ampere per 100 cm² of polished rock surface. About 90 percent of this ionization is due to alpha-rays from the rock, and about 10 percent to beta-rays. From hand specimens the gamma-radiation is too feeble to operate an ionization chamber, but can be measured with a Geiger-Müller tube-counter. Observations of the surface ionization due to alpha-rays, or of the gamma-ray activity with the tube-counter, represent the combined effect of the uranium, actinium and thorium series. They can be corrected for the effects of the uranium and actinium series by employing emanation measurements, and thus the thorium content of ordinary rocks may be obtained. Important applications lie in the field of geophysics and in certain cosmic-ray problems.

INTRODUCTION

FURTHER significant advances in such problems as the age of ordinary terrestrial rocks, the age of meteorites, the correlation of unshielded cosmic ray electroscope readings with the radioactive content of the surrounding rocks or soil, and the problem of the earth's heat, now wait upon the development of a reliable technique for determining the thorium content of ordinary rocks. The related problem of determining the radium or uranium in ordinary rocks, has been satisfactorily solved by methods involving the removal of radon from the rock, followed by accurate measurements of the *ca.* 10^{-18} g of radon so obtained. Because the half-period of thoron is some 6000 times shorter than that of radon, emanation methods encounter new difficulties when applied to the measurement of minute quantities of thorium. These difficulties are not prohibitive, however, and experiments now in progress indicate that the direct-fusion furnace technique,[1] combined with a gas flow procedure, will be sufficiently sensitive to make reliable measurements possible. The thoron from a few milligrams of monazite sand can be easily and accurately measured in this manner.

The gamma-radiation from two or three hundred grams of ordinary granite is too feeble to compare favorably with the cosmic and local radiation in an ordinary ionization chamber, but if a Geiger-Müller tube counter is employed the rock radiation can be easily detected above the background count. We find that 300 g of granite containing 1.5×10^{-12} g Ra per g will nearly double the background counting rate. The increased counting rate is not due to the uranium series alone, but is in part due to the thorium series, and the total effect is scarcely strong enough to permit reliable separation of the thorium and uranium series effects by means of absorption measurements. Work in progress indicates, however, that when combined with independent measurements of the uranium content, by the direct-fusion technique, the tube-counter measurements will give significant information on the thorium content of ordinary rocks. It may be pointed out that Vogt's[2] measurement of the radium content of rocks by means of a tube-counter, involves the tacit but basic assumption that the ratio of thorium to uranium is constant in ordinary rocks. Probably this is approximately true where the acidity of all the specimens is the same, but for the range of rocks from granites to basalts there is evidence that the thorium-uranium ratio may vary between 1.0 and 2.5.

Radioactive *ores*, such as carnotite, usually lose a large fraction of their radon to the surrounding air. The fraction lost is called the "emanating power." In investigations of the radium content

* National Research Fellow.

[1] Evans, Rev. Sci. Inst. **4**, 223 (1933).

[2] W. Vogt, Phys. Zeits. **34**, 79 (1933).

of a wide variety of rock specimens, the writer has studied the emanating power of these materials when ground to pass a 60-mesh screen. From granites to basic lavas and volcanic pumice, no igneous rocks were found to lose to the air a measurable amount of their radon. Two limestone specimens had an emanating power of 15 percent at room temperature. Rocks whose emanating power is zero are of the type discussed elsewhere;[3] in them the entire radioactive series is in equilibrium, and the alpha-particles emitted from smooth surfaces of such rocks produce a measurable ionization in the air near their surface. The equations describing this ionization can easily be modified to include the rare cases having an appreciable emanating power. In the experiments described below, the alpha-, beta-, and gamma-radiation from the surface of artificially prepared rocks is studied, with results confirming the theoretical treatment[3] and indicating that the effects are due almost wholly to alpha-radiation, in disagreement with the conclusions of Gräven,[4] who attributed similar effects to gamma-radiations.

Apparatus

Artificial rocks were used to provide conveniently shaped sources with smooth surfaces and known uranium and thorium contents. These sources were prepared by thoroughly mixing known amounts of finely powdered radioactive minerals with anhydrous calcium sulfate, then adding water and casting the resulting plaster of Paris source in shallow paper tubing moulds, 10 cm in diameter. The standard uranium mineral is carnotite containing 1.58 percent uranium. Its radium content was determined by the direct-fusion method, and comparison with Ledoux and Company's uranium analysis shows that the radium-uranium ratio is correct, hence the uranium series is in equilibrium, a condition which does not always hold for randomly selected carnotites.[5] The thorium mineral is a monazite sand containing 5.1 percent thorium. Radioactive equilibrium is assumed. Taking the formula for the finished dry casts as $CaSO_4 \cdot 2H_2O$, the uranium sources contain 2.53×10^{-5} g U per g, and the thorium sources contain 4.1×10^{-5} g Th per g. A second set of sources containing one-tenth of these concentrations was also prepared. Duplicate sets were made in thicknesses of 0.4 and 1.1 cm, all 10 cm in diameter. Blank sets, containing no radioactive material, were prepared in the same sizes.

The radiation from the surface of these sources is measured in a horizontal cylindrical electroscope 10 cm in diameter and 10 cm long, provided at each end with a window of 8×10^{-5} cm thick aluminum foil the full diameter of the electroscope. The detecting element is a *ca.* 15μ gold-coated quartz fiber hinged at one end in a nickel trough about 2 mm wide, 2 mm deep and 25 mm long. The insulation is a quartz rod, coated, while hot, with ceresin wax and mounted in a brass guard ring. The deflecting element is of the type described by Workman and DeVore[6] and was most generously supplied by Mr. Henry DeVore of the California Institute of Technology. It has the curious characteristic of high charge sensitivity over the working range of 200 to 300 volts, combined with low sensitivity at lower voltage, thus making over half of the microscope scale useful in the high voltage range where the relative saturation of the ion current is fairly constant.

The walls of the ionization chamber are 2 mm thick paper tubing, coated inside with lampblack in a shellac binder. The charging switch is insulated in a Bakelite plug in a pine yoke and is grounded when not in use. The electroscope support and the racks for supporting the artificial rocks are also pine. Metal is avoided by this construction, with a view to minimizing scattering and secondary radiation in the electroscope. A 2 cm diameter glass bulb in the bottom of the electroscope contains P_2O_5 for drying. Fig. 1 shows the arrangement of the apparatus.

In taking readings, the guard ring potential is held at a value about midway between the initial and final potential of the fiber, to minimize insulation leakage. The fiber position is plotted against time and the slope of the average curve taken as the discharge rate. When comparing the

[3] Evans, Phys. Rev. **45**, 29 (1934).

[4] H. Gräven, Akad. Wiss. Wien, Ber. **139**, 181 (1930); **141**, 515, 521 (1932).

[5] Lind and Whittemore, J. Am. Chem. Soc. **36**, 2066 (1914).

[6] Workman and DeVore, Phys. Rev. **41**, 262A (1932).

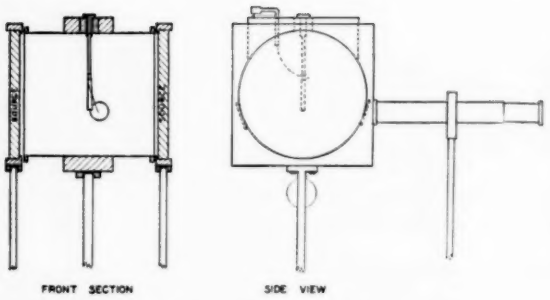

FIG. 1. Arrangement of the apparatus.

activity of two sources, observations are made on one source until the slope of the discharge line is well established, then the sources are changed and the readings continued until the new discharge rate is determined. This avoids alteration of the moving element's geometry and capacity by touching it with the charging electrode, and leads to much more closely reproducible results.

AGREEMENT BETWEEN THEORETICAL AND EXPERIMENTAL RESULTS

A. Predictions

It has been shown[3] that if q^U is the ionization in ion pairs per sec. per cm² of surface due to alpha-rays ejected from a solid emitting N^U alpha-particles per sec. per cm³ from each member of the uranium series, and if k is the specific ionization per alpha-particle of range R cm in air at 0°C, 760 mm, and μ the stopping power of air at 0°C, 760 mm relative to the emitting solid, then

$$q^U = N^U \sum \epsilon k R \mu, \qquad (1)$$

where ϵ is a numerical constant depending on R, and the summation is extended over all R in the uranium series. Now if an absorbing medium, such as air and the electroscope's aluminum window, is interposed between the radioactive surface and the ion collecting chamber, and if this absorber has a stopping power of a cm of air at 0°C, 760 mm, then Eq. (1) is written:

$$q_a^U = N^U \sum \epsilon_a k R \mu. \qquad (2)$$

There are analogous equations for the thorium and actinium series.

In the present apparatus, the windows have a stopping power of 0.13 cm of air and the distance between the active surface and the window is some 0.37 cm so that $a = 0.5$ cm of air. The Bragg-Kleeman rule gives $\mu = 4.85 \times 10^{-4}$ for air at 0°C, 760 mm relative to $CaSO_4 \cdot 2H_2O$, whose density is 2.32 g per cm³. Where $a = 0.5$ cm, the value[3] of $\sum \epsilon_a k R$ is 4.58×10^5 for the uranium series, 5.72×10^5 for the actinium series, and 5.23×10^5 for the thorium series. Substituting in Eq. (2) and recalling the activity ratio of 0.04 for the actinium relative to the uranium series, we find:

$$q_a^{Th} = 74.5$$
$$q_a^U + q_a^{Ac} = 174. \quad \text{ion pairs per cm}^2 \text{ per sec.}$$

The ratio of the activity of the thorium source to the uranium source should therefore be $74.5/174 = 0.43$, if the ionization is due to alpha-particles alone. Moreover, since the chamber is 10 cm long, and has a rock source at each end, the background ionization in ion pairs per cm³ per sec. should be $2 \times 74.5/10 \cdot s$ times the ratio of the fiber discharge rate for the background relative to the thorium source, or $2 \times 174/10 \cdot s$ times the similar ratio of the background to the uranium sources activity, where s is the fractional saturation of the alpha-particle ion current.

The ionization to be expected from the gamma-radiation from the radium plate can be roughly computed. Behounek[7] has recently shown that the effective mass absorption coefficient for the equilibrium mixture of uranium series gamma-rays in rocks is close to 0.065 cm² g⁻¹. The inner absorption of gamma-rays in the thickest sources here used will therefore be only 7 percent. If I is total ion pairs per sec.; ω the average solid angle subtended by the electroscope as seen from the source; l, the length of the electroscope; μ_1, the average absorption coefficient of the gamma-rays in air; and N_1 is the total number of ion pairs per sec. due to Ra B+C in equilibrium with 1 g of Ra; then, per g of Ra,

$$I = (\omega/4\pi) l \mu_1 N_1. \qquad (3)$$

Since $\mu_1 N_1 = 60 \times 10^9$ (Eve gives 50×10^9; Hess 61 and 72×10^9; Rutherford 64×10^9),[8] $l = 10$ cm, $\omega/4\pi = 0.14$, and the strongest uranium source

[7] Behounek, Zeits. f. Physik **79**, 590 (1932).

[8] A. S. Eve, Phil. Mag. **12**, 189 (1906); **22**, 551 (1911); **27**, 394 (1914). V. F. Hess, Akad. Wiss. Wien, Ber. **122**, 1053 (1913). Rutherford, Chadwick and Ellis, *Radiations from Radioactive Substances*, p. 497 (1930). Meyer and Schweidler, *Radioactivität*, p. 199 (1927).

contains 1.73×10^{-9} g Ra, we find the total ionization from two uranium sources, one at each end of the electroscope, to be 290 ion pairs per sec. due to Ra B+C. The total from the whole series is the same order of magnitude because Ra C is the important gamma-ray body in the uranium series. The electroscope volume is 785 cm^3, hence the gamma-ray activity is about 0.37 ion pairs per cm^3 per sec. The background, as will be shown later is 12 ion pairs per cm^3 per sec. The gamma-ray effect is thus less than 4 percent of the background, and is nearly the same as the statistical variations in the background.[9] Therefore the gamma-radiation should not be detected by this apparatus. This prediction is in agreement with the conclusions of Behounek,[7] but contrary to the conclusions of Gräven.[4] No gamma-rays were detected in the present experiments.

Because of their wide difference in penetrating power the ratio of the ionization produced by alpha- and beta-rays will depend on the thickness of the source, until a thickness of *ca.* 5 mm is exceeded. Rutherford[10] found the ratio of alpha- to beta-ray ionization above thin uranium oxide layers to be 12.7 to 1. No data on thorium are available. We may therefore expect that the ionization due to beta-radiation will be small, but detectable in the present apparatus. The observations confirm this prediction.

B. Observations

Aluminum filters 23 and 46×10^{-4} cm thick, hence with stopping powers of 3.6 and 7.2 cm of air, are used to screen out the alpha-rays. The ionization due to alpha-rays is the difference between the electroscope discharge rates for the screened and unscreened artificial rock sources. Within the observational uncertainty, the ionization due to alpha-rays is proportional to the uranium or thorium concentration of the source, and is independent of the thickness of these sources (0.4 to 1.1 cm). The average discharge rate for six runs with two 2.53×10^{-5} g U per g uranium sources is 3.8 ± 0.13 divisions per hour; and for three runs with two 4.1×10^{-5} g Th per g thorium sources, 1.6 ± 0.16 divisions per hour. The probable errors are computed from the residuals, by means of Peter's formula. The ratio of thorium to uranium series alpha-ionization is therefore $1.6\pm0.16/3.8\pm0.13=0.42\pm0.04$. This excellent agreement with the predicted value 0.43 is partly accidental, as is shown by the magnitude of the probable error, but taken with the following consideration of the background, it suggests the essential validity of the theoretical analysis of the alpha-ray ionization given previously.[3]

The background ionization due to cosmic and local radiation is measured when the radioactive artificial rock sources are replaced by blanks of identical shape, and does not vary when absorbing screens are used, thus showing the $CaSO_4$ used is free from appreciable radioactivity. The background is 1.1 ± 0.1 div per hr. As shown earlier, we can estimate the absolute value of this ionization by reference to the alpha-ray results. From the work of Moulins,[11] the alpha-ray ion current is about 85 ± 5 percent saturated at the field gradients here employed. Hence the background, computed from the uranium results, is $2\times174\times1.1/3.8\times0.85\times10=11.9\pm1.0$, and from the thorium results, $2\times74.5\times1.1/1.6\times0.85\times10=12.1\pm1.$ ion pairs per cm^3 per sec. The average value, $12.\pm1.$, agrees well with experience with other ionization chambers used for other work in the same laboratory room, and on which accurate capacity calibrations have been carried out.

The beta-ray ionization is measured by comparing the discharge rate for sources screened by the 46×10^{-4} cm aluminum alpha-ray screen with the rate when either a 5 mm aluminum or a 2 mm lead screen is added. The latter stop the beta-rays, but pass nearly all of the gamma-rays. The effects due to beta-rays are much smaller than those due to alpha-rays, and therefore cannot be measured with great precision. For 1.1 cm thick sources the ratio of beta-ray ionization to alpha-ray ionization is 0.10 ± 0.05 for the uranium series, and 0.20 ± 0.07 for the thorium series.

The gamma-ray ionization is isolated by comparing the discharge rate for the active plates screened by 5 mm Al or 2 mm Pb with the rate for blank plates similarly screened. Within the

[9] Evans, Phys. Rev. **39**, 1014 (1932).

[10] Rutherford, *Radioactivity*, p. 199 (1905).

[11] Moulins, *vide* Meyer and Schweidler, *Radioaktivität*, p. 281 (1927).

observational uncertainty, no gamma-radiation can be detected.

Absorption measurements were also made with 3.5 mm thick $CaSO_4 \cdot 2H_2O$ absorbers in place of the aluminum and lead screens. These screens stop all the alpha-ray ionization but seem always to pass most of the beta-ray ionization, a result which is not anticipated from mass absorption considerations. That this excess ionization is not due to intense secondary emission from the action of the gamma-rays on the gypsum screen was established as follows. A 2 mm Pb screen was placed between the 3.5 mm gypsum screen and the source; the lead stopped all alpha and beta-rays, but passed nearly all the gamma-rays on through the gypsum screen and into the electroscope. The discharge rate for this arrangement is identical with the background and with the rate when a blank plate is substituted for the radioactive source. Thus neither gamma-rays nor gamma-ray secondaries are measurable. This disagrees with the conclusions of Gräven,[4] which were based on indirect evidence.

Gräven reports the 3.5 mm gypsum screen to decrease a very measurable gamma-ray activity to 1/10 of its unscreened value for the uranium series, and to only 2/3 of its unscreened value for the thorium series. Employing the apparatus described by Workman,[12] and using strong radium and radiothorium γ-ray sources, DeVore[13] has shown that a 3.5 mm gypsum screen actually increases the ionization by 16 percent for the radium series, and by 21 percent for the thorium series. This is in keeping with the wall effects for other elements as observed by Workman, but is oppositely directed to the effects observed by Gräven. It seems probable that most of the ionization observed by Gräven is due to alpha-radiation, which he has regarded as negligible.

[12] Workman, Phys. Rev. **43**, 859 (1933); *vide* Fig. 2, p. 862.

[13] DeVore, personal communication, June, 1933.

Conclusion

Ordinary granites contain about 3×10^{-6} g uranium per g and about 6×10^{-6} g thorium per g of rock. The stronger sources employed in the present experiments contain 2.53×10^{-5} g U per g and 4.1×10^{-5} g Th per g, while the weaker sources contain one-tenth of these amounts, or slightly less than ordinary rocks. The alpha-radiation from ordinary rocks is therefore measurable.

No absorption measurements can differentiate sharply between the thorium and the uranium series. Observations on the alpha-radiation from polished rock surfaces measure the sum of the thorium and uranium series effects. By evaluating the uranium content in an independent analysis by the emanation method one can correct the surface alpha-radiation observations for uranium, and obtain an estimate of the thorium content of ordinary rocks.

The measurements are best carried out in a shallow ionization chamber, since the bulk of the alpha-ray ionization is within 2.5 cm of the rock surface. In this way the background is prevented from seriously interfering with the measurements. The alpha-rays from 100 cm^2 of ordinary granite will support an ion current of 10^{-15} amperes.

Rough rock surfaces present an unknown active area for the emission of alpha-particles which is approximately 1.5 times the exposed geometrical area, and has a correspondingly greater alpha-ray emission. Polished surfaces are therefore necessary, and these must be free from traces of surface moisture which strongly absorb the emerging alpha-rays.

It is my privilege to record here my cordial thanks for the generous assistance of Messrs. Henry DeVore, Alton Wangsgard and Sterling Gorrill in the experimental phases of this work, and to the Department of Physics of the University, particularly Professors L. B. Loeb and R. T. Birge for the excellent laboratory facilities provided.

Scattering of Electrons by Stibnite and Galena

A. G. EMSLIE,* *Cornell University*

(Received June 22, 1933)

A study has been made of the scattering of 20–60 kv electrons, produced in a hot cathode tube, by cleavage surfaces of stibnite and galena. The patterns from stibnite consist of spots, Kikuchi lines, bands, circles and parabolas. The spots are a surface grating effect with high resolving power for both surface directions. It is concluded that the crystal has relatively large mosaic units and that collisions with atoms, involving small energy losses, cause high absorption of the primary beam as it penetrates the crystal. Inelastic collisions, producing excitation of the thermal vibrations of the crystal, are considered. They cause increased scattering at angles just larger than the Bragg reflection angles and thus give a reason for the bands. The circles are considered to arise from the localizing of an electron's wave packet to the neighborhood of a single row of atoms, a process initiated by an inelastic encounter with a single atom. The measurements indicate a potential difference of about 26 volts between the row of atoms and the outside of the crystal. The parabolas, which occur also with galena, are thought to be due to the confinement of an electron to a single plane of atoms.

INTRODUCTION

AS first shown by Kikuchi and Nishikawa[1] for calcite, the diffraction of high energy electrons by crystal cleavage surfaces consists of a pattern of intersecting straight lines and bands and a number of spots. Kikuchi[2] has explained the lines as due to Bragg reflections of the diffusely scattered electrons in the crystal. The breadth of the Kikuchi lines has been worked out by Shinohara,[3] using Bethe's theory of electrons in crystals. It is sometimes sufficient to fill the space between a pair of parallel Kikuchi lines, thus affording an explanation of the bands.

The present paper is concerned chiefly with the scattering by stibnite crystals in which some new effects are observed.

APPARATUS

The apparatus is practically the same as that described by G. P. Thomson and C. G. Fraser,[4] except that a hot filament source of electrons replaces the gas discharge tube and the high tension is produced by a transformer in conjunction with rectifying Kenotrons and smoothing condensers. The cathode consists of a cylindrical nickel box with a 0.5 mm hole at one end and a filament of Konel strip just behind the hole. The electrons emerging from the hole, under the influence of the accelerating field, come to a focus just outside the hole. It is thus only necessary to have a single pinhole at the entrance to the crystal chamber in order to obtain a sharply defined beam. A ground-in plug, to which was attached a strip of metal carrying several pinholes of diameters varying down to 0.05 mm, allowed beams of any desired cross section to be obtained. The crystal could then be set by visual observation at the fluorescent screen with a large pinhole, and a fine pinhole substituted in making the photograph.

EXPERIMENTS WITH STIBNITE

Stibnite Sb_2S_3 is orthorhombic with a, b, $c=11.39$, 11.48, 3.89[5] and cleaves perpendicular to the b axis. Fig. 1 is a photograph taken with the a axis in the plane of incidence, which is horizontal. The pattern consists of spots, lines, bands, circles and parabolas.

The spots

The spots appear to be a surface grating effect. The reflection conditions for this are

$$\cos\alpha = \cos\alpha_0 - h\lambda/a$$

$$\cos\gamma = \cos\gamma_0 - l\lambda/c$$

* Commonwealth Fellow.

[1] Kikuchi and Nishikawa, Proc. Imp. Acad. Japan **4**, 475 (1928).

[2] S. Kikuchi, Jap. J. Phys. **5**, 83 (1928–29).

[3] Shinohara, Inst. Phys. Chem. Res. (Tokyo) **18**, 221 (1932).

[4] Thomson and Fraser, Proc. Roy. Soc. **A128**, 641 (1930).

[5] Gottfried, Zeits. f. Krist. **65**, 428 (1927).

where α_0, γ_0; α, γ are the angles the incident and reflected beams make with the a and c axes.

Let L be the distance from crystal to plate and take all angles to be small. Then the first condition gives a series of concentric circles of radii given by

$$r_h^2 = r_0^2 + 2L^2 h\lambda/a,$$

while the second condition gives a set of parallel layer lines separated by an interval $\eta = L\lambda/c$. From these we obtain $c/a = (r_{h+1}^2 - r_h^2)/2L\eta$. Table I shows that $(r_{h+1}^2 - r_h^2)/\eta$ is independent of h and also of the voltage. The mean value of c/a is found to be 0.339 agreeing with Gottfried's x-ray value of 0.342. The mean value of c obtained from $\eta = L\lambda/c$ is 3.86A agreeing with the x-ray value of 3.89A.

Kirchner and Raether[6] have found that at small angles of deviation the first reflection condition given above is not satisfied closely. This is probably due to their crystals possessing smaller mosaic units than stibnite which appears to have an unusually perfect cleavage.

The conclusion to be derived from the surface diffraction is that there is quite a high absorption of the incident beam as it penetrates the crystal. This must be caused by incoherent, and therefore presumably inelastic, collisions with the atoms of the crystal. The electrons scattered in this way reappear in the remainder of the pattern, which is independent of the direction of the primary beam by virtue of the incoherence produced at the first collision.

[6] Kirchner and Raether, Phys. Zeits. **33**, 510 (1932).

The lines and bands

The lines and bands are space grating effects, agreeing with the conclusion that an electron entering them starts as a spherical wave surrounding a single atom. However, the energy losses at the first collisions must be small compared to the initial energy on account of the sharpness of the pattern.

The pattern appears to stand out in relief, indicating that each Kikuchi line is bordered on one side by a dark strip. The various bands (marked 002, 063, etc.) have dark regions at both edges. In Table II b is the breadth of a band, α its inclination to the horizontal and d the spacing of the corresponding crystal planes obtained from $d = L\lambda/b$. The values of α and d agree with the values calculated from x-ray data. The breadths were measured out to the inner edges of the dark regions, so it seems that these edges, rather than the centers of the Kikuchi lines, mark the Bragg angles.

The fact to be explained, then, is that there is increased scattering at angles just larger than the

TABLE II. *Stibnite. Measurements of the bands.*

b (cm)	α	d (A)	X-rays α	X-rays d (A)	(lmn)
1.10	0°	1.95	0°	1.94	002
2.96	22°	0.72	22° 8′	0.72	065
1.80	24°	1.19	24° 30′	1.18	043
2.02	34°	1.06	34° 10′	1.07	063
1.58	45°	1.35	45° 30′	1.36	062
.96	54°	2.23	53° 32′	2.31	041
1.24	63°	1.73	63° 50′	1.72	061

TABLE I. *Stibnite. Measurements of the spots.*

v (volts)	r_0 (cm)	r_1 (cm)	r_2 (cm)	r_3 (cm)	η (cm)	$\frac{r_1^2 - r_0^2}{\eta}$	$\frac{r_2^2 - r_1^2}{\eta}$	$\frac{r_3^2 - r_2^2}{\eta}$	$\eta v^{\frac{1}{2}}$
19500	2.49	5.78	7.79		0.951	28.7	28.8		133.0
29000	2.20	5.15	6.98	8.32	.770	28.2	28.8	26.5	131.1
39000	1.77	4.55			.650	27.0			128.2
39500	1.75	4.50			.643	26.8			127.8
39800	1.71	4.48	6.12		.637	26.9	27.3		128.1
40000	2.70	5.00	6.50		.632	28.0	27.4		126.3
40800	1.74	4.45	6.10	7.36	.625	26.8	28.0	27.0	126.2
41000	2.97	5.12	6.66	7.90	.632	27.5	29.0	28.4	128.0
42000	1.80	4.55			.636	27.4			130.2
43500	2.20	4.60			.615	26.6			128.2
45000	1.07	3.24	5.88		.614	27.5	27.1		130.1
52500	1.40	4.20	5.80	7.05	.566	27.6	28.2	28.6	129.8
54800	2.36	4.55	6.00	7.14	.553	27.4	27.7	27.1	129.4
58000	1.26	4.05	5.58	6.80	.540	27.4	27.4	28.0	130.0

Bragg angles. From Bethe's theory of elastic reflection by the crystal planes, Shinohara[3] finds this effect but it is too small to account for the observed intensities. We are led, then, to consider the effects of absorption of energy by the thermal vibrations of the crystal. These vibrations can be resolved into a set of independent oscillations which can be excited separately.[7] The interaction energy between an electron and one of the oscillators will be the change in potential energy of the electron arising from a sine wave displacement of the crystal medium. For a long wave oscillator this change in potential will have approximately the same space periodicity as the undisturbed crystal potential. It can then be taken as

$$V=\sum_{lmn} V_{lmn}(t)\,\exp\left[2\pi i(\mathbf{j}_{lmn}\cdot\mathbf{r})/d_{lmn}\right],$$

where $\mathbf{j}_{lmn}$ is a unit vector normal to the (l, m, n) planes and d_{lmn} is the spacing of these planes. As a first approximation we take an initial plane wave electron $A\exp(2\pi i/h)(\mathbf{p}\cdot\mathbf{r}-p^2t/2m_0)$ of momentum $\mathbf{p}$. The matrix element corresponding to a transition in which the electron's momentum changes to $\mathbf{p}'$ is different from zero only if $(1/h)(\mathbf{p}-\mathbf{p}')=(1/d_{lmn})\mathbf{j}_{lmn}$. This means that, for absorption of energy by the crystal $(p^2>p'^2)$, scattering only occurs if the glancing angle on the plane (l, m, n) is greater than the Bragg angle $(p^2=p'^2)$. Corresponding to a loss of energy $\delta E=(1/2m_0)(p^2-p'^2)$ the deviation from the Bragg angle is $\delta\theta=(m_0\delta E/hp)d_{lmn}$ so the breadth of the absorption band should be large for large spacings, which is true. The intensity depends on $V_{lmn}(t)$ which in general should increase with d_{lmn}. The absorbed electrons go to form the bright bands and Kikuchi lines contained between pairs of dark bands.

The circles

The well-defined circle in Fig. 1 is surrounded by a narrow dark region, to the right of which appear Kikuchi lines of the group $(1, m, n)$. For $l=1$, the reflection condition $\cos\alpha=\cos\alpha_0-l\lambda/a$ is satisfied only at points lying outside the circle $r_1^{0^2}=2L^2\lambda/a$. The circle in the photograph, however, is definitely smaller than this. Another circle, too faint to be seen in the reproduction, occurs just inside the circle $r_2^{0^2}=4L^2\lambda/a$ corresponding to $l=2$. It is much narrower than any Kikuchi line near it, so the circles cannot be considered as envelopes of families of Kikuchi lines. Such envelopes, furthermore, can be shown to be always parabolas.

In Table III, the radii r_1 and r_2 of the two circles are compared with the calculated radii r_1^0 and r_2^0. The other columns give the crystal

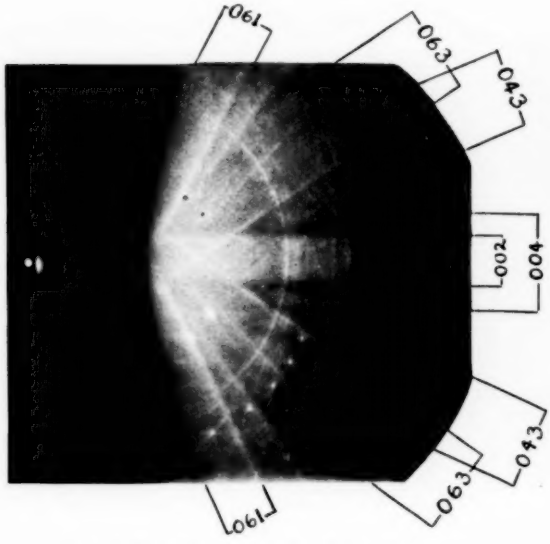

FIG. 1. Stibnite, a axis in plane of incidence.

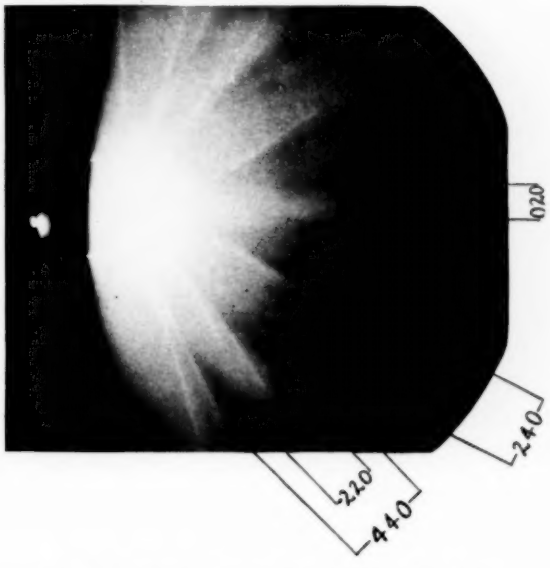

FIG. 2. Galena, cube edge in plane of incidence.

[7] A. H. Wilson, Proc. Roy. Soc. **A138**, 597 (1932).

TABLE III. *Stibnite. Measurements of the circles.*

V (volts)	r_1 (cm)	r_1^0 (cm)	ϕ_1 (volts)	r_2 (cm)	r_2^0 (cm)	ϕ_2 (volts)
18000	5.03	5.14	11	(7.28)	7.26	(−0.3)
27200	4.50	4.65	21	6.50	6.58	13
43700	3.98	4.14	32	5.72	5.85	37
50000	3.87	4.00	30	5.59	5.66	27
53600	3.82	3.93	26	5.45	5.56	42
56200	3.75	3.86	27	5.38	5.46	25

innerpotential ϕ required to deflect the calculated circles into the observed ones. The average value of 26.4 volts is much larger than the usual mean innerpotential of about 10 volts. But, to obtain the one-dimensional diffraction that the circles seem to be, an electron must have its wave packet confined chiefly to a single row of atoms parallel to the a axis. The potential in such a region may be high.

The mechanism whereby an electron wave packet becomes localized may be as follows. The original plane wave electron loses a little energy to an atom and becomes an approximately spherical wave radiating from that atom. If it leaves the atom in a direction nearly parallel to the a axis it may continue in that direction, entrapped in a kind of potential tube. It is scattered finally by the potential variations along the length of the tube.

The parabolas

Towards the right of Fig. 1, and also in Fig. 2 for galena, appear several symmetrical curves which measurements show to be parabolas. They can be explained in a manner similar to that for the circles. This time we imagine an electron confined initially to a *plane* of atoms perpendicular to the c axis. The diffraction will depend only on the atoms in that plane and the reflection conditions are

$$\cos \alpha_0 - \cos \alpha = l\lambda/a,$$

$$\cos \beta_0 - \cos \beta = m\lambda/b.$$

Since $\cos \gamma_0 = 0$ we have $(\cos \alpha + l\lambda/a)^2 + (\cos \beta + m\lambda/b)^2 = 1$. The surfaces determined by this equation meet the photographic plate approximately in a set of parabolas which fit the observed parabolas fairly well. The envelopes of some families of Kikuchi lines, however, are the same set of parabolas. The measurements are not exact enough to indicate whether an abnormal refraction occurs here as with the circles, and so decide which explanation to accept. The continuity of the curves and the correspondence with the case of the circles favor the former.

In conclusion, the writer wishes to thank Professors F. K. Richtmyer and C. C. Murdock for their kind interest in the work and Mr. H. R. Nelson for his valuable collaboration.

The Elastic Scattering of High Velocity Electrons by Mercury Atoms and the Agreement with Mott's Theory

EDWARD B. JORDAN,* *University of California, Berkeley, California*

(Received October 4, 1933)

The angular distribution of electrons scattered elastically by single mercury atoms has been studied for electrons of 900, 1160, 1600 and 2000 volts energy. The angle range was 8° to 48°. The values of the scattered intensities have been plotted and compared with the corresponding theoretical curves computed in accordance with Mott's theory. The theoretical and experimental curves for 900 volt-electrons differ markedly in shape. The slope of the experimental curve is much greater for small angles than that of the theoretical curve. The departure from Mott's curve decreases progressively for electron velocities corresponding to 1160, 1600 and 2000 volts energy. The 2000 volt curve shows good agreement with the corresponding theoretical curve.

THE scattering formula of Mott[1] $(e^4/4m^2v^4) \times (Z-F)^2 \operatorname{cosec}^4 \frac{1}{2}\theta$ gives an expression for the electron current scattered in a unit solid angle, in the direction θ, by a single free atom placed in a stream of unit electron current density. In this formula e is the charge on the electron, m its mass and v its velocity. Z is the atomic number of the scattering atom and F, a function of θ, is the atomic form factor.

The results of Dymond and Watson,[2] Harnwell,[3] McMillen,[4] Werner,[5] Hughes, McMillen and Webb[6] allow one to conclude that Mott's theory is adequate to describe the experimental facts for helium for energies above 200–400 volts. For mercury, Mott's theory was inadequate to describe the experimental facts for the highest energies used (700 volts) according to Tate and Palmer,[7] and Hughes.[8]

The purpose of the present research was to investigate the scattering by mercury atoms when higher velocity electrons were used and if possible to find at what voltage Mott's theory accurately accounted for the experimental data.

The apparatus used in this experiment was the same as that used by Jordan and Brode[9] in their measurements on the scattering of electrons by mercury vapor for low voltages. The apparatus was carefully aligned and only those measurements of the scattered current intensities which were the same on the two sides of the central beam were used. Each point shown on an experimental curve is the average of a number of measurements taken for the same scattering angle on the two sides of the central beam. Considerable precaution was taken to make sure that the electron beam was in the plane that passed through the center of the collector slit system.

Experimental Results and Discussion

The results of the measurements are given in Fig. 1. No attempt was made to compute the absolute magnitude of the scattered intensities from the experimental measurements because the solid angle of collection was not accurately known. The ordinates consequently represent the scattered intensities in arbitrary units. The angular range studied was 8° to 48°. The scattered currents at larger scattering angles were too small to measure accurately when these higher voltages were used.

In order to plot the theoretical curves shown in the figures it was necessary to calculate the atomic structure factor F for mercury for this

* Whiting Fellow, University of California.

[1] N. F. Mott, Proc. Roy. Soc. **A127**, 658 (1930).

[2] E. C. Dymond and E. E. Watson, Roy. Soc. Proc. **A122**, 571 (1928).

[3] G. P. Harnwell, Phys. Rev. **33**, 559 (1929).

[4] J. H. McMillen, Phys. Rev. **36**, 1034 (1930).

[5] S. Werner, Proc. Roy. Soc. **A134**, 202 (1931).

[6] A. L. Hughes, J. H. McMillen and G. M. Webb, Phys. Rev. **41**, 154 (1932).

[7] J. T. Tate and R. R. Palmer, Phys. Rev. **40**, 731 (1932).

[8] A. L. Hughes, Phys. Rev. **42**, 147 (1932).

[9] E. B. Jordan and R. B. Brode, Phys. Rev. **43**, 112 (1933).

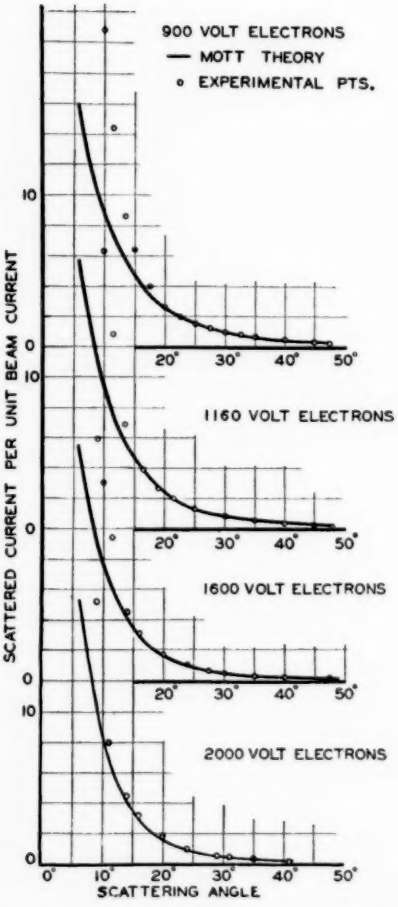

FIG. 1. Atomic scattering coefficient in arbitrary units.

angular range. The F values for caesium together with a formula which enables one to calculate the F values for any other heavy element are given in James and Brindley's[10] paper. These data were used in the present calculations. The magnitudes of the experimental and corresponding theoretical curves have been adjusted so that the curves are in agreement at 30°. It is evident that

[10] R. W. James and G. W. Brindley, Phil. Mag. **12**, 81 (1931).

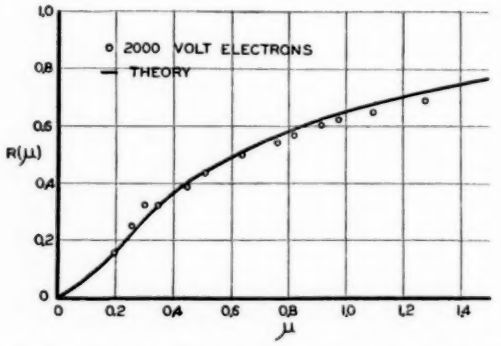

FIG. 2. $R(\mu)$, ratio of the actual scattered amplitude to the Rutherford amplitude, as a function of μ for mercury.

theory does not account for the scattering of electrons by mercury atoms when the energy of the electrons is 900 volts or less. The slope of the experimental curve is much greater than that of the theoretical curve for the smaller angles. This is in accord with the results of Hughes, McMillen and Webb[6] for helium when the energy of the electrons was less than about 400 volts. The departure from Mott's curve decreases correspondingly for the 1160, 1600 and 2000 volt curves. The 2000 volt curve shows good agreement with the corresponding theoretical curve. Morse[11] has suggested another method for comparing the theoretical and experimental values. If $R(\mu)$, the ratio of the actual scattered amplitude to the Rutherford amplitude is plotted as a function of μ, $[\mu = \sin(\theta/2)/\lambda]$, where λ is the de Broglie wave-length, then the plot shown in Fig. 2 is obtained. The solid line is the theoretical curve, and the circles are the experimental points obtained using 2000 volt electrons. This method of comparison shows the agreement at larger angles to a better advantage.

I am indebted to Professor R. B. Brode for many valuable discussions and comments.

[11] Philip M. Morse, Rev. Mod. Phys. **4**, 596 (1932).

On the Spatial Distribution of Photoelectrons Ejected from the Atomic *K*-Shell

J. A. VAN DEN AKKER, *Washington University, St. Louis*

(Received October 26, 1933)

With an electron velocity analyzer and modified Geiger-Mueller electron counter, the longitudinal space-distribution of electrons ejected from the *K* energy level of copper by Mo $K\alpha_1$ has been determined. Asymmetries in the experimental and theoretical distributions are compared and lack of satisfactory accord with wave mechanics is found. The effects of nuclear scattering are briefly discussed. A convenient asymmetry factor, *k*, is introduced. It is possible to compute *k* from data given by other investigators and, from an analysis of the statistical errors in the C. T. R. Wilson method, to compute probable errors. This is done and it is shown that a probably real difference, amounting to 10 percent, exists between the experimental and wave-mechanical asymmetries. Computations from an early but erroneous wave-mechanical treatment are in excellent accord with experimental results.

I. INTRODUCTION

IN 1927, Auger and Perrin[1] and Wentzel[2] announced, respectively, their "classical" and wave-mechanical expressions for the distribution in space of x-ray photoelectrons. Since then, several experimental studies[3, 4, 5, 6] on photoelectrons produced in gases have been carried out. For the most part, the investigations have been on the longitudinal distribution of electrons ejected from the *K*-shells of the heavier atoms or from the lighter atoms where the binding energy was negligible. Auger[3] and Anderson[5] succeeded in studying the fog-tracks of electrons from the *L*-shells and agreed in the important finding that the distribution curves for these electrons are markedly more isotropic than those for the *K*-electrons. Watson and Van den Akker[7, 8] found that the "spread" in the distribution of electrons ejected from very thin metallic films is definitely a function of the type of level from which the electron is ejected, as well as of the binding energy and the frequency of the incident x-rays. As regards comparison of experiment with theory, we may say that the distribution of *L*-electrons is only in qualitative agreement with wave-mechanics, while the distribution for *K*-electrons seems generally to be regarded as being in agreement with theory. Sommerfeld and Schur[9] and Auger and Miss Meyer[3] have noted, however, that the asymmetry in the experimental distributions for *K*-electrons seems to be in better agreement with an early but erroneous wave-mechanical treatment which has since been corrected.[9] It is the purpose of this paper to present new results on the longitudinal distribution of electrons ejected from the *K*-shell of atoms composing a very thin metallic film and to analyze results obtained in the past by other investigators who used the C. T. R. Wilson method. There appears to be a real discrepancy between experiment and present wave-mechanical theory.

II. APPARATUS

Photoelectrons ejected from the *K*-shell of copper by Mo $K\alpha_1$ were counted with a modified Geiger-Mueller tube[8] after they had been sepa-

[1] P. Auger and F. Perrin, J. de Physique **8**, 93 (1927).

[2] G. Wentzel, Zeits. f. Physik **41**, 828 (1927).

[3] P. Auger, C. R. **186**, 758 (1928); J. de Physique **9**, 225 (1928); C. R. **187**, 1141 (1928); C. R. **188**, 447 (1929); C. R. **188**, 1287 (1929); P. Auger and Miss Meyer, C. R. **192**, 672 (1931).

[4] E. J. Williams, J. M. Nuttall and H. S. Barlow, Proc. Roy. Soc. **A121**, 611 (1928).

[5] C. D. Anderson, Phys. Rev. **35**, 1139 (1930).

[6] E. Lutze, Ann. d. Physik (5) **9**, 853 (1931).

[7] E. C. Watson and J. A. Van den Akker, Proc. Roy. Soc. **A126**, 138 (1929).

[8] J. A. Van den Akker and E. C. Watson, Phys. Rev. **37**, 1631 (1931).

[9] A. Sommerfeld and G. Schur, Ann. d. Physik (5) **4**, 409 (1930).

rated from other electrons by an electrostatic refocusing analyzer of the type devised by Hughes and Rojansky[10] and Hughes and McMillen.[11] The copper film, deposited on cellophane by evaporation, was approximately 130 atoms thick and 0.23 cm wide. This film was mounted at the center of an evacuated brass chamber, the latter being capable of rotation and having 16 ports for the admission of the x-ray beam so that θ (the angle between the forward direction of the x-ray beam, and the initial direction of ejection) could be varied in 10° steps from 10° to 170°, 90° excluded. To reduce scattering to a minimum, the copper film was oriented so that the initial direction of all electrons received by the analyzer was normal to the surface of the copper film. Since the entrance slit of the analyzer was 2.85 cm from the film, the uncertainty produced in θ by the width of the film was only 2.3° (a negligible figure in the longitudinal distribution). The entrance and exit slits of the analyzer were 0.031 cm wide and the radii of the cylindrical analyzer plates were 4.85 cm and 5.15 cm. These dimensions ensure good resolution, which made it possible to resolve the Mo $K\alpha_1$: Cu K-electrons from the Mo $K\alpha_2$: Cu K, and Mo $K\alpha_1$: Cu K-electrons which had suffered energy losses in escaping from the film. The x-ray beam, generated in an oil-immersion balanced-circuit outfit,[12] was sufficiently wide to include the copper film at all angular settings.

III. Method and Results

Since the electron currents were, at maximum, less than 5 electrons per minute, it seems desirable to outline the method of measurement. Happily, one electron-counter served throughout the period of nearly three months required for the results given in this paper, without suffering change of sensitivity or exhibiting erratic behavior.[13] The residual count (analyzer voltage zero, x-rays on or off) was only 1.6 ions per minute. The residual count was not usually taken but, rather, the procedure was to take electron counts over the Mo $K\alpha_1$: Cu K peak and at the high energy foot of the peak (the latter being the true background count). All counts were taken over ten-minute intervals, alternating from the peak to the foot of the energy distribution curve, until eleven ten-minute counts had been recorded for the peak and an equal number for the foot. All counts were reduced to number per minute. The difference between the average number of impulses (Geiger-Mueller) per minute at peak (P) and foot (F) was taken as a measure of the electron current at the given angular setting. In a typical case, the average number of impulses at peak and foot were, respectively, 7.46/min. and 3.30/min. Thus, a period of four hours of continuous observation was required for the measurement of a current of about 4.2 electrons/min. In general, several of these four-hour determinations were made to establish the current at a given angle. The results of 69 four-hour determinations are shown in Fig. 1.

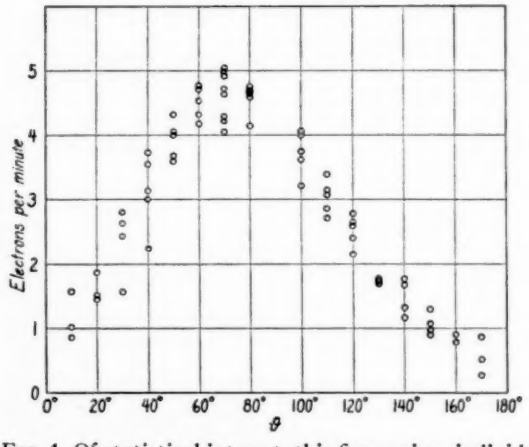

FIG. 1. Of statistical interest, this figure gives individual determinations of electron currents. Each of the 69 determinations results from 22 ten-minute counting periods over the peak and foot of the energy-distribution curve at the given angular setting.

Averages of the points shown in Fig. 1 are given in Fig. 2, with twice the probable errors

[10] A. L. Hughes and V. Rojansky, Phys. Rev. **34**, 284 (1929).

[11] A. L. Hughes and J. H. McMillen, Phys. Rev. **34**, 291 (1929).

[12] R. D. Bennett, N. S. Gingrich and W. C. Pierce, Rev. Sci. Inst. **2**, 226 (1930).

[13] It is perhaps incorrect to speak of the "sensitivity" of a Geiger-Mueller tube, because this device records the formation of individual ions; when imperfect, spurious impulses are recorded in such a way that the "sensitivity" apparently *increases*.

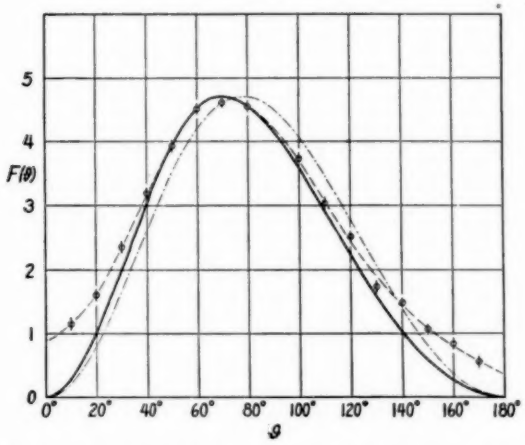

FIG. 2. Experimental and theoretical distributions, giving relative probabilities of ejection per unit *solid angle*. Dashed curve, experimental; full curve, wave-mechanics; dot-dash curve, classical.

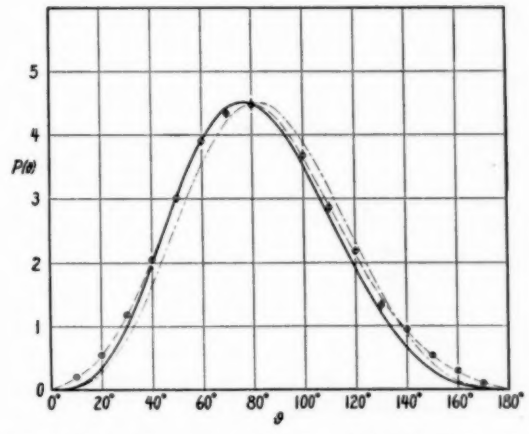

FIG. 3. Experimental and theoretical distributions, giving relative probabilities per *unit angle;* the ordinates of this figure are those of Fig. 2 multiplied by sin θ.

represented by the vertical lines drawn through the points. The probable errors were computed from the relation, $r=0.67[(P+F)/(10\times 11\ m)]^{\frac{1}{2}}$ where P and F are defined as above and m is the number of four-hour determinations at the angle in question. (This relation is essentially the square root of the sum of the squares of the probable errors in P and F.)

Determination of the longitudinal distribution by the C. T. R. Wilson method involves counting the number of fog-tracks occurring in a given angular range and hence, by this method, the probability per unit angle, $P(\theta)$, is found. Since the solid angle for a given angular range tends to go to zero at $\theta=0°$ and $\theta=180°$, actually few electrons are counted at these extreme angles and consequently little weight can be attached to the corresponding experimental values of $P(\theta)$. It therefore seems probable that effects due to weak scattering would not be noticeable where this method is used. In the present work, on the other hand, the electrons were received by a slit and hence the probability per unit solid angle, $F(\theta)$, was determined directly. Electron counts taken near 0° and 180°, therefore, possess considerable weight. Inspection of Fig. 2 shows that the electron currents at 0° and 180° do not go to zero; it cannot be said, at the present time, whether the major part of these currents are real or due to the spurious action of nuclear scattering.

The solid curve in Fig. 2 represents the wave-mechanical expression for K-electrons ejected by unpolarized rays,[14, 15, 16, 17]

$$F(\theta) \propto \frac{\sin^2\theta}{[1-(\beta/a)\cos\theta]^4},$$

adjusted to fit the experimental points at the peak. In this expression β is the ratio of the speed of the photoelectron to that of light and $a=1+\alpha/2=1+h\nu/2mc^2$, where ν is the frequency of the incident x-rays. The classical expression given by Auger and Perrin[1] is given by the dash-dot curve.

For the comparison of experiment with theory, it is convenient (for mathematical and graphical reasons) to convert the experimental results and theory into the form $P(\theta)$. This is simply effected by multiplying all experimental and theoretical ordinates in Fig. 2 by sin θ. The result of doing this is shown in Fig. 3, in which the ordinates express the probability per unit angle; and, again, twice the probable errors are given by the vertical dashes through the points.

---

[14] G. Wentzel, reference 2; result announced in Lecture Series of Norman Bridge Laboratory, Pasadena.

[15] J. Fischer, Ann. d. Physik (5) **8**, 821 (1931).

[16] F. Sauter, Ann. d. Physik (5) **9**, 217 (1931).

[17] F. Sauter, Ann. d. Physik (5) **11**, 454 (1931), deduces expressions valid when $\beta\sim 1$, $\beta^2\ll 1$, on the basis of Dirac's relativistic wave-mechanics. The latter expression becomes the same as the one given in this paper when the frequency of the incident x-rays is low.

It is readily seen that both the classical and wave-mechanical curves fit the points as to *form* but that the asymmetry of the classical curve is unquestionably too weak. We may compare the experimental and theoretical asymmetries by evaluating the quantities defined by the following equations:

$$\rho = \int_0^{\pi/2} P(\theta)d\theta \Big/ \int_{\pi/2}^{\pi} P(\theta)d\theta;$$

$$\theta_0: \int_0^{\theta_0} P(\theta)d\theta = \int_{\theta_0}^{\pi} P(\theta)d\theta;$$

$$\overline{\cos\theta} = \int_0^{\pi} P(\theta)\cos\theta d\theta \Big/ \int_0^{\pi} P(\theta)d\theta;$$

$$k = \mu\,\overline{\cos\theta}/(h\nu_0/c), \quad \mu = m\beta c/(1-\beta^2)^{\frac{1}{2}}.$$

The last quantity, k, is defined as the ratio of the average forward momentum of the electrons to the momentum of a quantum having an energy equal to that of the electrons. This quantity is particularly useful when the binding energy of the K-electrons is not negligible but is comparable with $h\nu$ of the incident x-rays.

The experimental values of these quantities were obtained by graphical methods from the experimental curve in Fig. 3. These values, with the corresponding theoretical values, are given in Table I. In each case, the experimental value

TABLE I.

	θ_0	ρ	$\overline{\cos\theta}$	k
Experimental	81.0°±.33°	1.55±.028	0.121±.0039	1.32±.042
Wave mechanics	79.8°	1.72	0.1424	1.57
Auger-Perrin	84.0°	1.37	0.0822	0.90

deviates from the corresponding wave-mechanical value in the direction of weaker asymmetry, while there appears to be real lack of accord between experiment and classical theory.

How does scattering of the electrons affect the experimental values recorded in Table I? We may assume that the nuclear scattering is appreciable over only small angles of scattering. This assumption, combined with the fact that most of the electrons are ejected in the neighborhood of $\theta=90°$, leads to the conclusion that the relative spurious effect of scattering is a maximum in the regions of $\theta=0°$ and $\theta=180°$. This means that the experimental value of $\overline{\cos\theta}$ is affected by scattering, with the change toward a smaller value. Inspection of the experimental curve in Fig. 3 shows, however, that there is a tendency toward compensation, in that scattering raises the curve at both ends. Because of the rough symmetry of the curve about the bipartition angle, $\theta_0=81°$, and the fact that, for a given angular range $\delta\theta$, the solid angle is roughly constant in the neighborhood of 81°, it is probable that scattering affects the experimental bipartition angle only inappreciably. A somewhat larger effect is to be expected in the case of ρ, for, while the solid angle for a given range $\delta\theta$ is very nearly constant in the vicinity of $\theta=90°$, the experimental curve is quite asymmetric with respect to this angle and, consequently, the effect of scattering would be to make the value of ρ too small.

The actual differences between the wave-mechanical and experimental values of $\overline{\cos\theta}$, θ_0 and ρ bear the ratios to the respective probable errors, 5.7, 3.6 and 6.1. In line with the above argument, θ_0 is in best agreement with theory; but this, of course, does not mean that the whole difference between theory and experiment can be accounted for by scattering.

IV. Computation of k from Data Given by Other Observers

It can be shown (with relativity correction) that

$$k = (1+2/\alpha_e)^{\frac{1}{2}}\,\overline{\cos\theta},$$

where $\alpha_e = 1/(1-\beta^2)^{\frac{1}{2}} - 1$. On the basis of wave-mechanics,

$$k = \frac{4}{5}\cdot\frac{1}{1+\alpha/2}\cdot\frac{2+\alpha_e}{1+\alpha_e} + \cdots.$$

The factor k is convenient in comparing experiment with theory because its wave-mechanical value is nearly constant over the ordinary range of values of α and α_e. When the binding energy is negligible, $\alpha_e \leqq \alpha$ and $k = 1.6(1-\beta^2)^{\frac{1}{2}}$, which has the limiting value (when $\beta=0$), $k=1.6$. The limiting classical value is 0.8.

Values of k computed from other observers' published values of $\overline{\cos\theta}$ are not in satisfactory

TABLE II.

Quantity	Probable error	Values when $N=400$, $\gamma=8/7$
$\cos\theta_0\left\{=\frac{1}{\gamma}\left[\left(1+\frac{\gamma^2}{2}\right)^{\frac{1}{2}}-1\right]\right\}$	$\pm\frac{89.3\tan\theta_0}{1+2.5\left(\frac{\gamma}{4}\right)^2-5.6\left(\frac{\gamma}{4}\right)^4}\cdot\frac{1}{N^{\frac{1}{2}}}$ percent	0.255 ± 14.5 percent
θ_0	$\pm\frac{51.2}{1+2.5\left(\frac{\gamma}{4}\right)^2-5.6\left(\frac{\gamma}{4}\right)^4}\cdot\frac{1}{N^{\frac{1}{2}}}$ degrees	$75.2°\pm2.2°$
$\rho[=(8+3\gamma)/(8-3\gamma)]$	$\pm67(\rho+1)\left(\frac{1}{\rho N}\right)^{\frac{1}{2}}$ percent	2.5 ± 7.4 percent
$\overline{\cos\theta}_k[=\gamma/5]\}$	$\pm\frac{67}{\overline{\cos\theta}(5N)^{\frac{1}{2}}}$ percent	$\left\{\begin{matrix}0.229\pm6.6\text{ percent}\\ \pm6.6\text{ percent}\end{matrix}\right.$

accord with wave-mechanical theory. The C. T. R. Wilson method was used in all these investigations and hence, in some cases, the results have been subject to large statistical errors. Assuming the distribution function[9]

$$P(\theta)\propto\sin^3\theta(1+\gamma\cos\theta),$$

(a close approximation to the wave-mechanical distribution when $\gamma=4\beta/a$), a statistical analysis was carried out for the C. T. R. Wilson method. The results of this analysis are given in Table II in which N is the total number of fog-tracks measured. Application of the analysis to the typical case, $N=400$ and $\gamma=8/7$ (or $\rho=2.5$), is included in the tabulation, while in Table III, probable errors in the ordinates of the longitudinal distribution are given. The rather typical range of 15° was used in the calculations for Table III. As Table III is only illustrative of how large the errors are, the calculations have been made for only the forward half of the curve.

TABLE III.

Range (degrees)	0–15	15–30	30–45	45–60	60–75	75–90
Percent (prob. error)	71	22	12	8.3	7.1	7.2

Other reasons for the worth of the factor k are that the probable error in this quantity is relatively small, and that, to compute the error, one need know only N and $(\overline{\cos\theta})_{\text{exp.}}$. In Table

TABLE IV.

Ref.	Gas	λ(A)	β	N	$\overline{\cos\theta}$	$k_{\text{exp.}}$	Probable error	$k_{\text{theor.}}$	$k_{\text{theor.}}-k_{\text{exp.}}$
5	C_2H_5Br	0.586	0.172	233(K)	0.133	1.54	±0.23	1.56	+0.02
3	A in H_2	.709	.231	1200(K)	.169	1.44	± .07	1.56	+ .12
3	A in H_2	.21	.433	1000(K)	.313	1.38	± .04	1.46	+ .08
3	A in H_2	.21	.433	450(K)	.277	1.22	± .06	1.46	+ .24
3	A in H_2	.134	.532	?	?	1.30*	?	1.41	+ .11
5	air	.709	.254	272	.182	1.40	± .14	1.55	+ .15
5	air	.562	.285	200	.210	1.45	± .15	1.54	+ .09
4	N_2	.614	.262	200	.189	1.36	± .15	1.54	+ .18
4	N_2	.545	.288	93	.179	1.22	± .21	1.53	+ .31
4	O_2	.709	.254	159	.202	1.56	± .18	1.55	− .01
4	O_2	.614	.262	179	.207	1.49	± .16	1.54	+ .05
4	O_2	.545	.288	148	.193	1.31	± .17	1.53	+ .22
Present Work		.7078	.180	22,000(K)	.121	1.32	± .04	1.57	+ .25

* Value given by Auger for σ, where $\sigma\leqq k$ when binding energy is small..

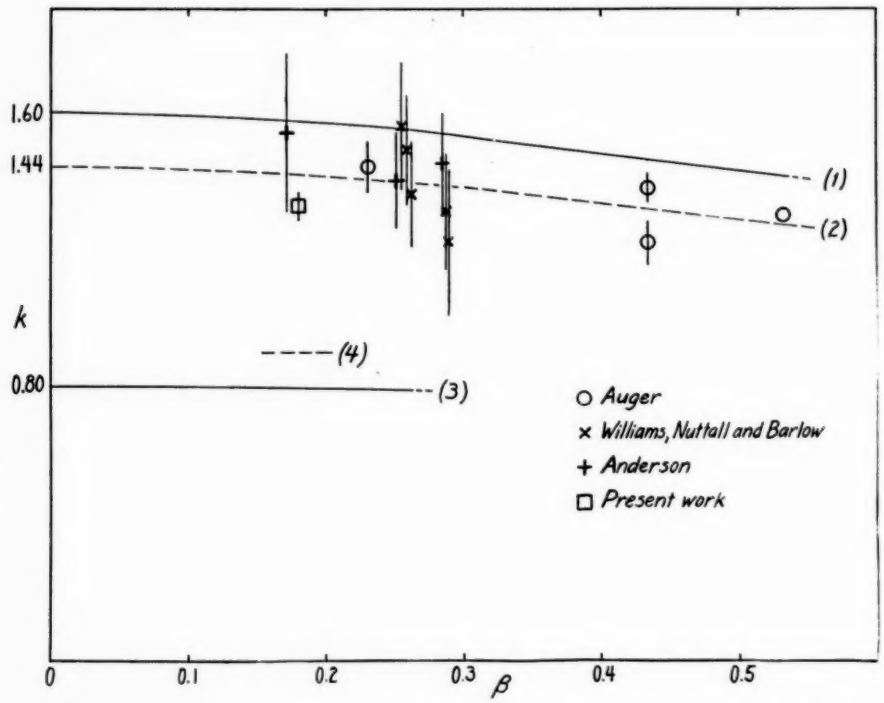

FIG. 4. Comparison of experimental and theoretical values of k. (1) Wave-mechanics, binding energy negligible *or* small but not negligible; (2) wave-mechanical values multiplied by 0.9; (3) classical theory of Auger-Perrin, binding energy negligible; (4) classical theory appropriate to present work, binding energy not negligible.

IV, experimental values of k, with probable errors computed by the simple formula of Table II, are compared with the appropriate wave-mechanical values. These values are plotted in Fig. 4, with twice the probable errors given by the vertical lines.

It is seen that all but one of the experimental values deviate from theory in the direction of weaker asymmetry in the space-distribution. Only one-third of the experimental values include the theoretical values within their respective probable-error ranges, and the probable errors in these particular values are large, varying from 10 percent to 15 percent. The most reliable values (computed from Auger's data) differ from theory by 1.6, 1.9 and 3.9 times the respective probable errors.

The value of k given by the erroneous wave-mechanical treatment referred to in the Introduction is just nine-tenths the present wave-mechanical value. While this value is of no theoretical significance, it is worthy of note that it is in striking agreement with experiment. The former theory, regarded as empirical, is represented by the dashed curve (2) in Fig. 4. The average weighted difference between the experimental values (excepting the one point for which the probable error is not known) and the appropriate wave-mechanical values multiplied by 0.9 is $+0.004$ or only 0.3 percent; the corresponding probable error is about 3.0 percent and hence we may say that experiment is in excellent accord with the older, erroneous theory. The deviation from present theory is about 10 percent, or more than three times the probable error, and, consequently, the discrepancy appears real.

An indication that scattering cannot account for the discrepancy is found in the circumstance that no real difference seems to exist between the results of Auger and of Williams, Nuttall and Barlow, in spite of Auger's effort to reduce scattering by diluting the gas studied (argon) in hydrogen, while in the latter work, in which N_2 and O_2 were used, scattering should have been stronger.

In the present work, as we have seen, small angle nuclear scattering affects the bipartition angle less than it does $\overline{\cos\theta}$ or ρ and we may therefore take, as the most reliable asymmetry factor given by the present work, $\theta_0 = 81.0° \pm 0.33°$. The bipartition angle calculated on the basis of the erroneous theory is 80.8°, in very good agreement with the experimental angle.

This work was aided, in part, by a grant made by the Rockefeller Foundation to Washington University for research in science. The writer is indebted to Mr. P. S. Williams, who assisted in taking observations. Appreciation is extended to Dr. L. A. DuBridge, with whom the writer has enjoyed several stimulating discussions throughout the course of the work.

Vibrational Isotope Effects in Three-Particle Systems. Part I

ARTHUR ADEL, *University of Michigan*

(Received October 25, 1933)

Proceeding on the assumption of valence forces between the units of a general three-particle system, an analysis is made of the effects of isotopy on the three fundamental frequencies of oscillation. In conformity with Salant and Rosenthal, the effects are classified as end and central isotope effects. The quantities $\Delta\omega_1/\omega_1$, $\Delta\omega_2/\omega_2$ and $\Delta\omega_3/\omega_3$ are derived for both cases. It is demonstrated that the analysis provides a criterion for deciding between several hypothetical models of a single molecule.

I. INTRODUCTION

DENOTING the three fundamental frequencies of the general triatomic molecule of Fig. 1 by ω_1, ω_2 and ω_3 we seek to determine the quantities $\Delta\omega_1/\omega_1$, $\Delta\omega_2/\omega_2$ and $\Delta\omega_3/\omega_3$, where $\Delta\omega$ is the shift of ω which follows an isotopic change in mass Δm. For the molecule under consideration it can be shown that an evaluation of the quantity $\Delta\omega/\omega$ presupposes a complete knowledge of the forces governing the vibrations

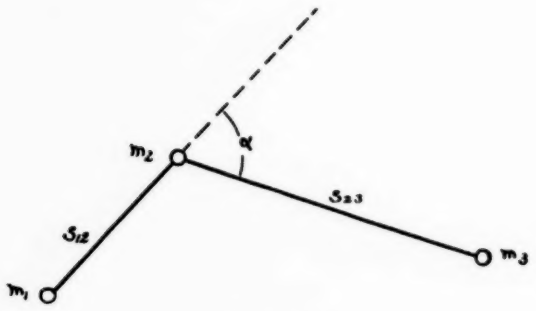

FIG. 1.

of the molecule. (As in the case of diatomic and symmetrical polyatomic molecules, the assumption will be made that the forces in the molecule are invariant for an isotopic change in mass.) However, in the absence of such simplifying assumptions as central or valence forces, the quadratic potential energy of the molecule involves four independent coefficients. The three data ω_1, ω_2 and ω_3, therefore, do not suffice for a determination of the potential function and are thus incapable of fixing the value of $\Delta\omega/\omega$. Furthermore, no other data gleaned from the infrared spectrum of the molecule are of service in an attack upon the problem. Consequently, in order to render the isotopic displacements of the bands computable we must resort to a potential possessing but three independent constants. For symmetrical triangular molecules this procedure has been followed with considerable success.[1] Urey and Johnston took as their starting point Bjerrum's equations for the vibrations of symmetrical triatomic molecules as derived upon the special assumption of valence forces. It is the purpose of the present paper to perform a similar analysis based upon Lechner's valence force equations for the vibrations of unsymmetrical triatomic molecules.[2]

In conformity with the notation introduced by Salant and Rosenthal in their general treatment of isotope effects in symmetrical molecules,[3] the phenomena will be classified as end isotope effect when the isotopic change in mass occurs at either m_1 or m_3 and as central isotope effect when the isotopic change in mass takes place in the central particle. In accordance with the approximations to be made in the analysis, the results of the investigation will be applicable to the isotopes of hydrogen only when the latter is a member of a particle of considerably greater mass, as, for example, the hydrogen atom in the groups CH_3 and CH_2 which behave as dynamical

[1] H. C. Urey and H. Johnston, Phys. Rev. **38**, 2131 (1931).

[2] F. Lechner, Monatshefte f. Chemie **61**, 385 (1932).

[3] E. O. Salant and J. E. Rosenthal, Phys. Rev. **42**, 812 (1932).

units in three of the vibrations of the molecule $(CH_3)(CH_2)I$.[4]

II. Analysis

On the assumption of the valence forces f_{12}, f_{23} and d, the potential energy of the molecule of Fig. 1 takes the form:

$$V_0=(\tfrac{1}{2})\{f_{12}(\Delta S_{12})^2+f_{23}(\Delta S_{23})^2+d(S\Delta\alpha)^2\}$$

where $d_{12}S_{12}^2=d_{23}S_{23}^2=dS^2$ is a constant of the configuration. Lechner[2] has shown, on the basis of this potential, that the three fundamental frequencies have the following dependence upon the molecular constants and forces:

$$n_1^2+n_2^2+n_3^2=f_{12}/\mu_{12}+f_{23}/\mu_{23}+d/\mu_4,$$

$$n_1^2n_2^2+n_1^2n_3^2+n_2^2n_3^2=(f_{12}/\mu_{12})(f_{23}/\mu_{23})\{1-(\mu_{12}\mu_{23}/m_2^2)\cos^2\alpha\}$$
$$+(f_{12}/\mu_{12})(d/\mu_4)\{1-(\mu_{12}\mu_4/m_2^2)\sin^2\alpha\}+(f_{23}/\mu_{23})(d/\mu_4)\{1-(\mu_{23}\mu_4/m_2^2)\sin^2\alpha\},$$

$$n_1^2n_2^2n_3^2=(f_{12}/\mu_{12})(f_{23}/\mu_{23})(d/\mu_4)\{1-\mu_{23}\mu_{12}/m_2^2\},$$

where $n=2\pi\omega$ and $1/\mu_{12}=1/m_1+1/m_2$, $1/\mu_{23}=1/m_2+1/m_3$, $1/\mu_4=(1/\mu_{12})(S/S_{12})^2+(1/\mu_{23})(S/S_{23})^2+(2\cos\alpha/m_2)(S^2/S_{12}S_{23})$.

Rewriting these equations in the form: $x+y+z=A$, $xy+xz+yz=B$, $xyz=C$, we obtain by differentiation the following set of linear equations:

$$xr+ys+zt=dA,$$
$$x(A-x)r+y(A-y)s+z(A-z)t=dB,$$
$$C(r+s+t)=dC,$$

where $r=2d\omega_1/\omega_1$, $s=2d\omega_2/\omega_2$, $t=2d\omega_3/\omega_3$. Ordinary methods of solution now yield $d\omega/\omega=Kdm/m^2$, where m is the mass of the isotopic atom and dm is the isotopic change of mass. The explicit form of the constant of proportionality is easily determined in terms of the molecular constants and forces and is thus readily evaluated by applying Lechner's equations to the fundamental frequencies ω_1, ω_2 and ω_3.

Specialization of the results to the case of the linear molecule is achieved by equating α to 0°. For this case we give the solution in all detail. Here,

$$d\omega_1/\omega_1=\{dB-(A-y)dA\}/2x(x-y),$$
$$d\omega_2/\omega_2=\{dB-(A-x)dA\}/2y(y-x),$$
$$d\omega_3/\omega_3=dC/2z,$$

where dA, dB and dC assume the following values for the end and central isotope effects:

End isotope effect

$$dA=-f_{12}(dm_1/m_1^2),$$
$$dB=-(f_{12}f_{23}/\mu_{23})(dm_1/m_1^2),$$
$$dC=-d\cdot(S/S_{12})^2(dm_1/m_1^2).$$

Central isotope effect

$$dA=-(f_{12}+f_{23})(dm_2/m_2^2),$$
$$dB=-\{f_{12}f_{23}(1/\mu_{12}+1/\mu_{23})-2f_{12}f_{23}/m_2\}(dm_2/m_2^2),$$
$$dC=-d\cdot\{(S/S_{12})^2+(S/S_{23})^2+2S^2/S_{12}S_{23}\}(dm_2/m_2^2).$$

III. Discussion

The theory developed above may clearly be applied not only to triatomic molecules such as N_2O, ClCN, HCN, COS, BrCN, ICN but with equal profit to many molecules containing more than three atoms. For example,[4] the molecules CH_3CH_2I, CH_3CH_2Cl, CH_3CH_2Br, etc., possess three modes of vibration in which the groups CH_3 and CH_2 behave very nearly like dynamically independent units and for these three frequencies the system may rightfully be looked upon as a triangular molecule. It is only in connection with molecules of the latter type that the results of the analysis may be applied to the isotopes of hydrogen.

[4] P. C. Cross and J. H. Van Vleck, J. Chem. Phys. 1, 350 (1933).

In conclusion, it may be pointed out that the above analysis, apart from its value in correlating the phenomena of isotopic displacements of vibrational frequencies in the infrared spectra of three-particle systems, may also serve to determine the relative positions of atoms or groups of atoms within a molecule. The molecule of carbonoxysulfide is a case in point. It is still undecided which of the structures

O———C———S
C———O———S

is to be associated with the actual molecule. Now the isotope effect of the carbon atom is central in the first model but ends in the second. Consequently, the quantity $d\omega/\omega$ will be a function of the structure. It is easily shown that $d\omega_3/\omega_3 = -1/30$ for the first model and $-1/105$ for the second, where ω_3 is the frequency of the perpendicular or deformation vibration. The large factor of difference between the two displacements provides a direct criterion for discriminating between the structures diagrammed above.

In Part II of this work the problem of vibrational isotope effects will be attacked through a general, non-central molecular force field and it will be shown how measurements on the isotopic shifts of frequency can be applied to an evaluation of the potential energy of the molecule.

The Stern-Gerlach Experiment with Iron

W. KLABUNDE[1] AND T. E. PHIPPS, *Laboratory of Physical Chemistry, University of Illinois*

(Received November 15, 1933)

An atomic ray of iron was investigated by the method of Stern and Gerlach. The intensity of the ray was sufficient to make the deposit upon the target directly visible in the vacuum after many hours. The trace was found to be widened when the ray was subjected to the magnetic field, an indication that iron in the vapor state has a magnetic moment. This positive result may remove the apparent discrepancy between spectroscopic prediction and the original negative result of Gerlach.

INTRODUCTION

THE first investigation of the magnetic moment of iron by the molecular ray method was carried out by Gerlach,[2] who found, after wet development of the target outside of the vacuum, a single trace only, at the position of zero deflection. Since deflected traces were expected from spectroscopic prediction, the result appeared to be in disagreement with theory. However, because of the inherent crudeness of the development method, as a result of which deflected traces might have been lost entirely, the result of Gerlach has been regarded as inconclusive rather than negative.[3]

It seemed desirable to determine definitely whether iron in the vapor state has a magnetic moment, the more so since a nonmagnetic condition[4] has been observed in thin films of iron formed by condensation of the sputtered metal on cold surfaces. To answer the question it was necessary to produce a ray of iron of intensity sufficient to make its trace upon the target directly visible in the vacuum. A comparison, then, of the width of traces obtained with and without magnetic field should decide the point. The more difficult problem of attempting a quantitative check upon the spectroscopic prediction was considered too difficult for present technique.

APPARATUS

Fig. 1 shows essential details of the furnace. Two water-cooled brass posts passed through a brass plate, one of them being insulated from it. The brass plate could be joined with sealing wax to the metal jacket. Two small molybdenum rods, 2 mm in diameter, were connected to the posts by tapered steel bushings and to the graphite furnace by force-fit through slightly

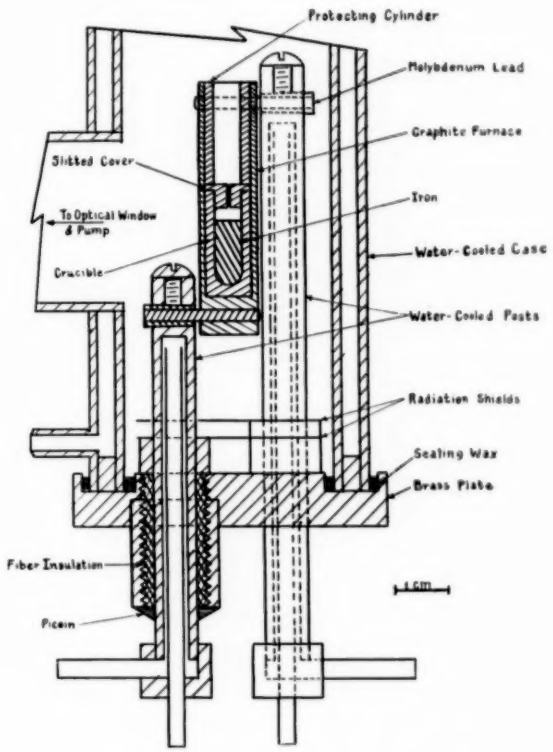

FIG. 1. Details of furnace construction.

[1] This communication is an abstract of a thesis submitted in partial fulfillment of the requirements for the degree of Doctor of Philosophy in Chemistry at the University of Illinois.

[2] W. Gerlach, Ann. d. Physik **76**, 163 (1925).

[3] See R. G. J. Fraser, *Molecular Rays*, p. 142.

[4] L. R. Ingersoll, Nature **119**, 234 (1927).

undersized holes drilled through the graphite. The graphite furnace was massive at the ends but was thinned at the middle to a shell having a wall thickness of 1 mm. The shell was a resistor unit, heated by a heavy current from a low voltage transformer. Below, a double radiation shield of polished nickel sheet protected the wax seal from direct radiation.

Inside the graphite shell was a pure magnesium oxide crucible with a slitted lid of the same material and above the lid a magnesium oxide cylinder, which protected the upper part of the graphite furnace from direct contact with the iron vapor. At 1700°K this furnace was found to have a life of about forty hours. Eventual diffusion of iron through the magnesium oxide to the graphite shell appeared to be the factor which limited the life of the furnace.

The slit in the magnesium oxide crucible cover was aligned optically with a metal slit which was fixed to one of the pole pieces of the magnetic field. The magnetic field was produced by pole pieces of the type which produce a region of constant inhomogeneity.[5]

The target, an optical Pyrex plate, was held by vacuum grease to the brass case and could be moved in its own plane without disturbing the vacuum. Other details of apparatus and operating conditions are given in Table I.

TABLE I. *Details of apparatus and operating conditions.*

Sample of iron	Hilger's H. S. Brand, Laboratory No. 8038
Furnace temperature	(T) 1450° C±50°
Inhomogeneity of magnetic field ($\partial H/\partial z$)	41,500 gauss$-$cm^{-1}
Distance between slits	6.5 cm
Distance from second slit to target	7.8 cm
Length of pole pieces (l_1)	6.0 cm
Distance from end of magnetic field to target (l_2)	1.8 cm
Width of first slit	0.015 cm
Width of second slit	0.0036 cm
Length of slits	0.4 cm
One-half the width of undeflected line, without field, (a)	0.009 cm.

RESULTS

Fig. 2 is a photomicrograph (6×) by reflected light of the result of a typical run, taken before the vacuum was broken. The three exposures were made consecutively without disturbing furnace or vacuum. After an exposure was complete, the target was displaced slightly and another exposure was begun. Table II gives details of the exposures of Fig. 2.

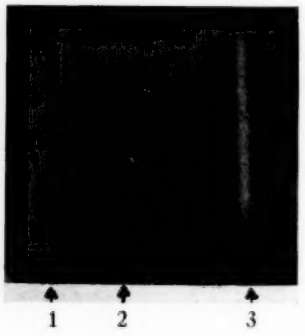

FIG. 2. Photomicrograph (6×) of three successive exposures in a typical experiment, traces 1 and 3 without magnetic field, trace 2 with field.

TABLE II. *Details of the exposures of Fig. 2.*

Trace	Magnetic field	Time of appearance (hours)	Total exposure (hours)
1	Off	$4\frac{1}{4}$	$4\frac{1}{2}$
2	On	8	$14\frac{1}{4}$
3	Off	$4\frac{1}{2}$	22

It will be seen in Fig. 2 that trace 2 (magnetic field on) is very much broader than traces 1 and 3 (field off) and that its density is less; and in Table II it will be seen that the time of appearance of trace 2 is greater than for the other two.

Microphotometer records were made from the negative of Fig. 2. Owing to the faintness of the image no detailed information about the intensity distribution in trace 2 could be obtained from these records. It was apparent from the records (as to the eye in Fig. 2) that trace 2 was wider and less intense than the others.

THEORETICAL INTENSITY DISTRIBUTION CURVE

The normal states of the iron atom are $^5D_{4,\,3,\,2,\,1,\,0}$, giving rise to the five Bohr magneton values ± 6, $\pm 9/2$, ± 3, $\pm 3/2$, and 0. From the term values of the different states, the relative probabilities, w, of the magneton values have been computed[6] to be (in order) 0.234,

[5] A. Leu, Zeits. f. Physik **41**, 551 (1927).

[6] For details of a similar calculation see Kurt and Phipps, Phys. Rev. **34**, 1365 (1929).

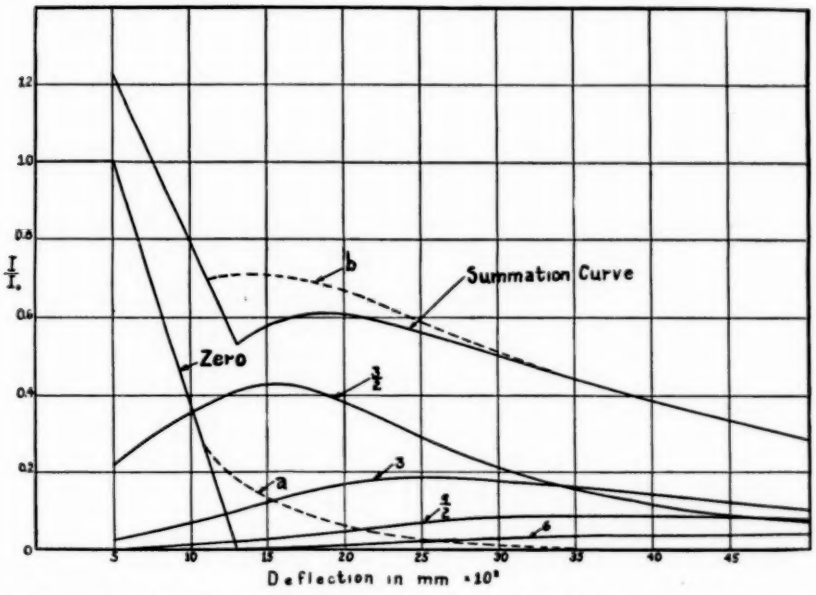

FIG. 3. Theoretical intensity distribution curves for the individual magneton values and the summation curve, for the conditions of Table I.

0.398, 0.582, 0.782 and 1.000. Values of s_α, the deviation in the magnetic field of atoms having the most probable velocity, were calculated for each of the magneton values from the equation

$$s_\alpha = \frac{\mu_i}{4kT} \cdot \frac{\partial H}{\partial z} l_1^2 \left\{ 1 + \frac{2l_2}{l_1} \right\}.$$

These values in cm were calculated to be 0.142, 0.106, 0.071, 0.035 and zero. From these values of s_α an intensity distribution curve for each species was constructed using the equation of Stern.[7]

These curves are given in Fig. 3. The "zero" curve is the ideal curve for magneton value zero, calculated from the geometry of the slit system. Actual molecular rays show a departure in the direction indicated by the dotted curve *a*. The "summation curve" is the expected distribution curve.

The effective magnetic moment of the iron atom was calculated from the summation curve to be 2.03 Bohr magnetons. The dotted curve *b* shows the effect upon the summation curve of a "tailing out" of the undeflected trace. It is seen from this analysis that in the actual experiment the maximum may be obscured in the general broadening of the trace.

The maximum might be realized with narrower slits and a considerably longer exposure. This would involve further improvements in slit alignment and furnace construction.

[7] O. Stern, Zeits. f. Physik **41**, 563 (1927).

LETTERS TO THE EDITOR

Prompt publication of brief reports of important discoveries in physics may be secured by addressing them to this department. Closing dates for this department are, for the first issue of the month, the twentieth of the preceding month; for the second issue, the fifth of the month. The Board of Editors does not hold itself responsible for the opinions expressed by the correspondents.

A Possible Explanation of the Frequency Distribution of Sizes of Hoffmann Stösse

The cloud chamber photographs of Blackett and Occhialini, Anderson, and Locher[1] have brought to light the suggestion that Hoffmann Stösse may not originate in a single atom, but may arise from several atoms as the result of a primary cosmic ray acting through intermediaries. Each of these observers finds groups of ray tracks, apparently all formed simultaneously. These tracks are possibly produced by the particles which give rise to the bursts of ions observed in a pressure chamber. However, these tracks do not diverge from a common point, but seem, in many cases, to be formed in several groups, each group of tracks diverging from a separate point. The existence of these multiple centers has been attributed by Locher[1] to the action of neutrons which, coming from any one nuclear disintegration, serve to precipitate others. Experiments by W. F. G. Swann and the author are in progress at the present time for the purpose of testing this conclusion further and particularly to ascertain whether the size of a Stoss depends upon the amount of material involved.

Data showing the frequency of occurrence of Stösse of different sizes have been published by Steinke and Schindler, and by Messerschmidt[2] and similar data have been taken at the Bartol Foundation with an apparatus which has been previously described.[3] These data all show the surprising fact that although a greater portion of the Stösse is grouped around a definite size, Stösse ten times this size occur fairly often. The object of the present note is to show how the cooperation of several atoms in the production of a Stoss would give rise to such a frequency distribution of Stoss sizes as is observed.

Let us suppose we have a block of material placed over an ionization chamber and suppose a group of rays is formed near the top of the block. These rays will contain among them entities capable of producing other groups and such secondary groups will be produced within the block. If the ranges of the ionizing rays are greater than the thickness of the block, then rays from both the primary and secondary groups will reach the ionization chamber and be recorded. Thus, on the average, if the primary group is formed near the top of the block of material, the number of ionizing rays which penetrate the ionization chamber will be larger than if the primary group is formed near the bottom of the block. Then the recorded Stösse will consist of a whole range of sizes similar to the observed range.

We can put the matter into a more quantitative form and obtain a rather good agreement with the observed distribution curves if we make a few simplifying assumptions. Let us suppose that the primary group will produce p ions in the chamber, and that p is independent of the position of the origin of the group. Also let us suppose that the rays of the primary group will produce a secondary group of size s ions, on the average, every a centimeters. Further let us suppose that each secondary group also

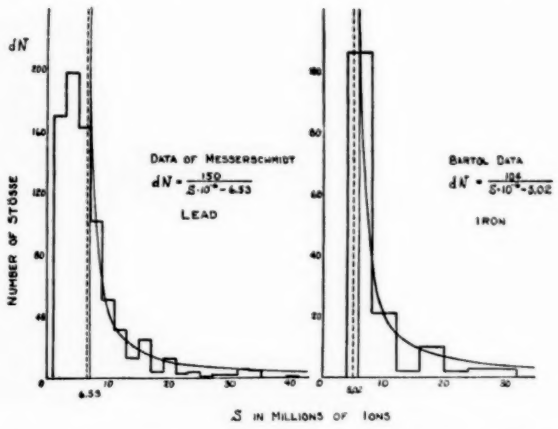

FIG. 1. Observed and computed distributions of sizes of Stösse.

produces groups of size s every a centimeters, and so forth. Then, if the primary group is formed at a distance r from the top of the block of material of thickness D, the size[4] of the resultant Stoss will be

$$S = p + s(2^{(D-r/a)} - 1). \quad (1)$$

Let us assume that the number of primary groups formed

[1] P. M. S. Blackett and G. Occhialini, Proc. Roy. Soc. Lond. **A139**, 699 (1933); C. D. Anderson, Phys. Rev. **43**, 368 (1933); G. L. Locher, Phys. Rev. **44**, 779 (1933).

[2] E. Steinke and H. Schindler, Zeits. f. Physik **75**, 115 (1932); W. Messerschmidt, Zeits. f. Physik **78**, 688 (1932).

[3] W. F. G. Swann and C. G. Mongtomery, Phys. Rev. **44**, 52 (1933).

in the element of thickness dr is independent of r, then we can write $dN=kdr$ where k is a constant. From relation (1), we obtain

$$dS=-(\log 2/a)[S-(p-s)]dr$$

or

$$dr=-adS/\{\log 2[S-(p-s)]\}.$$

Then the form of the distribution curve will be given by

$$dN=-\frac{ak/\log 2}{S-(p-s)};\quad dS=-\frac{A}{S-b}dS.$$

This depends on only two parameters, and we may fit it to the observed distribution curves. The data of Steinke and Schindler are unsuitable for consideration in the present connection since they give a distribution curve for the difference in size of Stösse occurring simultaneously in two chambers placed side by side. However, we can compare Messerschmidt's results and those obtained at the Bartol Foundation with this empirical formula. The accompanying curves show how well this elementary theory fits the observations. For Messerschmidt's data, we obtain $A=75$, $b=6.53\times10^6$ ions, and for the Bartol data $A=26$, $b=5.02\times10^6$ ions. b represents the difference in size of a primary and a secondary group, while $A=ak/\log 2$, where k is the total number of primary groups per centimeter. Since the observations do not extend to sufficiently small sizes, we can only set a lower limit to it. For the Bartol data, $D=2.5$ cm iron, $k>59$ and hence $a<0.3$ cm. For Messerschmidt's data, $D=10$ cm lead, $k>81$ and $a<0.6$ cm.

We see that the observed curves, in their middle range at least, are well represented by such a picture of the Stoss-forming process as is given here. The deviations at either end are certainly to be ascribed to the overly simplified picture used. An elaboration of the theory would involve a closer specification of the probabilities of formation of the secondary groups, rather than the assumption that they are all equal. Although this would improve the agreement, it would only tend to complicate the calculations and would add nothing to the picture of the mechanism. However, the agreement is certainly good enough to regard the model used as a fair approximation to what actually happens. It is to be noticed that the essential idea in the process is that all groups, whether primary or secondary, are capable of producing other groups. The application of the picture of a primary group producing secondary groups all along its path (S in this case would vary linearly with r) is not capable of giving a distribution curve of the type observed.

The real importance of this picture of the formation of Stösse lies in the predictions that can be made from it. First, there should be a lower limit to the sizes of Stösse, and this limit is the size of the primary group of rays. If an upper limit of size exists, it probably depends upon the energy of the primary cosmic ray. Second, the distribution curves of Stoss sizes will depend upon the thickness of the material from which the Stösse come: thicker materials should give larger Stösse. There should also be observed "transition" effects if there is a primary or secondary Stoss size characteristic of the material. The lower limit of the size should, however, be dependent only upon the last material through which the Stoss particles pass.

In conclusion, the author wishes to express his thanks to Dr. W. F. G. Swann for his helpful encouragement and discussion of the ideas involved here.

C. G. MONTGOMERY

Bartol Research Foundation
of The Franklin Institute,
November 26, 1933.

[4] The "2" in this expression results from the assumption that the number of groups doubles every "a" centimeters. As Dr. Swann has pointed out to the author, if the number of groups is derived by an integration process, the "2" becomes an "e."

Gamma-Rays from Lithium Bombarded with Protons

In a previous letter to the *Physical Review*[1] we reported the production of neutrons by the bombardment of lithium chloride with hydrogen ions. The measurements were made with an ionization chamber lined with paraffin and enclosed in a lead cylinder of 5 cm wall thickness. That the ionization was, in part at least, due to neutrons was concluded from the observation that less ionization was observed when the paraffin was removed from the chamber. We observed, however, that the difference in ionization with and without paraffin was in this case less than in the measurements of neutrons produced by other disintegrations previously investigated by us. This suggested that in the case of lithium a considerable part of the ionization might be due to γ-rays.

It is well established that lithium when bombarded with protons yields a group of long range α-particles and one or more groups of shorter range. Oliphant, Kinsey and Rutherfore[2] have recently made very careful measurements of the ranges and numbers of these particles and have found ranges of 0.65, 1.15 and 8.3 cm, the relative numbers of which are 0.5, 1 and 1, respectively. The 8.3 cm particles are satisfactorily accounted for by the reaction $Li^7+H^1\rightarrow 2He^4$, but this does not explain the two short range groups observed, unless the excess energy (about 12×10^6 e.v.) goes into a γ-ray. A search for such γ-rays has been made by Traubenberg, Eckartt and Gebauer,[3] but the evidence is not very conclusive. It is clear, therefore, that if all of these particles result from the disintegration of Li^7 with protons, the process must be more complicated than indicated by the above equation.

[1] Crane and Lauritsen, Phys. Rev. **44**, 783 (1933).

[2] Oliphant, Kinsey and Rutherford, Proc. Roy. Soc. **A141**, 722 (1933).

[3] Traubenberg, Eckartt and Gebauer, Zeits. f. Physik **80**, 557 (1933).

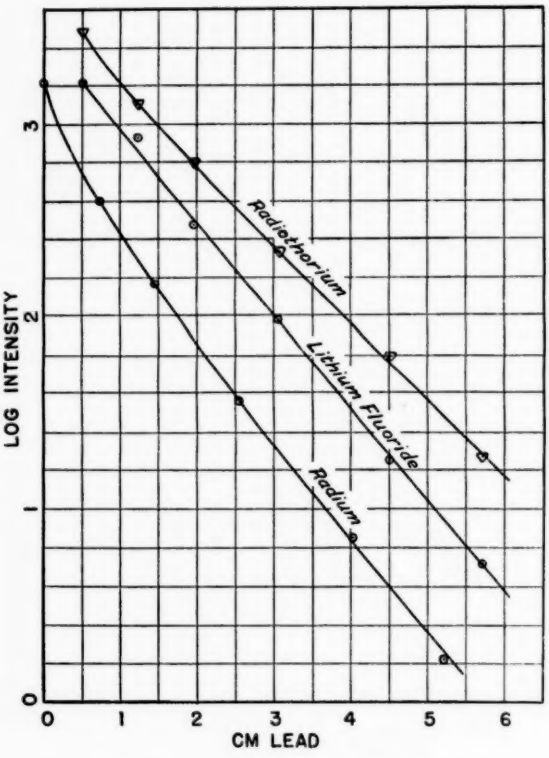

FIG. 1. Absorption of rays in lead.

To investigate the problem more closely, we have made provision for varying the amount of lead between the target and the ionization chamber. Measurements with much reduced lead filtration produced a large increase in the ionization which enabled us to make absorption measurements. The presence of strong γ-radiation was indicated by the observation that the absorption, per electron, was nearly the same for lead as for paraffin. The experimental arrangement was not suitable for an absolute determination of absorption coefficients as it was necessary to use a rather large solid angle. For this reason the absorption was compared directly with the absorption of γ-rays from radium and thorium sources placed in the exact position of the target.

The results of such a series of measurements at 600 kv with a lithium fluoride target and lead absorbers are shown in Fig. 1, from which we conclude that the γ-rays from lithium fluoride have about the same quantum energy as γ-rays from radium filtered through about 2 cm of lead. The plot is a straight line, within the accuracy of our measurements, indicating that the radiation is monochromatic, or at least nearly so. There is no evidence of a component of much harder radiation and, if such a component is present, it must be of very much smaller intensity. It is tempting to associate this γ-radiation with the short range α-particles, as the quantum energy corresponds approximately to the energy difference between two 1.15 cm particles and two 0.65 cm particles, namely, about 1.5×10^6 e.v.

It may be of interest to note that the intensity of γ-radiation at 600 kv and 20 microamperes ion current is about equal to that from 0.1 milligram of radium. The number of quanta is therefore not very different from the number of α-particles in the 1.15 cm group, thus giving support to the above suggestion.

C. C. LAURITSEN
H. R. CRANE

Kellogg Radiation Laboratory,
California Institute of Technology,
December 1, 1933.

The Nature of the "Forbidden" Lines in the Pb I Spectrum

In a recent letter to the *Physical Review*,[1] one of us has reported the appearance of some Pb I lines which are forbidden for the normal dipole radiation. These lines were obtained in the spectrum of high frequency electric discharges in mixtures of lead vapor with inert gases.

The strongest of these lines λ4618.0A, corresponding to the transition from $6p^2\,{}^1S_0$ to $6p^2\,{}^3P_1$ energy level, cannot be explained by quadrupole radiation as violating the $0\rightarrow1$ interdiction for the change of the resultant angular momentum quantum number J. The appearance of this line was therefore attributed to the electrically perturbed dipole radiation although the absence of sufficiently strong external or intermolecular electric fields hardly supports this view. Hence the remaining "forbidden" lines λ4659.4 ($6p^2\,{}^3P_0-6p^2\,{}^1D_2$), λ5312.7 ($6p^2\,{}^3P_2-6p^2\,{}^1S_0$) and λ7330 ($6p^2\,{}^3P_1-6p^2\,{}^1D_2$) which are allowed for the quadrupole radiation could also be interpreted as the electrically perturbed dipole radiation.

The emission of the line λ4618.0 can be explained however by the *magnetic dipole radiation* thus avoiding the hypothesis of strong electric fields under the described experimental conditions. A detailed examination, which will be published shortly, has shown that there exists a finite probability of the transitions from the energy state ${}^1S_0$ to that ${}^3P_1$ for the magnetic dipole radiation. Brinkman's[2] selection rules for the change of the quantum numbers L and S in the magnetic dipole radiation ($\Delta L=0$ and $\Delta S=0$) cannot be applied here since they are strictly valid only for extreme Russell-Saunders coupling for which electric dipole and quadrupole intercombination lines are also forbidden. A deviation from Russell-Saunders coupling in the case of the energy states of the neutral lead atom belonging to the electron configuration $6s^2\,6p^2$ is indicated by the wide relative separation of the ${}^3P$ levels.

---

[1] H. Niewodniczański, Phys. Rev. **44**, 854 (1933).

[2] H. C. Brinkman, Dissertation, Utrecht (1932), also quoted by A. Rubinowicz and J. Blaton, Ergebnisse der exakten Naturwiss. **11**, 190 (1932).

The probabilities of the analogous transitions from $^1S_0$ to $^3P_1$ energy state in C I, N II and O III were calculated by Stevenson[3] who found finite values for these probabilities. However, Stevenson does not separate the multipole radiation into the quadrupole and magnetic dipole radiation and interprets accordingly the radiation corresponding to the transitions between the energy states $^1S_0$ and $^3P_1$ as quadrupole radiation in contradiction to the $J_1+J_2 \geqq 2$ selection rule for this radiation.

Assuming the line λ4618.0 to be due to the pure magnetic dipole radiation, the lines λ4659.4 ($^3P_0-{}^1D_2$) and λ5312.7 ($^3P_2-{}^1S_0$) can be explained as pure quadrupole lines and the line λ7330 ($^3P_1-{}^1D_2$) as due to the mixed magnetic dipole and quadrupole radiation.

We hope to confirm the above explanation of the forbidden Pb I lines by the Zeeman effect.

J. Blaton
H. Niewodniczański

Physical Laboratory
Stefan Batory University,
Wilno, Poland,
November 27, 1933.

[3] A. F. Stevenson, Proc. Roy. Soc. **A137**, 298 (1932).

Concerning the Thermoelectric Effects of the Alkalis

In an extensive article,[1] I have presented an elementary treatment of the electron theory of metals in a simpler and more complete manner than I had given in my paper of 1928[2] and H. Bethe has followed this with a basic wave-mechanical formulation of the theory. In this note I should like to extend one phase of this treatment.

From my elementary theory the Thomson coefficient μ defined by $U=-\mu J\,(dT/dx)$ (U=rate of heating, J=current density), is given by

$$\mu=-\frac{\pi^2}{3}\frac{k^2}{|e|}\frac{\Lambda T}{\zeta}; \qquad \Lambda=1+\tfrac{1}{2}\frac{d\log l}{d\log v} \tag{1}$$

with the simplifying assumptions that Λ and ζ are independent of T. $|e|$ is the absolute value of the charge on an electron, ζ the internal potential per electron in the Gibbs sense which I formerly denoted by W_i, l the free path, and in the expression for Λ the derivative is to be taken for the limiting velocity ($v=\bar{v}$) of the Fermi distribution. Originally I had chosen silver as an example and placed $\Lambda=1$ as a reasonable approximation. Now μ is *positive* for Cu, Ag and Au (also for Hg) and hence Eq. (1) seemed to predict the *wrong sign*. However, the alkalis rather than the noble metals are the true representatives of metals with "free" electrons. Their ionization potentials (with the exception of Li) are particularly small, their mono-valence most pronounced and the closed shell of eight electrons inside the valence electron (again excepting Li) is most clearly defined (better than the shell of eighteen electrons inside the valence electron of the noble metals).

At the time of the preparation of my *Handbuch* article measurements of the Thomson coefficients of the alkalis were not known to me. However, even at that time I could conclude from older measurements of the thermoelectric force by Bernini, et al., that, because of thermodynamic relations, the Thomson coefficient of Na and K must be negative and hence the sign required by Eq. (1) actually occurred for Na and K. In a note I postulated that reliable measurements on Rb and Cs would agree with formula (1) and expected that the comparison for Li would be less satisfactory than for the remaining alkalis.

Meanwhile my attention has been called to an article by C. C. Bidwell.[3] Here measurements of the thermoelectric force are given ($\Theta_1=d\Theta/dT$ if Θ denotes the thermoelectric difference of potential) for the complete series of the alkalis. They show a good *linear falling off* of Θ_1, above the melting point, if all the measurements are referred to lead as the second metal. Li is an exception and shows a *linear rise* above the melting point. Since the thermodynamic relation

$$\mu=Td\Theta_1/dT \tag{2}$$

must hold if μ is taken zero for lead, the linear decrease of Θ_1 denotes *proportionality of μ with T* and a *negative sign* as is required by Eq. (1). It is also understandable that these relations are best satisfied in the *molten state*. For the elementary theory does not take the crystal lattice into account but replaces its action schematically by a free path l, which is independent of all regularity in space. In the *solid state* Bidwell finds an α- and a β-modification. The β-modification joins at the melting point and also shows a passable linear decline of Θ_1 with T, while in the neighborhood of the melting point μ rises rather suddenly. The transition point between α and β lies at lower temperatures (−100°C for K, etc.). In the α-phase Θ_1 rises with T; for such low temperatures, however, our elementary theory is certainly not valid.

For the molten state our formula (1) yields the *correct order and order of magnitude* of the Thomson coefficients. Table I shows this, the numbers denoting microvolts per degree. The experimental data are the values given by Bidwell in his Table III under "liquid" (denoted there by d^2E/dt^2); the theoretical values are calculated from Eq. (1):

Table I.

μ/T	Li	Na	K	Rb	Cs
Exp.	+0.40	−0.0282	−0.0275	−0.069	−0.062
Theor.	−0.016	−0.023	−0.036	−0.041	−0.048

Li is an exception; the remaining alkalis check surprisingly well. With respect to the order we prefer to give more credence to the theoretical numbers than to the experi-

[1] A. Sommerfeld, Handb. d. Physik **24**, 2 (in press), Springer.

[2] A. Sommerfeld, Zeits. f. Physik **47**, 1–32, 43–60 (1928).

[3] C. C. Bidwell, Phys. Rev. **23**, 357 (1924).

mental ones and would be inclined to look upon the departure from the natural order Na, K, . . . as unreal.

In this connection another point must be discussed, *viz.*, the magnitude of Λ. The elementary theory can make no predictions about the free path and must turn to wave mechanics for information about this point. The latter leads us to expect as the simplest possible law: l proportional to the square of the kinetic energy of the electron. From this it follows from Eq. (1) that $\Lambda=3$. This value has been used in constructing Table I. One can also readily see (compare Bethe, loc. No. 50a) that the above law relating l and Λ must hold for and only for the alkalis.

In the same manner as for the Thomson effect, the thermoelectric power of the alkalis may be calculated from the elementary theory, especially for the liquid state (Li excepted). It seems very noteworthy to me that such simple formulas as Eq. (1) (the formula for the thermoelectric effect is quite similar), at least for the simplest metals, can predict the sign, order and magnitude approximately correctly for these complicated effects. To indicate the method of the calculations which lead to the values in Table I, I give the values of n (number of free electrons = number of metal ions per cc) and for ζ (the internal potential) in Table II. n is calculated in the usual manner from the atomic weight and density, ζ from the formula

$$\zeta=(h^2/2m)(3n/8\pi)^{2/3}. \tag{3}$$

TABLE II.

	Li	Na	K	Rb	Cs
$n\times10^{-22}$	4.66	2.67	1.30	1.08	0.86
$\zeta\times10^{12}$	7.4	5.1	3.2	2.8	2.4

A. SOMMERFELD

University of München,
December 11, 1933.

Magnetic Properties of Rochelle Salt

In conjunction with Müller's[1] recent note in *Physical Review* on the electric properties of Rochelle salt, it may be of interest to communicate a few tests of the magnetic properties of this substance which we have recently made. Through the courtesy of Dr. R. M. Bozorth of Bell Telephone Laboratories, a single crystal of the salt was supplied to us which in turn was cut into two smaller rectangular crystals approximately $1.2\times0.3\times0.3$ cm, the b and c axes being parallel to the long side of the rectangles respectively in the two prisms. The susceptibility along the a, b and c axes was then measured by using a Weiss magnetic balance and a field strength of about 8000 gauss. No variation in the susceptibility in these three principal directions could be found within the experimental error (half percent). The value of the mass-susceptibility was $\chi=-0.54\times10^{-6}$ if $\chi_{Au}=0.145\times10^{-6}$. In addition, the susceptibility at various temperatures, in the range 10°C to 30°C, for the three principal crystallographic directions was determined. No variation in the mass-susceptibility could be detected for any of the three directions to within an accuracy of about one-quarter of one percent. Apparently, therefore, the Weiss electrical field postulated by Müller to account for the anomalous behavior of the electric properties of Rochelle salt is without influence on its magnetic properties.

C. T. LANE

Sloane Physics Laboratory,
Yale University,
December 13, 1933.

[1] H. Müller, Phys. Rev. **44**, 854 (1933).

Periodic Unequal Potential Minima and Torsion Oscillation of Molecules

The problem of the torsion oscillation of molecules of the ethane type has been treated by Nielsen,[1] Teller and Weigert[2] and Koenig.[3] Molecules, however, in which each of the two identical groups is composed of different atoms, as for example in the symmetric dichloroethylenes, have to be treated differently since the potential fields corresponding to the cis and the trans positions are different. The problem of the quantization of the oscillations of the two groups is reduced to solving the Hill equation $d^2\psi/d\theta^2+(8\pi^2I/h^2)[E-V(\theta)]\psi=0$ in which the potential $V(\theta)$ has two unequal minima in 2π, is symmetrical about each minimum, and $V(\theta)=V(\theta+2\pi)$ subject to the periodicity condition that $\psi(\theta)=\psi(\theta+4\pi)$.

The fact that both the cis and the trans forms of the molecules of the type ClHC : CHCl are stable and do not transform from one to the other appreciably at low temperature justifies the assumption that the two minima are separated by a relatively large potential barrier and that their lower energy levels lie much below the maximum value of the barrier. On this assumption the solution of the wave equation by the W-K-B method can be carried out by generalizing the cases treated by Koenig[3] and the writer.[4] For levels below the top of the potential maximum, corre-

[1] H. H. Nielsen, Phys. Rev. **40**, 445 (1932).

[2] Teller and Weigert, Gött. Nachr. **2**, 218 (1933).

[3] H. D. Koenig, Phys. Rev. **44**, 675 (1933).

[4] T. Y. Wu, Phys. Rev. **44**, 727 (1933). It should be made more explicit here that in the above article, there are two levels for each quantum number n, given by expressions (3), (6) and (7) corresponding to the two possible signs of δ and ϵ in Eqs. (2) and (5), namely, $\tan\delta=\pm|D/2E|$ and $\tan\epsilon=\pm|E/2D\alpha^4|$. When applied to the calculation of the F levels of heavy atoms, the atomic field is such that only the lower level in each pair, corresponding to the negative sign for δ and ϵ, is stable.

sponding to each value of the quantum number, there are four eigenvalues given by the two equations

$$\tan\frac{\Gamma}{2}\tan\frac{\gamma}{2}+(-1)^{n+1}\frac{1+\epsilon^2}{1-\epsilon^2}\left(\tan\frac{\Gamma}{2}+\tan\frac{\gamma}{2}\right)+1=0 \qquad (1)$$

$$\tan\frac{\Gamma}{2}\tan\frac{\gamma}{2}+(-1)^{n}\frac{1-\epsilon^2}{1+\epsilon^2}\left(\tan\frac{\Gamma}{2}-\tan\frac{\gamma}{2}\right)-1=0 \qquad (2)$$

where

$$\Gamma=(2\pi/h)\int_{\theta_1}^{\theta_2}P^{\frac{1}{2}}d\theta, \qquad \gamma=(2\pi/h)\int_{\theta_3}^{\theta_4}P^{\frac{1}{2}}d\theta,$$

$$\epsilon^2=\tfrac{1}{4}\exp\left[-(4\pi/h)\int_{\theta_2}^{\theta_3}P^{\frac{1}{2}}d\theta\right]$$

$$P=2I\left|E-V(\theta)\right|,$$

$\theta_1<\theta<\theta_2$, $\theta_3<\theta<\theta_4$ being the two classical regions, $\theta_2<\theta<\theta_3$, the region under the potential hill (Fig. 1). Eq. (1) gives two energy levels (a and b in the figures) which, in the case where the potential valleys are identical, become given by $\Gamma=(n+\frac{1}{2})\pi\pm 2\arctan\epsilon$. Eq. (2) also gives two levels (c and d in the figures) which in the case of identical minima degenerate into one and are then given by $\Gamma=(n+\frac{1}{2})\pi$. In the limiting case in which the potential barrier is infinite, i.e., $\epsilon=0$, the four levels given by Eqs. (1) and (2) degenerate into two, E_n' and E_n'', given by $\Gamma=(n+\frac{1}{2})\pi$ and $\gamma=(n+\frac{1}{2})\pi$ respectively. The lowest levels E_0' and E_0'' of the trans and the cis forms of the isomers will then be approximately given by $\Gamma=\pi/2$ and $\gamma=\pi/2$, respectively.

In Fig. 2, the connection of the energy levels between the limits of pure rotation and pure oscillation is indicated. In the case of identical minima, the levels c and d degenerate into one and $E_n'=E_n''$. It may also happen that $E_{n+1}'<E_n''$, and in that case the connection curves will cross.

The torsion oscillation of the trans form is active in emission and absorption in the infrared, while that of the cis

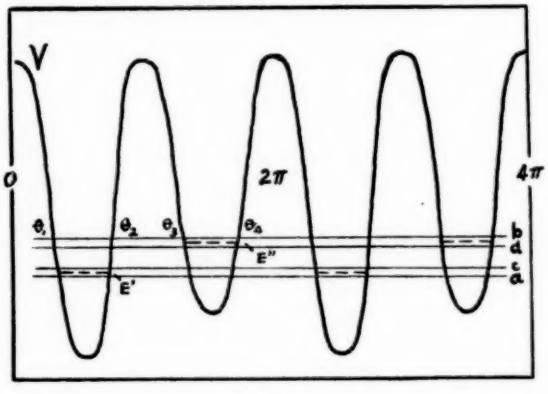

FIG. 1.

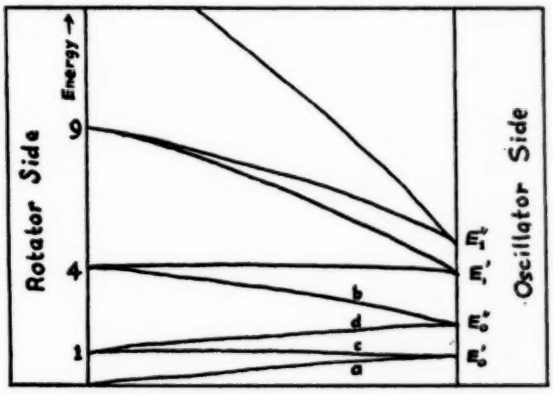

FIG. 2.

form is not active. The infrared spectra of the cis and the trans dichloroethylene are being studied by the writer[5] with the hope of finding the oscillation frequency of the trans form, in addition to differences in other fundamental vibrations of the two forms arising from difference in their geometrical symmetry.

The suggestion of Wolf[6] on the temperature dependence of the electric moment of the isometric molecules applies here. One starts with the cis form at ordinary temperature, whose lowest levels E_0'' lies above that of the trans form E_0'. When the temperature is raised sufficiently high enough, the cis form will pass into the trans form by going over and through the top of the potential barrier, the proportion of the two in the equilibrium state being determined by the Boltzmann theorem. As the cis form has a permanent electric moment while the trans form has none, if the dielectric constant be measured as a function of temperature by first raising and then lowering the temperature, a "hysteresis" curve for the dielectric constant-temperature variation will be obtained. When data of this kind are available, it will be possible to estimate the height of the potential barrier. Such experiments on the dichloroethylenes are being carried out by Mr. Stone in this laboratory. The writer is grateful to Professor Uhlenbeck for helpful discussions.

TA-YOU WU*

University of Michigan,
December 14, 1933.

* China Foundation Fellow.

[5] The spectra of these two forms together with C_2H_3Cl, asym. $C_2H_2Cl_2$, C_2HCl_3 and C_2Cl_4 in the region from 1 to 25μ are being studied. Results will be published in the near future.

[6] K. L. Wolf, article in Molekülstruktur, Leipziger Vorträge, 1931.

An Infrared Band of Arsine

A very weak band[1] of arsine at 1.63μ has been investigated with an automatic recording spectroscope[2] by using a one-meter cell with the gas at atmospheric pressure. Under these conditions the zero branch showed a 25 percent absorption. The characteristics of this band are very similar

TABLE I.

AsH_3 band	$\Delta\nu$ cm^{-1}	Branch	$I\times10^{40}$ g cm^2
10μ	8.5	R	6.51
11	10.0	P	5.53
1.63	7.32	R	7.57
	9.75	P	5.68

to those of the ammonia band[3] at 3.0μ. The positive branch has a decidedly smaller line spacing than the negative branch and the intensity of the lines is much less in the latter. The zero branch is broad, symmetrical and relatively intense and it overlaps the first line of the + and − branches because of insufficient resolving power.

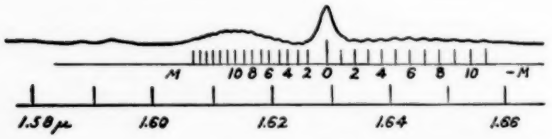

FIG. 1. M indicates line numbers measured from the zero branch and not the initial j values giving the rotational energy changes,

$$W=(h^2/4\pi^2I)(\pm(j+\tfrac{1}{2})+\tfrac{1}{2}).$$

There is an apparent divergence of the line spacing on the high frequency side of the R-branch and the low frequency side of the P-branch which indicates some coupling between the rotational and vibrational states of the molecule. The average line spacings in the branches of this band are a little smaller than those of the bands[1] at 10μ and 11μ, which indicates that the moment of inertia is not constant but increasing for the higher vibrational states.

WILL V. NORRIS
HILBERT J. UNGER

School of Science,
University of Oregon,
December 13, 1933.

TABLE II.
$\nu=6137.99+8.187M-0.1304M^2-0.00104M^3$

M	$\lambda(\mu)$	ν	$\Delta\nu$ cm^{-1}
14	1.6020	6242.2	
			10.1
13	1.6046	6232.1	
			9.4
12	1.6070	6222.7	
			9.2
11	1.6094	6213.5	
			8.1
10	1.6115	6205.4	
			6.6
9	1.6132	6198.8	
			6.1
8	1.6148	6192.7	
			5.7
7	1.6163	6187.0	
			5.4
6	1.6177	6181.6	
			5.7
5	1.6192	6175.9	
			6.5
4	1.6209	6169.4	
			7.1
3	1.6227	6162.5	
			7.5
2	1.6247	6155.0	
			15.1
0	1.6287	6139.9	
			20.0
−2	1.6340	6120.0	
			9.4
−3	1.6365	6110.6	
			9.3
−4	1.6391	6101.3	
			8.9
−5	1.6414	6092.4	
			8.2
−6	1.6436	6084.2	
			8.9
−7	1.6460	6075.3	
			9.5
−8	1.6486	6065.8	
			10.3
−9	1.6513	6055.5	
			11.0
−10	1.6544	6044.5	
			11.7
−11	1.6576	6032.8	

[1] Robertson and Fox, Proc. Roy. Soc. **A120**, 161 (1928).
[2] H. J. Unger, Phys. Rev. **43**, 123 (1933).
[3] G. A. Stinchcomb and E. F. Barker, Phys. Rev. **33**, 305 (1929).